

Coupling between Voltage Sensor Activation, Ca^{2+} Binding and Channel Opening in Large Conductance (BK) Potassium Channels

FRANK T. HORRIGAN¹ and RICHARD W. ALDRICH²

¹Department of Physiology, University of Pennsylvania School of Medicine, Philadelphia, PA 19104

²Department of Molecular and Cellular Physiology, Howard Hughes Medical Institute Stanford University School of Medicine, Stanford, CA 94305

ABSTRACT To determine how intracellular Ca^{2+} and membrane voltage regulate the gating of large conductance Ca^{2+} -activated K^+ (BK) channels, we examined the steady-state and kinetic properties of *mSlo1* ionic and gating currents in the presence and absence of Ca^{2+} over a wide range of voltage. The activation of unliganded *mSlo1* channels can be accounted for by allosteric coupling between voltage sensor activation and the closed (C) to open (O) conformational change (Horrigan, F.T., and R.W. Aldrich. 1999. *J. Gen. Physiol.* 114:305–336; Horrigan, F.T., J. Cui, and R.W. Aldrich. 1999. *J. Gen. Physiol.* 114:277–304). In 0 Ca^{2+} , the steady-state gating charge-voltage (Q_{ss-V}) relationship is shallower and shifted to more negative voltages than the conductance-voltage (G_K-V) relationship. Calcium alters the relationship between $Q-V$ and $G-V$, shifting both to more negative voltages such that they almost superimpose in 70 μM Ca^{2+} . This change reflects a differential effect of Ca^{2+} on voltage sensor activation and channel opening. Ca^{2+} has only a small effect on the fast component of ON gating current, indicating that Ca^{2+} binding has little effect on voltage sensor activation when channels are closed. In contrast, open probability measured at very negative voltages (less than -80 mV) increases more than 1,000-fold in 70 μM Ca^{2+} , demonstrating that Ca^{2+} increases the C-O equilibrium constant under conditions where voltage sensors are not activated. Thus, Ca^{2+} binding and voltage sensor activation act almost independently, to enhance channel opening. This dual-allosteric mechanism can reproduce the steady-state behavior of *mSlo1* over a wide range of conditions, with the assumption that activation of individual Ca^{2+} sensors or voltage sensors additively affect the energy of the C-O transition and that a weak interaction between Ca^{2+} sensors and voltage sensors occurs independent of channel opening. By contrast, macroscopic I_K kinetics indicate that Ca^{2+} and voltage dependencies of C-O transition rates are complex, leading us to propose that the C-O conformational change may be described by a complex energy landscape.

KEY WORDS: calcium • potassium channel • BK channel • gating current • ion channel gating

INTRODUCTION

Ion channels activate by sensing stimuli such as membrane voltage or ligand binding and transducing this information into conformational changes that open the channel pore. Thus, a key question to understanding ion channel function is how the protein domains involved in sensing stimuli (sensors) and opening the pore (gates) communicate. We addressed this question in *mSlo1* large conductance Ca^{2+} -activated K^+ (BK) channels by measuring ionic and gating currents over a wide range of voltage and $[\text{Ca}^{2+}]$ (for abbreviations and parameters used in this paper, see Table I).

To characterize sensor-gate interaction ideally, one would like to monitor both sensor and gate activity and determine what effect the state of one has on the functional properties of the other. However, this approach

is problematic for many channels because the kinetics and equilibrium properties of sensor activation and channel opening are too similar to allow one process to be studied while the other remains in a fixed state. In addition, for cases in which certain combinations of sensor and gate conformation are prohibited, the conditions under which interactions can be probed will be restricted. For instance, channel opening in many voltage-gated channels cannot be studied when voltage sensors are in a nonactivated state (Isla and Sigworth, 1999).

Large conductance BK channels possess many advantages as a system for studying interactions between sensors and gates. First, voltage- and ligand-dependent gating mechanisms can be studied in the same channel. Second, the mechanisms of voltage sensor activation, Ca^{2+} -binding, and channel opening appear simple and reasonably represented as two-state processes. The homotetrameric nature of the channel and the absence of inactivation also help to limit the potential complexity of interactions between sensors and gates. Third, closed to open state transition kinetics in *Slo1* channels are

Address correspondence to Dr. Frank T. Horrigan, Department of Physiology, University of Pennsylvania School of Medicine, A401 Richards, 3700 Hamilton Walk, Philadelphia, PA 19104. Fax: (215) 573-5851; E-mail: horrigan@mail.med.upenn.edu

T A B L E I

Commonly Used Abbreviations and Parameters

BK	Large conductance Ca^{2+} -activated K^+ channel.
MWC	Monod-Wyman-Changeux.
LFER	Linear-free energy relationship.
C,O	Closed and open conformations of the channel.
R,A	Resting and activated conformations of voltage sensor.
X,Xca	Unliganded and Ca^{2+} -bound state of Ca^{2+} -sensor.
L	C-O equilibrium constant (unliganded channel, resting voltage sensors).
L_0, z_L	The zero voltage value of L and its partial charge, respectively.
J	R-A equilibrium constant (closed, unliganded channel).
J_0, z_J	The zero voltage value of J and its partial charge, respectively.
$V_h(J)$	The voltage where $J = 1$, corresponding to the half-activation voltage of Q_C .
K_D	Ca^{2+} dissociation constant (closed channel, resting voltage sensors).
K	Equilibrium constant for Ca^{2+} -binding ($K = [\text{Ca}^{2+}] / K_D$).
C	Allosteric factor describing interaction between channel opening and Ca^{2+} -binding. The ratio of $K_{D\text{S}}$ for closed and open channels.
D	Allosteric factor describing interaction between channel opening and voltage sensor activation. The ratio of R-A equilibrium constants for open and closed channels.
E	Allosteric factor describing interaction between voltage-sensor activation and Ca^{2+} -binding.
	The ratio of $K_{D\text{S}}$ for activated and resting voltage sensor.
$V_h(P_0)$	Half activation voltage of the P_0 -V relationship.
R_0	Ratio of NP_0 in the presence and absence of Ca^{2+} at extreme negative voltages where voltage-sensors are not activated.
Q_p	Gating charge moved during a voltage pulse.
$I_{g\text{Fast}}$	The fast component of ON or OFF gating current.
Q_{fast}	Fast component of gating charge movement.
$\tau_{g\text{Fast}}$	Time constant of fast gating charge movement.
$\tau_{g\text{Slow}}$	Time constant of slow gating charge movement (limited by C-O transition).
Q_{ss}	Steady-state gating charge.
Q_C, Q_O	Steady-state gating charge distribution for closed or open channels.
Q_T	Total gating charge associated with opening and voltage-sensor activation.
$\langle q_a \rangle$	Mean activation charge displacement/slope of $\log(P_0)$ -V (Eq. 7).
C_g	Gating capacitance determined by admittance analysis.
α, β	Forward and backward rate constant, respectively, for R-A transition.
δ, γ	Forward and backward rate constant, respectively, for C-O transition.
i_j	The number of voltage sensors activated and Ca^{2+} ions bound, respectively.
$\tau(I_K)$	The time constant of I_K relaxation after voltage-sensor activation.
τ_N, τ_P	$\tau(I_K)$ at extreme negative or positive voltages, respectively.
z_N, z_P	Partial charges of τ_N, τ_P , respectively.
V_{dn}	The voltage where $\tau(I_K)$ deviates from an exponential voltage-dependence at extreme negative voltages.

slow relative to voltage sensor activation and Ca^{2+} -binding (Cox et al., 1997a; Horrigan and Aldrich, 1999; Horrigan et al., 1999). This simplifies the analysis of

macroscopic I_K kinetics and allows sensor function to be examined while channels are maintained in either an open or closed conformation. Fourth, voltage sensors and Ca^{2+} sensors appear to interact with channel opening through allosteric mechanisms such that no combination of sensor and gate conformation is prohibited. Finally, the sensitivity of BK channels to both Ca^{2+} and voltage allows the manipulation of channel function in ways that facilitate analysis of sensor-gate interaction.

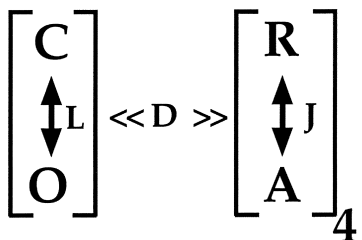
In the present study, we address several features of BK channel gating that are readily explained by allosteric models. Our ability to test this mechanism and to characterize sensor-gate interaction in BK channels depends on isolating subsets of transitions under extreme conditions and measuring both ionic and gating currents. For example, we show that the effect of Ca^{2+} -binding on channel opening is best characterized when the C-O equilibrium constant is reduced by forcing voltage sensors into a resting state at extreme negative voltages. Conversely, some effects of channel opening on voltage sensor activation are best detected when the open conformation is stabilized by high $[\text{Ca}^{2+}]$. The observed properties of Ca^{2+} - and voltage-dependent transitions and their relationship to each other define how Ca^{2+} and voltage interact to determine *mSl01* channel activity.

The BK Channel Gating Mechanism

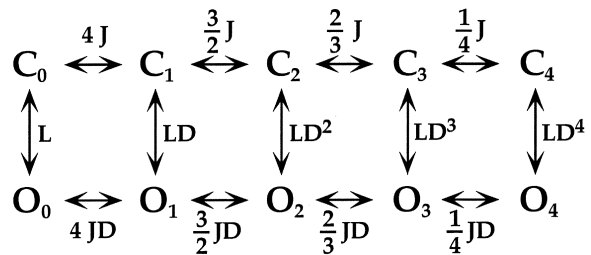
Because the response of BK channels to Ca^{2+} and voltage is complex, it is useful to present our results in the framework of a plausible general model. BK channel gating involves voltage sensor activation, Ca^{2+} binding, channel opening, and some interaction among these three processes. Previous analysis of ionic and gating currents from *mSl01* in 0 Ca^{2+} ($[\text{Ca}^{2+}] < 1 \text{ nM}$) showed that voltage sensor activation promotes channel opening through an allosteric mechanism, illustrated in Fig. 1 A, Scheme I (Horrigan and Aldrich, 1999; Horrigan et al., 1999). In Scheme I, voltage sensors in each of the four identical subunits can undergo transitions between resting (R) and activated (A) conformations. In addition, the channel can undergo a transition between closed (C) and open (O) conformations. Voltage sensor activation and channel opening interact through an allosteric mechanism, represented by a factor D, such that the C-O equilibrium constant increases D-fold for each voltage sensor activated, and the R-A equilibrium constant increases D-fold when the channel opens.

A key feature of an allosteric interaction is that the two processes involved influence each other but are not coupled obligatorily. That is, channels can open even if voltage sensors are not activated and voltage sensors can activate whether channels are closed or open. Therefore, Scheme I specifies a 10-state gating scheme (Fig. 1 B, Scheme I*) with 5 closed and 5 open states representing

A Scheme I (Activation by Voltage)



B Scheme I*



C Scheme II (Activation by Voltage and Ca²⁺)

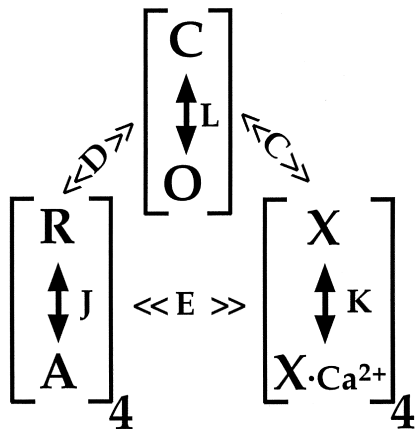


FIGURE 1. *Slo1* gating mechanisms. (A) The unliganded gating mechanism (Scheme I) involves an allosteric interaction between channel opening (C-O) and voltage sensor activation (R-A). L is the C-O equilibrium constant when all voltage sensors are in the resting (R) state. J is the R-A equilibrium constant when channels are closed. D is the allosteric interaction factor such that the C-O equilibrium constant increases D-fold for each voltage sensor activated, and the R-A equilibrium constant increases D-fold when the channel opens. (B) Scheme I specifies a 10-state gating scheme (Scheme I*) with the indicated equilibrium constants. Subscripts for closed and open states denote 0–4 activated voltage sensors. (C) A general allosteric gating mechanism (Scheme II) includes a Ca²⁺ binding transition (X-XCa) for each subunit with an equilibrium constant K = [Ca²⁺]/K_d when channels are closed and voltage sensors are not activated. Allosteric interactions of Ca²⁺ binding with channel opening and voltage sensor activation are determined by allosteric factors C and E, respectively, as described in the text.

the C and O conformations with 0–4 activated voltage sensors. Similar schemes have been proposed to describe the activation of other voltage-dependent channels (Marks and Jones, 1992; Rios et al., 1993; McCormack et al., 1994), and the basic finding that channels undergo both independent and concerted (or cooperative) transitions is well established (Sigworth, 1994; Zagotta et al., 1994). The kinetic and equilibrium properties of *mSlo1* channels allow us to study these transitions in isolation (Horriigan and Aldrich, 1999; Horriigan et al., 1999), an advantage that will be exploited here to determine the mechanism of Ca²⁺ action.

Several lines of evidence indicate that Ca²⁺-binding also influences channel opening through an allosteric mechanism. The voltage-dependent activation of unliganded channels shows that Ca²⁺-binding is not obligatory for channel opening or for voltage sensor activation (Cui et al., 1997; Nimigean and Magleby, 2000; Talukder and Aldrich, 2000). Similarly, macroscopic I_K relaxation kinetics are altered by Ca²⁺ in a saturable manner, indicating that Ca²⁺ binding is not a rate-limiting step in channel activation. The kinetic and steady-state properties of *mSlo1* activation in the presence and absence of Ca²⁺ exhibit similar voltage dependencies (Cox et al., 1997a; Cui et al., 1997; Rothberg and Magleby, 2000), suggesting that a similar gating scheme with altered rate constants might account for the activation of unliganded and Ca²⁺-bound channels. In line with this prediction, single channel data from native BK channels in high Ca²⁺ are consistent with a two-tiered gating scheme for Ca²⁺-bound channels similar to Scheme I* (Rothberg and Magleby, 1999). Moreover, an allosteric model of Ca²⁺ action reproduces many features of macroscopic *mSlo1* I_K over a wide range of Ca²⁺ despite the use of a simplified voltage-gating mechanism (Cox et al., 1997a; Cui et al., 1997).

A General Allosteric Model of BK Channel Gating

Any BK channel gating scheme that incorporates four identical subunits and accounts for the effects of both Ca²⁺ and voltage must necessarily contain a large number of states (Cox et al., 1997a). In addition to the four voltage sensors, each channel presumably contains at least four high affinity Ca²⁺ binding sites, since dose-response relationships describing the effect of micro molar Ca²⁺ on steady-state open probability require Hill coefficients greater than three (Cox et al., 1997a; Rothberg and Magleby, 2000). To describe a channel that can be open or closed with any number (0–4) of Ca²⁺-bound and voltage sensors activated requires a minimum of 50 states, divided into two interconnected tiers of open and closed states (Horriigan et al., 1999; Rothberg and Magleby, 1999; Cox and Aldrich, 2000; Cui and Aldrich, 2000; Rothberg and Magleby, 2000).

Despite the apparent complexity of a large gating

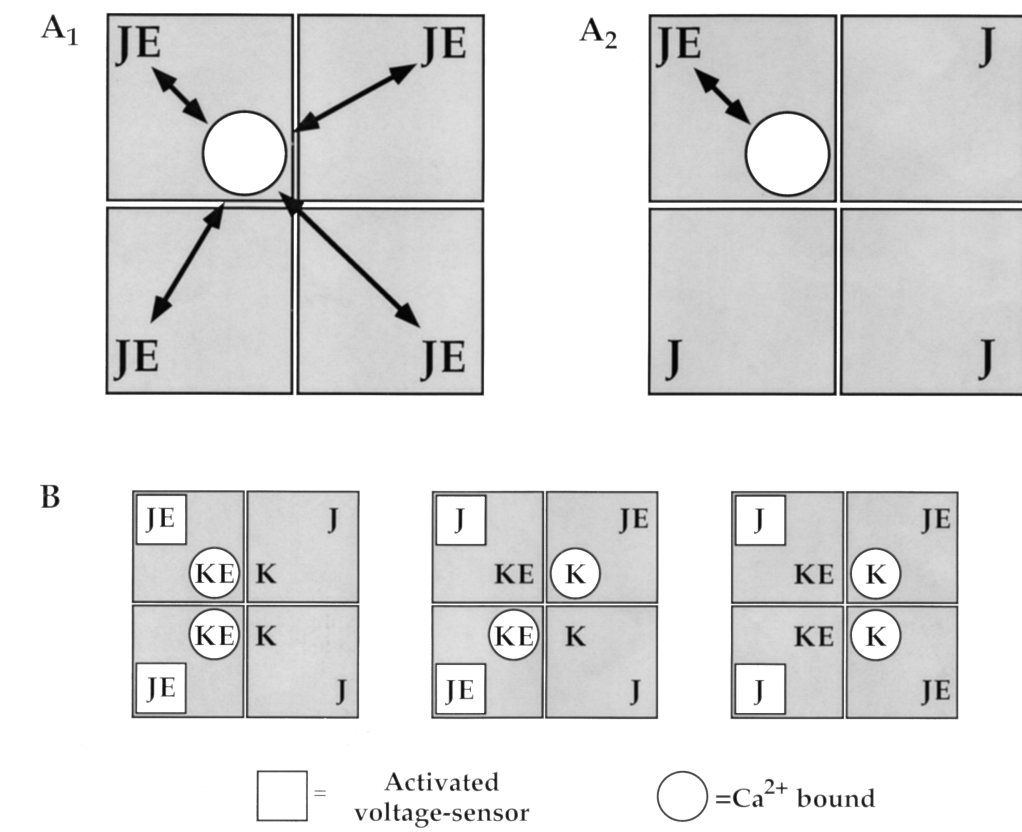
FIGURE 2. Mechanisms of interaction between voltage sensors and Ca^{2+} -binding sites. (A₁) If the binding of Ca^{2+} to a single subunit affects voltage sensors equally then voltage sensor equilibrium constants in all four subunits will increase E-fold to JE as indicated. (A₂) In Scheme II, we assume Ca^{2+} binding only affects the voltage sensor in the same subunit. Consequently, the A₂ mechanism predicts more states than the A₁ mechanism. (B) For example, when a channel has two Ca^{2+} -bound (open circles) and two voltage sensors activated (open squares), the A₂ mechanism specifies three states depending on the relative location of Ca^{2+} and activated voltage sensors. That the states are functionally distinct can be seen by comparing the different Ca^{2+} -binding equilibria for the unoccupied binding sites (K,K), (K,KE), and (KE,KE). Equilibrium constants for voltage sensor activation are also different. By contrast, the A₁ mechanism specifies a single state with equilibrium constants KE² for Ca^{2+} binding and JE² for voltage sensor activation (not depicted).

scheme, the mechanism underlying such a model and the parameters required to describe it may be relatively simple as illustrated by Fig. 1 C, Scheme II. The homotetrameric nature of the *mSlo1* channel implies that high affinity binding sites are identical. Thus, in Scheme II, Ca^{2+} binds to these subunits with identical equilibrium constants K. The independence of the binding sites is an initial simplifying assumption. As in Scheme I, the gating of unliganded channels is specified by an allosteric interaction between voltage sensor activation (R-A) and channel opening (C-O). Similarly, Ca^{2+} is coupled to channel gating through allosteric interactions represented by the factors C and E that connect the Ca^{2+} -binding transitions to the C-O and R-A voltage sensor transitions respectively. The steady-state properties of this model are fully described by three allosteric factors (C, D, E) and three equilibrium constants (J, K, L):

$$P_0 = \quad (1)$$

$$\frac{L(1 + KC + JD + JKCDE)^4}{L(1 + KC + JD + JKCDE)^4 + (1 + J + K + JKE)^4},$$

where



$$L = L_0 \exp\left(-\frac{z_L V}{kT}\right); J = J_0 \exp\left(-\frac{z_J V}{kT}\right); K = \frac{[\text{Ca}^{2+}]}{K_D}.$$

z_L and z_J are the partial charges associated with channel opening and voltage sensor activation respectively, and K_D is the elementary Ca^{2+} dissociation constant when the channel is closed and voltage sensors are not activated.

Scheme II highlights an important strategy used in our analysis: to define the simplest mechanism—rather than the gating scheme with the fewest kinetic states—that can account for the data. The simplest or most physically plausible mechanism often does not produce the fewest states. The number of states specified by Scheme II is determined by the nature of interactions between C-O, R-A, and X-X Ca^{2+} transitions. Interactions of channel opening with voltage sensors and Ca^{2+} binding sites are the most easily defined. If the C-O transition is concerted, channel opening should affect individual subunits equally. Therefore, by energy conservation, each bound Ca^{2+} or activated voltage sensor must have an additive effect on the energy of the C-O transition, increasing the C-O equilibrium constant C- or D-fold, respectively. By contrast, interactions between the X-X Ca^{2+} and R-A transitions in Scheme II do not involve a con-

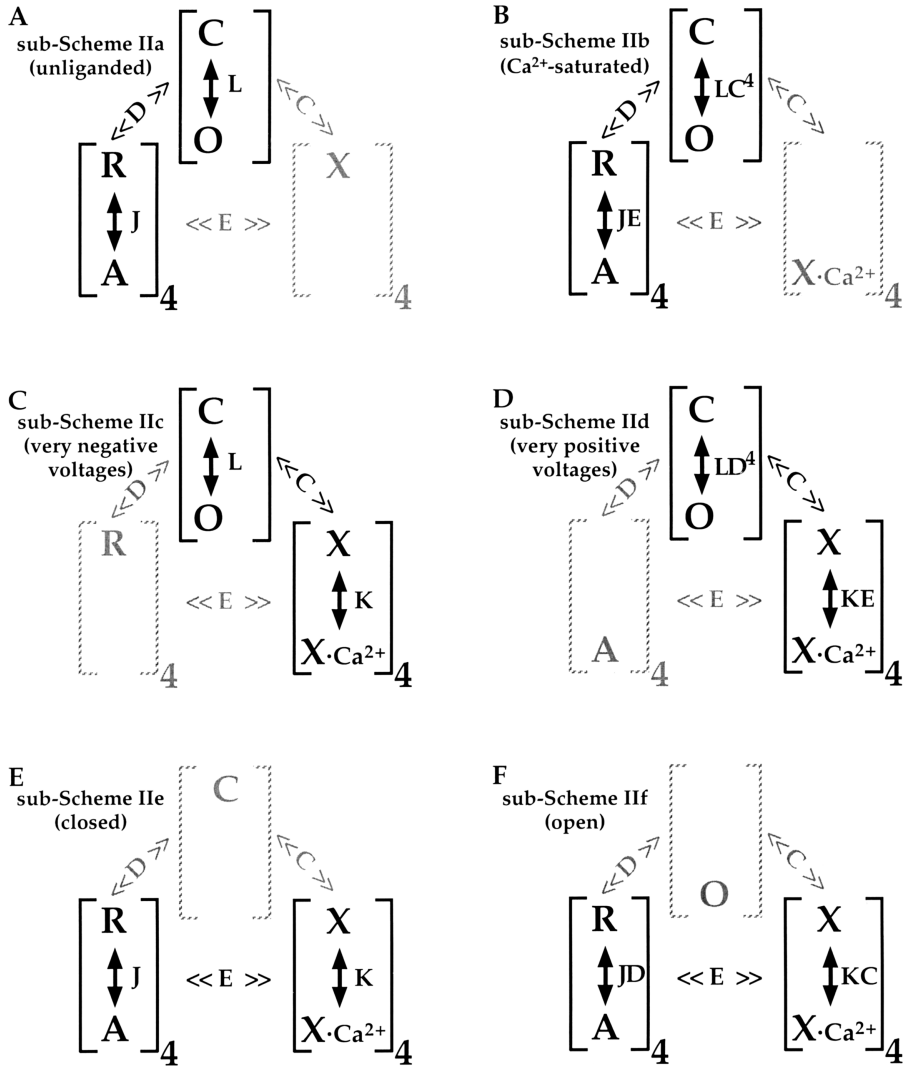


FIGURE 3. Sub-Schemes derived from Scheme II. Under extreme conditions that limit Ca^{2+} -binding, voltage sensor activation, or channel opening, the number of interactions that govern *mSlo1* gating is reduced and Scheme II is reduced to the following subschemes. (A) unliganded, (B) Ca^{2+} -saturated, (C) very negative voltages (voltage sensors resting), (D) very positive voltages (voltage sensors activated), (E) closed, and (F) open.

certed transition and several mechanisms can be postulated, each resulting in a different number of functionally distinct states.

In cases where no interaction between Ca^{2+} binding sites and voltage sensors exist, Scheme II will define a gating scheme with the minimum 50 states and P_O can be described by Eq. 1 with $E = 1$ (Cox and Aldrich, 2000; Shi and Cui, 2001; Zhang et al., 2001). A 50-state scheme is also generated if Ca^{2+} binding to one subunit affects voltage sensors in all subunits equally and the activation of a voltage sensor affects all Ca^{2+} -binding sites equally (Fig. 2 A₁). However, this would require a complex mechanism for coordinated communication among subunits independent of their relative positions in the tetramer. The equation describing such a mechanism is more complex than Eq. 1 (Cui and Aldrich, 2000). We will instead make the simplifying assumption that Ca^{2+} binding sites and voltage sensors can only interact within the same subunit (Fig. 2 A₂). This assumption, although mechanistically and mathematically simpler, increases

the number of states to 70 because interactions between voltage sensors and Ca^{2+} binding sites now depend on their relative location within the tetramer, and some combinations of i-activated voltage sensors and j-occupied binding sites are no longer energetically equivalent. For example, a channel with two activated voltage sensors and two Ca^{2+} bound can exist in three distinct states depending on whether Ca^{2+} and activated voltage sensors are in the same or different subunits (Fig. 2 B). More general gating schemes that distinguish the relative Ca^{2+} occupancy and/or voltage sensor conformation in adjacent and diagonally opposed subunits result in even more than 70 states (Cox et al., 1997a) but, like the 50-state model, require additional mechanisms to account for interactions between or among voltage sensors and Ca^{2+} binding sites in different subunits.

The general allosteric model (Scheme II) illustrates some questions and strategies that motivated this study. Does the allosteric effect of Ca^{2+} on BK channel activation occur via effects on voltage sensor activation, chan-

nel opening or both? In terms of Scheme II, the answer to this fundamental question reduces to the evaluation and comparison of the interaction factors C and E. To accomplish this and to characterize Ca^{2+} -binding, voltage sensor activation, and channel opening transitions, we studied *mSlo1* gating under a range of conditions that allow us to isolate subsets of the interactions in Scheme II. Fig. 3 shows the sub-schemes that describe *mSlo1* for various conditions that are approximated in our results. The unliganded (sub-Scheme IIa) or Ca^{2+} -saturated (sub-Scheme IIb) conditions were approximated in sub-nanomolar or 70–100 μM Ca^{2+} respectively. Voltage sensors were forced into resting (sub-Scheme IIc) or activated (sub-Scheme IId) states at extreme negative or positive voltages. Finally, by taking advantage of the relatively slow C-O transition kinetics, we studied gating while channels remain briefly in a closed (sub-Scheme IIe) or open (sub-Scheme IIIf) conformation.

MATERIALS AND METHODS

Channel Expression

Experiments were performed with the mbr5 clone of the mouse homologue of the *Slo1* gene (*mSlo1*) (Butler et al., 1993) expressed in *Xenopus* oocytes or HEK 293 cells. The clone was modified to facilitate mutagenesis and was propagated and cRNA transcribed as described previously (Cox et al., 1997b). *Xenopus* oocytes were injected 3–7 d before recording with ~0.5–5 ng or ~50 ng of cRNA for ionic current or gating current experiments respectively (50 nl, 0.01–1 ng/nl). *mSlo1* was also subcloned into a mammalian expression vector (SRα, provided by Dr. A.P. Braun, University of Calgary, Calgary, Canada) containing the SV-40 promoter. HEK 293 cells expressing the large T-antigen of the SV-40 virus were cotransfected with *mSlo1* and green fluorescent protein (GFP, as a marker) using LipofectAMINE (GIBCO BRL/Life Technologies, Inc.) 3 d before recording.

Electrophysiology

Currents were recorded using the patch clamp technique in the inside out configuration (Hamill et al., 1981). Upon excision, patches were transferred to a separate chamber and washed with at least 20× volumes of internal solution. K^+ currents were recorded with internal solutions containing (in mM) 110 KMeSO₃, 20 HEPES, and an external (pipette) solution containing 104 KMeSO₃, 6 KCl, 2 MgCl₂, 20 HEPES. Gating currents were recorded with internal solutions containing 135 N-methyl-d-glucamine (NMDG)-MeSO₃, 20 HEPES, and an external solution containing 125 tetraethylammonium (TEA)-MeSO₃, 6 TEA-Cl, 2 MgCl₂, 20 HEPES. Internal solutions contained 40 μM (+)-18-crown-6-tetracarboxylic acid (18C6TA) to chelate con-

taminant Ba^{2+} (Diaz et al., 1996; Neyton, 1996; Cox et al., 1997b). “0 Ca^{2+} ” solutions contained 2 mM EGTA reducing free Ca^{2+} to an estimated 0.8 nM based on the presence of ~10 μM contaminant Ca^{2+} (Cox et al., 1997b). Ca^{2+} solutions were buffered with 2 or 5 mM HEDTA and CaCl₂, and free Ca^{2+} was measured with a Ca^{2+} -electrode (Orion Research, Inc.). Total Cl[−] was adjusted to 10 mM with HCl. The pH of all solutions was adjusted to 7.2. Solutions were prepared and experiments performed at 20°C (approximately ±1°C).

Electrodes were pulled from thick walled 1010 glass (World Precision Instruments), coated with wax (KERR sticky wax) to minimize electrode capacitance (~1 pF), and fire-polished before use. Pipette access resistance measured in the bath solution (0.5–1.5 MΩ) was used as an estimate of series resistance (R_s) to correct the pipette voltage (V_p) at which I_K was recorded. The corrected pipette voltage, V_m , was used in determining membrane conductance (G_K) from tail current measurements and in plotting the voltage dependence of G_K or the time constant of I_K relaxation ($\tau[I_K]$). Series resistance error was <15 mV for all data presented and <10 mV for $\tau[I_K]$ measurements.

Data were acquired with an Axopatch 200B amplifier (Axon Instruments, Inc.) set in patch mode with the Axopatch's internal 4-pole Bessel filter set at 100 kHz. Currents were subsequently filtered by an 8-pole Bessel filter (Frequency Devices, Inc.) at 20 kHz (I_g) or 50 kHz (I_K) and sampled at 100 kHz with a 16 bit A/D converter (Instrutech ITC-16). Macroscopic currents were recorded at a relatively low gain (1–2 mV/pA) to avoid saturation of capacitive transients in response to voltage steps that often exceeded 300 mV. In addition, for gating currents, the voltage command was filtered at 20 kHz to limit the speed of fast capacitive transients so that they could be sampled accurately and subtracted. Gating current records were typically signal averaged in response to at least eight voltage pulses. A P/4 protocol was used for leak subtraction (Armstrong and Bezanilla, 1974) except at voltages less than the holding potential where a P/8 protocol was used to avoid channel activation during the leak pulses. The holding potential was adjusted from −80 mV in 0 Ca^{2+} to −120 mV in 1,000 μM Ca^{2+} .

A Macintosh-based computer system was used in combination with Pulse Control acquisition software (Herrington and Bookman, 1995) and Igor Pro for graphing and data analysis (WaveMetrics, Inc.). A Levenberg-Marquardt algorithm was used to perform non-linear least-squared fits. Error estimates for fit parameters are given as ± SD.

Single Channel Analysis

Under conditions where the open probability (P_O) is small (<10^{−3}), single channel opening events were ob-

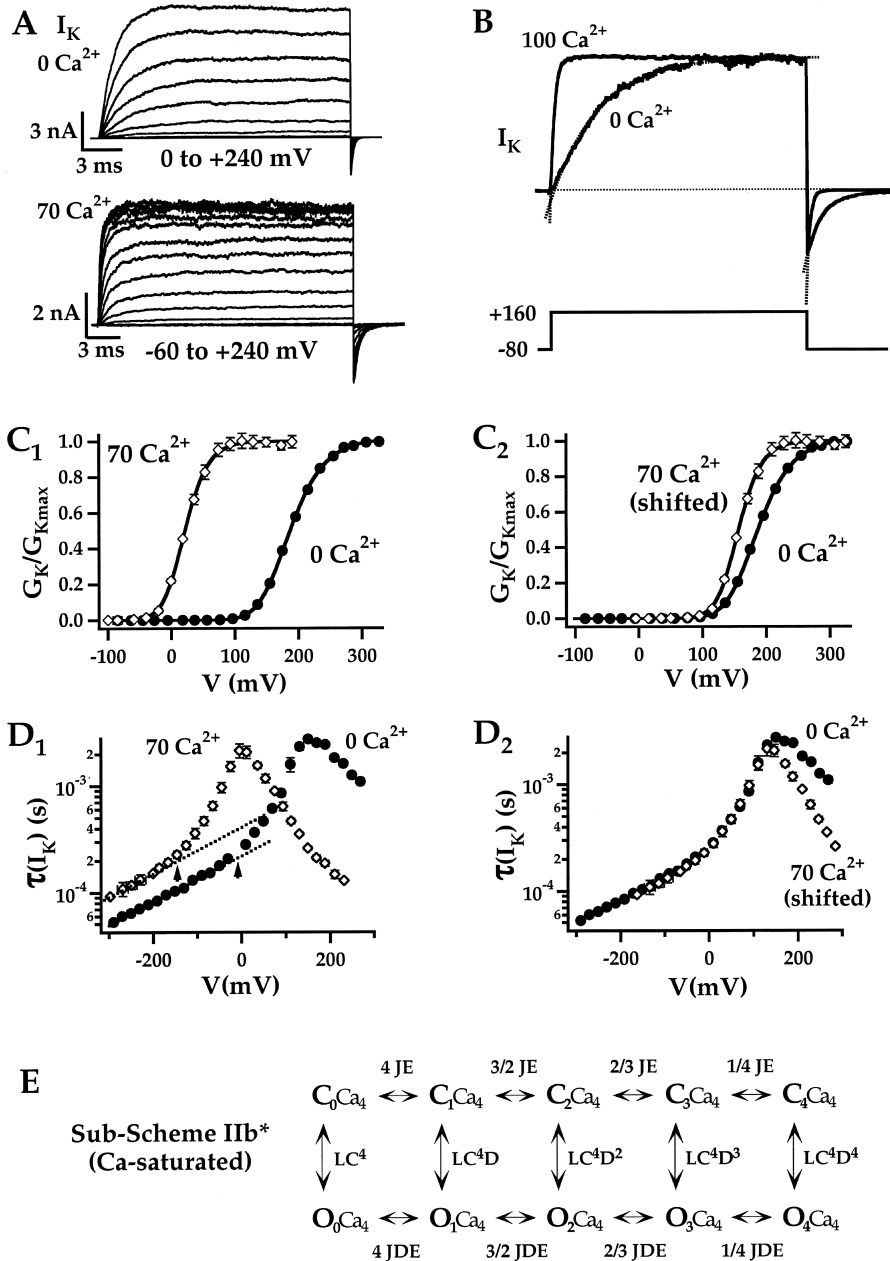


FIGURE 4. Effects of Ca^{2+} on I_K . (A) Families of I_K evoked by 20-ms depolarizations to different voltages (20 mV steps over the indicated range) are compared in 0 and 70 μM Ca^{2+} (different patches). (B) I_K evoked by 10-ms pulses to 160 mV in 0 and 100 μM Ca^{2+} (same patch) are normalized to steady-state current during the pulse and superimposed together with exponential fits (dashed lines) to both activation and deactivation time courses. (C₁) Normalized G_K -V relationships (mean \pm SEM) in 0 Ca^{2+} ($n = 51$) and 70 μM Ca^{2+} ($n = 3$) obtained from isochronal tail currents following 20-ms pulses. G -Vs were normalized by fitting with Boltzmann functions raised to a power n (solid lines) (0 Ca: $z = 0.73$ e , $V_h = 144$ mV, $n = 2.93$; 70 μM Ca^{2+} : $z = 1.22$ e , $V_h = 12.9$ mV, $n = 1.39$). (D₁) Mean time constants of I_K relaxation ($\tau[I_K]$) are plotted on a log scale versus voltage for the same experiments as in C₁. Dashed lines indicate similar exponential voltage dependencies of $\tau[I_K]$ at negative voltages in the presence or absence of Ca^{2+} . The shapes of the G -V and $\tau[I_K]$ -V relationships from C₁ and D₁ are compared in C₂ and D₂, respectively, by shifting the 0 Ca^{2+} plot along the voltage-axis by 135 mV, which is sufficient to align the $\tau[I_K]$ -V relationships at voltages less than the peak voltage. (E) The 10-state gating scheme (sub-Scheme IIb*) specified by Scheme II in saturating Ca^{2+} .

served in patches containing hundreds of channels and NP_O was determined from steady-state recordings of 5–45 s duration. Currents were filtered at 20 kHz, yielding a dead-time of $\sim 10 \mu\text{s}$, and were sampled at 100 kHz. NP_O was then determined from all-points amplitude histograms by measuring the fraction of time spent (P_k) at each open level (k) using a half-amplitude criteria and summing their contributions $\text{NP}_O = \sum k P_k$. NP_O was also determined by fitting P_k with a Poisson distribution $P_k = e^{-\text{NP}_O} (\text{NP}_O)^k / k!$. The values of NP_O obtained by these two methods differ by $< 5\%$, consistent with the assumption that the observed currents represent the activity of a large uni-

form population of channels opening with very low probability (Horrigan et al., 1999).

Normalized open probability ($P_O / P_{OMAX} = \text{NP}_O / \text{NP}_{OMAX}$) was determined by combining NP_O measurements with an estimate of NP_{OMAX} obtained from the macroscopic G_K -V relationship in the same patch ($\text{NP}_{OMAX} = G_{KMAX}/g_K$, where g_K is the single channel conductance). Patches that were used to measure single channel activity at negative voltages often produced currents that were too large to measure ($> 20 \text{nA}$) at voltages that activate *mSl01* channels maximally. In these cases, G_{max} was estimated by fitting the macroscopic G_K -V with a Boltzmann function

$\{1 + \exp[-z(V - V_h)/kT]\}$ raised to a power n (e.g., Fig. 4 C₁), where z and n were determined at each $[Ca^{2+}]$ from other patches where the entire G_K - V relationship was measured.

For voltages >60 mV from the reversal potential (0 mV), single channel amplitudes were large enough that false opening events due to noise were not detected using 20 kHz filtering. The prevalence of false events was assessed by evaluating the number of current transients from the closed level that exceed the 1/2 amplitude criterion in a direction opposite to that of channel opening. When determining P_O - V relationships over a large voltage range, currents were digitally filtered at 5 kHz before determining NP_O such that false events were not observed at 20 or -20 mV. For $V > 60$ mV no difference in NP_O was observed with 5 or 20 kHz filtering. However, for $V < -60$ mV a decrease in NP_O was observed at 5 kHz, reflecting the brevity of open times at these voltages. The largest decreases ($\sim 30\%$) were observed at the most negative voltages in 0 Ca^{2+} and little change was observed for $[Ca^{2+}] > 1$ μM . Thus, P_O in low Ca^{2+} may be underestimated. To minimize this effect, dose-response relationships used to quantify the effect of Ca^{2+} on channel activation (Fig. 9) were determined from NP_O at $V < -80$ mV using 20 kHz filtering.

Shifts in Voltage-dependent Parameters

Patch to patch variations in the half-activation voltage (V_h) of G_K - V and Q - V relationships are observed for *mSlo1* (Horrigan and Aldrich, 1999; Horrigan et al., 1999) and *hSlo1* (Stefani et al., 1997), possibly due to differences in the redox state of channels (DiChiara and Reinhart, 1997; Tang et al., 2001). Such shifts do not appreciably alter the shape of voltage-dependent relationships but make comparison of data between different experiments difficult and cause broadening in averaged voltage-dependent relationships. To compensate for this effect, V_h was determined for each patch and compared with the mean for all experiments ($\langle V_h \rangle$) at the same $[Ca^{2+}]$. Data from individual experiments were then shifted along the voltage-axis by $\Delta V_h = (\langle V_h \rangle - V_h)$ before averaging. This procedure yields average relationships that accurately represent the shape of individual G_K - V and Q - V relationships.

Admittance Analysis

Admittance analysis was performed as described previously (Horrigan and Aldrich, 1999). Briefly, in gating current solutions, the membrane was clamped with a sinusoidal voltage command (868 Hz, 60 mV peak to peak) superimposed on a 1 s voltage-ramp. The voltage command and current signal were both filtered at 20 kHz and current was sampled at 18- μs intervals (64

samples/period). Admittance was determined for each cycle of the sinusoid. Gating capacitance ($C_g[V]$) was determined as the voltage-dependent component of patch admittance appearing at a phase angle of 90° relative to the command voltage (after correction for instrumentation phase delays).

RESULTS

Effects of Ca^{2+} on *mSlo1* Ionic Currents

The basic effects of micromolar Ca^{2+} on BK channel gating are shown in Fig. 4, which compares macroscopic I_K recorded from *mSlo1* channels in the presence of internal solutions containing 0 Ca^{2+} or 70–100 μM Ca^{2+} , which correspond approximately to unliganded (sub-Scheme IIa) or Ca^{2+} -saturated (sub-Scheme IIb) conditions, respectively. 70 μM Ca^{2+} may be insufficient to completely saturate high affinity Ca^{2+} binding sites, which we estimate later to have K_D s on the order of 1 and 10 μM for open and closed channels, respectively (Cox et al., 1997a). However, concentrations of Ca^{2+} or other divalent cations in the 100 μM to 100 mM range produce distinct effects on channel gating that have been attributed to nonselective, low-affinity (millimolar) binding sites (Shi and Cui, 2001; Zhang et al., 2001). As a compromise, 70–100 μM Ca^{2+} was used throughout this study to approximate the Ca^{2+} -saturated condition for high affinity binding sites while minimizing possible contributions from low affinity sites.

Fig. 4 A compares I_K evoked at different voltages in 0 or 70 μM Ca^{2+} . Ca^{2+} increases the steady-state open probability (P_O) such that conductance-voltage (G_K - V) relationships shift to more negative voltages (Fig. 4 C₁). The records in Fig. 4 A indicate that Ca^{2+} speeds I_K activation during the pulse and slows deactivation at -80 mV after the pulse. This effect is illustrated in Fig. 4 B, where currents evoked by pulses to 160 mV in 0 and 100 μM Ca^{2+} from the same patch have been superimposed and normalized. Activation and deactivation kinetics are well fit by exponential functions following a brief delay (dashed lines) (Horrigan et al., 1999). The time constants ($\tau[I_K]$) of such fits over a wide range of voltages in 0 and 70 μM Ca^{2+} are plotted in Fig. 4 D₁.

Figs. 4, C₁ and D₁, show that Ca^{2+} shifts the G_K - V and $\tau(I_K)$ - V relationships along the voltage axis with little change in shape, suggesting that unliganded and ligand-bound channels gate by similar mechanisms. Indeed, Scheme II reduces, in saturating Ca^{2+} (Fig. 3, sub-Scheme IIb), to a 10-state gating scheme (Fig. 4 E, sub-Scheme IIb*) analogous to the unliganded scheme (Fig. 1, Scheme I*) (Horrigan and Aldrich, 1999; Horrigan et al., 1999). Despite this general similarity, significant changes in the shape of G_K - V and $\tau(I_K)$ - V relationships are observed when the plots obtained in 70 μM Ca^{2+} are shifted by 135 mV to align them with the 0 Ca^{2+}

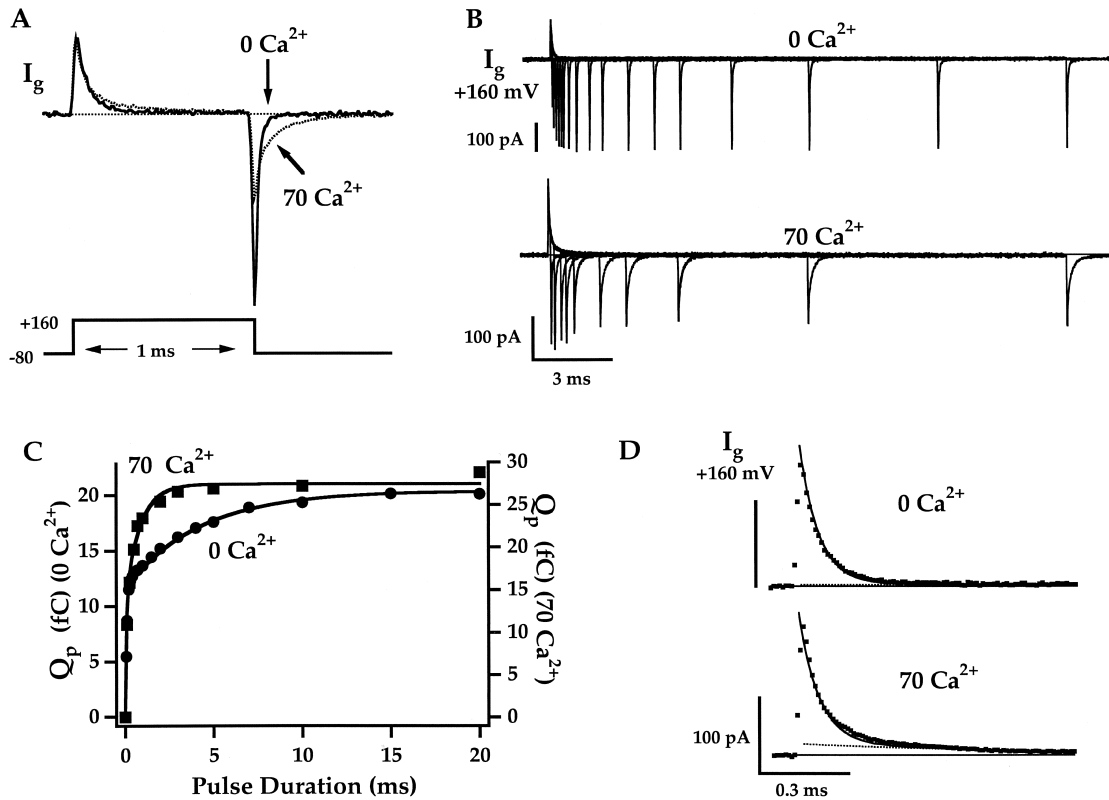


FIGURE 5. Effects of Ca^{2+} on gating currents (A) Gating currents evoked by 1-ms pulses to 160 mV in 0 and 70 μM Ca^{2+} . I_g was recorded in the absence of K^+ and the presence of 125 mM external TEA to eliminate ionic currents. (B) Families of I_g evoked by depolarizations to 160 mV of different duration (0.1–20 ms) in 0 and 70 μM Ca^{2+} from two different patches. Total OFF charge for each pulse (Q_p) was determined by integrating $I_{g\text{OFF}}$ for 5 ms and is plotted against pulse duration in (C). Results were fit with double exponential functions (0 μM Ca^{2+} : $\tau_1 = 63 \mu\text{s}$, $A_1 = 11.7 \text{ fC}$, $\tau_2 = 4.2 \text{ ms}$, $A_2 = 8.7 \text{ fC}$; 70 μM Ca^{2+} : $\tau_1 = 68 \mu\text{s}$, $A_1 = 14.6 \text{ fC}$, $\tau_2 = 0.85 \text{ ms}$, $A_2 = 12.8 \text{ fC}$). (D) The derivative of the fits to Q_p (solid lines) are superimposed with $I_{g\text{ON}}$ at 160 mV. Dashed lines represent the slow component of the fits.

data (Fig. 4, C₂ and D₂). Such differences are expected if *mSlo1* gating is governed by multiple voltage-dependent processes (e.g., C-O and R-A transitions).

In general, Ca^{2+} will shift the G_K -V and $\tau(I_K)$ -V relationships without changing their shape only if the rate constants in the unliganded scheme (Fig. 1, Scheme I*) at any voltage V are identical to those for the Ca^{2+} -saturated scheme (Fig. 4 E, sub-Scheme IIb*) at $V-\Delta V$. Since the horizontal (R-A) transitions are more voltage dependent than the vertical (C-O) transitions, this condition can only be satisfied if voltage sensor activation is more Ca^{2+} dependent than channel opening. In fact we will show that the opposite is true. Therefore, the relationship between the horizontal and vertical transitions in Schemes I* and IIb* is altered by Ca^{2+} in a manner that cannot be compensated for by voltage, producing a change in the shape of the G_K -V and $\tau(I_K)$ -V relations.

Effects of Ca^{2+} on Gating Current

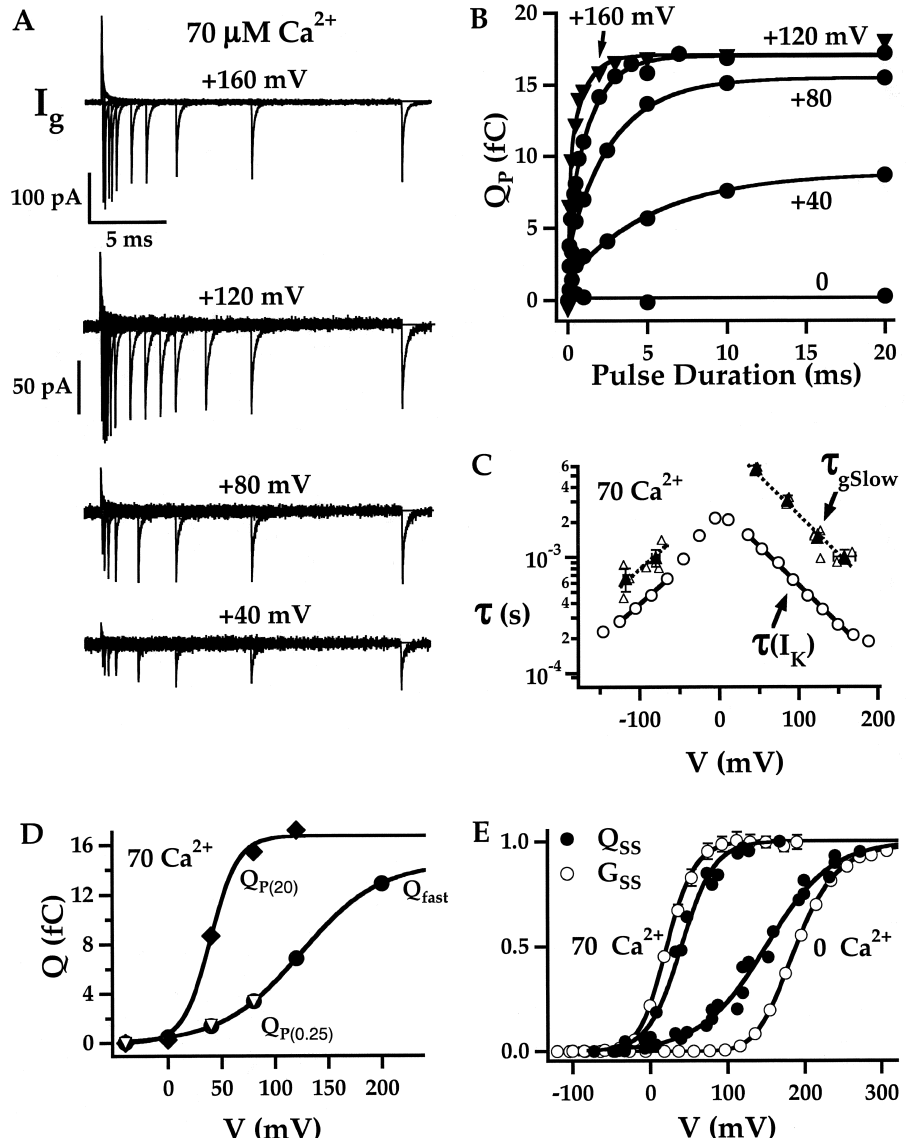
The data in Fig. 4 are insufficient to determine if Ca^{2+} effects channel opening (C-O) or voltage sensor acti-

vation (R-A) because I_K kinetics and steady-state activation are generally dependent on both processes (Horrigan et al., 1999). To help address this question *mSlo1* gating currents (I_g) were compared in 0 Ca^{2+} and 70 μM Ca^{2+} . As the following analysis indicates (Figs. 5–7), the Ca^{2+} sensitivity of I_g can be attributed mainly to an effect on channel opening and the interaction between Ca^{2+} binding and voltage sensor activation is weak.

I_g evoked by 1-ms pulses to 160 mV in 0 or 70 μM Ca^{2+} are superimposed in Fig. 5 A. ON gating currents ($I_{g\text{ON}}$) decay with a similar but not identical time course in the presence or absence of Ca^{2+} . However, the 0 Ca^{2+} record can be approximated by a single exponential function (Horrigan and Aldrich, 1999), whereas the 70 μM Ca^{2+} trace has an obvious slow component (see also Fig. 5 D). In addition, OFF gating currents ($I_{g\text{OFF}}$) recorded at -80 mV after the pulse are slowed substantially in the presence of Ca^{2+} .

Since Ca^{2+} affects gating current and shifts the voltage dependence of G_K and $\tau(I_K)$, it might appear reasonable to conclude that Ca^{2+} acts by promoting volt-

FIGURE 6. Properties of gating charge movement in 70 μM Ca^{2+} . (A) Families of I_g evoked by depolarizations of different duration to the indicated voltages in 70 μM Ca^{2+} ($\text{HP} = -80 \text{ mV}$). (B) Plots of Q_p versus pulse duration determined from A and fit with double exponential functions. The 160-mV trace (\blacktriangledown) was obtained from a different patch than the others (\bullet) and was normalized to the 120 mV trace because the steady-state Q_V relationship is saturated for $V \geq 120 \text{ mV}$ in 70 μM Ca^{2+} (see E). (C) $\tau_{g\text{SLOW}}$ - V relationships in 70 μM Ca^{2+} were determined at positive voltages from the slow component of Q_p and at negative voltages from the slow component of Q_{OFF} (e.g., Fig. 13 C). Individual data points (Δ) and mean \pm SEM (\blacktriangle) are plotted. The mean $\tau(I_K)$ - V relationship (\circ) was fit by exponential functions (solid lines) over voltage ranges corresponding to the $\tau_{g\text{SLOW}}$ data. These fits were then scaled (dashed lines) to match the $\tau_{g\text{SLOW}}$ - V relationships. (D) Q_p - V relationships determined following brief (0.25 ms) or prolonged (20 ms) pulses (from B) are compared with Q_{fast} - V determined by integrating the fast component of $I_{g\text{ON}}$ in the same patch (see Fig. 7 A). $Q_{p(20)}$ - V and Q_{fast} - V relationships are fit by Boltzmann functions (Q_{fast} : $z = 0.68$, $V_h = 123 \text{ mV}$, $Q_{p(20)}$: $z = 1.95$, $V_h = 40 \text{ mV}$). (E) Normalized steady-state Q_V s (solid symbols) and G_V s (open symbols) in 0 Ca^{2+} and 70 μM Ca^{2+} . Q_{ss} was determined from 10–20-ms pulses and data from three experiments in each $[\text{Ca}^{2+}]$ are plotted. Individual Q_V s were normalized based on fits to Boltzmann functions. Boltzmann fits to the cumulative data are shown (0 Ca^{2+} : $z = 0.59$, $V_h = 150 \text{ mV}$, 70 μM Ca^{2+} : $z = 1.19$, $V_h = 40 \text{ mV}$). G_V s (mean \pm SEM) were measured and fit as in Fig. 4 C.



age sensor activation (Diaz et al., 1998). However, a closer examination of gating charge movement reveals that this is not the case. Although gating currents provide a direct assay of voltage sensor activation, they are also influenced by channel opening. Indeed, we have shown previously that *mSlo1* I_g exhibits multiple kinetic components reflecting C-C, O-O, and C-O transitions in Scheme I* (Horrigan and Aldrich, 1999). These components must be isolated before conclusions can be drawn about the mechanism of Ca^{2+} action.

The Ca^{2+} Dependence of Slow Gating Charge Movement

$I_{g\text{ON}}$ evoked during a pulse to 160 mV in 0 Ca^{2+} (Fig. 5 A) consists of a prominent fast component, represent-

ing voltage sensor activation while channels are closed, and an additional component that is \sim 100-fold slower. The relaxation of the slow component, like I_K activation, is limited by the speed of channel opening (Horrigan and Aldrich, 1999) and therefore should exhibit a Ca^{2+} and voltage dependence similar to that of $\tau(I_K)$ (Fig. 4 B). To examine the slow component in detail, I_g was measured in response to pulses of different duration to 160 mV in 0 Ca^{2+} and 70 μM Ca^{2+} (Fig. 5 B). The total charge moved during each pulse (Q_p) was determined by integrating $I_{g\text{OFF}}$ and is plotted versus pulse duration in Fig. 5 C. These Q_p time courses, which indicate the kinetics of ON charge movement, are fit with double exponential functions (solid lines). Prominent slow components are observed in both 0 and 70 μM Ca^{2+} representing 43% and 47% of the

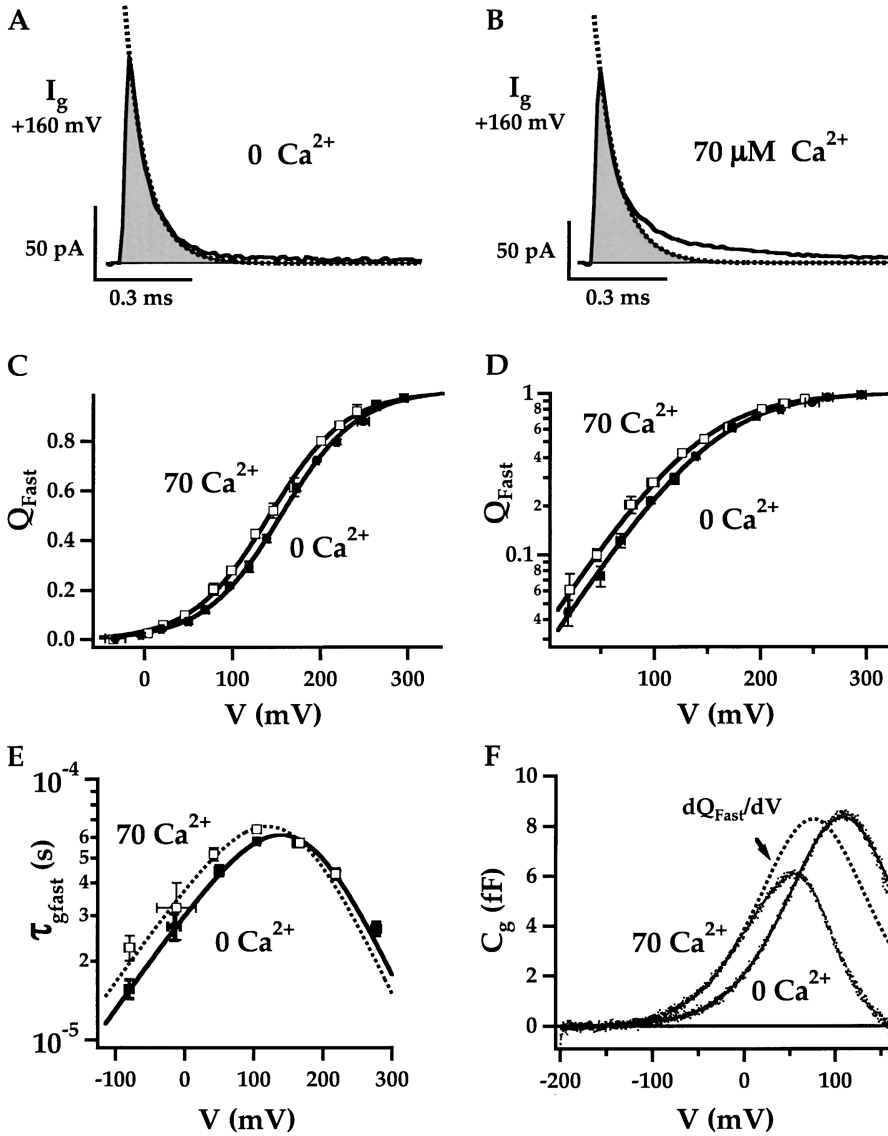


FIGURE 7. Ca²⁺ has little effect on fast gating charge movement. The fast components of I_{gON} evoked at 160 mV in 0 Ca²⁺ (A) and 70 μM Ca²⁺ (B) are determined by fitting the first 100 μs of the decay with exponential functions (dashed lines; 0 Ca: $\tau_{\text{gfast}} = 69.7 \mu\text{s}$, 70 μM Ca: $\tau_{\text{gfast}} = 73.6 \mu\text{s}$). Fast charge movement (Q_{fast}) was estimated by integrating under the exponential fits (shaded areas in A and B). Q_{fast} -V relationships (mean ± SEM) are plotted on linear (C) and semilog (D) scales for 0 Ca²⁺ (solid symbols, $n = 10$) and 70 μM Ca²⁺ (open symbol, $n = 7$). To determine mean Q_{fast} , normalized Q_{fast} -V relationships from individual experiments were shifted along the voltage-axis by $\Delta V_h = \langle V_h \rangle - V_h$ to align their half-activation voltages (V_h) to the mean (0 Ca²⁺: $\langle V_h \rangle = 155 \text{ mV}$; 70 μM Ca: $\langle V_h \rangle = 135 \text{ mV}$). Then the shifted data were averaged in 25 mV bins (see MATERIALS AND METHODS). The mean Q_{fast} -Vs are fit by Boltzmann functions (lines) where the valence $z = 0.58 e$ was constrained to the mean voltage sensor charge determined from fits to individual Q_{fast} -Vs in 0 Ca²⁺ and 70 μM Ca²⁺. (E) Mean τ_{gfast} -V relationships were determined in 60 mV bins after individual τ_{gfast} -V relationships were normalized to peak τ_{gfast} and shifted by ΔV_h (as determined from Q_{fast} -V relationships in C). The curves are fit with functions of the form $\tau_{\text{gfast}} = [\alpha_0 e^{-z\alpha/kT} + \beta_0 e^{-z\beta/kT}]^{-1}$ where $z_\alpha = 0.33 e$, $z_\beta = -0.22 e$ and 0 Ca: $\alpha_0 = 1,020 \text{ s}^{-1}$, $\beta_0 = 32,500 \text{ s}^{-1}$; 70 Ca: $\alpha_0 = 1,220 \text{ s}^{-1}$, $\beta_0 = 25,500 \text{ s}^{-1}$. (F) C_g-V relationships measured with admittance analysis in 0 and 70 μM Ca²⁺ for a single patch indicate a Ca²⁺-dependent shift in the voltage dependence of fast

charge movement. The membrane was clamped with a sinusoidal voltage command (868 Hz, 60 mV peak to peak) superimposed on a 1-s voltage-ramp from -200 to 160 mV. C_g was determined for each cycle of the sin wave. The C_g-V relationships were fit with the derivative of Boltzmann functions: $C_g = A * z((1 + e^{-z(V - V_h)/kT}) / (kTe^{z(V - V_h)/kT}))^2$ over voltage intervals where most channels are closed (0 Ca, -160 to 100 mV; 70 Ca, -160 to -10 mV). The 0 Ca²⁺ data were fit first (A = 1,390, z = 0.61 e, V_h = 108 mV) and the 70 Ca²⁺ data were fit with identical amplitude and charge (A, z) while V_h was reduced to 75 mV.

steady-state charge movement, respectively. Time-derivatives of the fits to Q_p superimpose with I_{gON} (Fig. 5 D) demonstrating that I_g kinetics reflect large slow components of ON charge movement.

Slow charge movement is evident as a distinct component of I_{gON} in 70 μM Ca²⁺ (dashed line – Fig. 5 D) but not in 0 Ca²⁺ because its time constant (τ_{gSLOW}) is decreased from 4.2 ms in 0 Ca²⁺ to 0.85 ms in 70 μM Ca²⁺ (Fig. 5 C). This fivefold change in kinetics produces a fivefold increase in slow gating current amplitude in 70 μM Ca²⁺. The marked Ca²⁺-sensitivity of τ_{gSLOW} is consistent with the ability of Ca²⁺ to speed I_K activation (Fig. 4 A).

The Voltage Dependence of Slow Gating Charge Movement in 70 μM Ca²⁺

The properties of slow charge movement in 70 μM Ca²⁺ are examined in more detail in Fig. 6. Families of I_g evoked after pulses of different duration to various voltages are shown in Fig. 6 A. Time courses of ON charge movement (Q_p) determined from these data are plotted in Fig. 6 B and fit with double exponential functions. The time constant of the slow component is plotted against voltage in Fig. 6 C together with τ_{gSLOW} at negative voltages, determined from the slow component of OFF charge movement (Horriigan and Aldrich,

1999) (see also Fig. 13 C). Also shown are the mean time constants of I_K relaxation ($\tau[I_K]$) in 70 μM Ca^{2+} . At both positive and negative voltages the voltage dependencies of τ_{gSLOW} and $\tau(I_K)$ are identical (Fig. 6 C, compare solid and dashed lines), supporting the idea that slow charge movement is limited by channel opening. However, τ_{gSLOW} is approximately fourfold slower than $\tau(I_K)$ at positive voltages and twofold slower at negative voltages. Differences between $\tau(I_K)$ and τ_{gSLOW} were also reported previously in 0 Ca^{2+} and may reflect the different ionic conditions used to measure I_K and I_g (Horrigan and Aldrich, 1999).

Ca^{2+} Alters the Relationship between Q-V and G-V

The Q_p -V curves in Fig. 6 D compare the voltage dependence of charge movement for pulses of different duration (from Fig. 6 B). The Q-V determined with brief 0.25 ms pulses ($Q_{p(0.25)}$) reflects fast charge movement. The voltage dependence of fast charge movement was also determined over a wider voltage range by integrating the fast component of I_{gON} (Q_{fast} , Fig. 6 D) (Horrigan and Aldrich, 1999). The steady-state Q_{ss} -V relationship determined with a 20 ms pulse ($Q_{p(20)}$, Fig. 6 D) is steeper and shifted to more negative voltages than Q_{fast} -V. This difference reflects the voltage dependence of slow charge movement and contrasts with results in 0 Ca^{2+} where Q_{ss} -V and Q_{fast} -V curves are similar in shape (Horrigan and Aldrich, 1999).

The steady-state Q-V and G-V relationships in 0 and 70 μM Ca^{2+} are compared in Fig. 6 E and indicate that Ca^{2+} -binding changes the relationship between charge movement and open probability. In 0 Ca^{2+} the Q-V is shallower and activates at more negative voltages than the G-V, exhibiting an approximate fourth-power relationship between the two, as in many voltage-dependent channels (Horrigan and Aldrich, 1999). In 70 μM Ca^{2+} , however, the Q-V and G-V almost superimpose. Calcium has changed the coupling between charge movement and channel opening so that less charge moves, on average, at voltages where most channels are closed. That is, Ca^{2+} allows channels to open when fewer voltage sensors have been activated.

The Effects of Ca^{2+} on Voltage Sensor Activation

To determine whether Ca^{2+} affects voltage sensor activation directly, we compared the fast components of gating charge movement in the presence and absence of Ca^{2+} (Fig. 7). This analysis shows that the interaction between Ca^{2+} binding and voltage sensor activation is weak.

Because voltage sensor movement in BK channels is rapid compared with channel opening and closing, the fast component of ON or OFF gating current (I_{gfast}) assays voltage sensor movement while channels remain in either a closed or open conformation (Horrigan and Aldrich, 1999) corresponding to sub-Schemes IIe and

IIIf, respectively (Fig. 3). For example, I_K activates with a delay of $\sim 100 \mu\text{s}$ after a voltage step (0 Ca^{2+} , 20°C) (Horrigan et al., 1999). During this period, I_g reflects voltage sensor activation while channels are closed. If voltage sensor activation is a two state process as in Scheme II, then the initial decay of I_g should be exponential, reflecting the R to A transition (Horrigan and Aldrich, 1999). Therefore, I_{gfast} at positive voltages was isolated by fitting the first 100 μs of I_{gON} with an exponential function (Fig. 7, A and B, dashed lines). Because channels are closed, the Ca^{2+} dependence of I_{gfast} must reflect a direct interaction between Ca^{2+} binding and voltage sensor movement that is independent of the ability of Ca^{2+} to alter channel opening.

Ca^{2+} Increases the Equilibrium Constant for Voltage Sensor Activation

The amount of fast charge movement (Q_{fast}) was estimated by integrating the area under the exponential fit to I_{gfast} , corresponding to the shaded regions in Fig. 7, A and B. Normalized Q_{fast} (mean \pm SEM) is plotted against voltage on linear and log scales in Fig. 7, C and D, respectively for 0 Ca^{2+} and 70 μM Ca^{2+} . The mean half-activation voltage ($\langle V_h(Q_{fast}) \rangle$) determined by fitting Boltzmann functions to individual Q-V records was shifted by -20 mV from $155 \pm 7 \text{ mV}$ in 0 Ca^{2+} ($n = 10$) to $135 \pm 8 \text{ mV}$ in 70 μM Ca^{2+} ($n = 8$), whereas the shape of the curves represented by the voltage sensor charge z_j was not appreciably altered (0 Ca^{2+} : $z_j = 0.59 \pm 0.03 \text{ e}$; 70 μM Ca^{2+} : $z_j = 0.57 \pm 0.03 \text{ e}$).

Because of the considerable patch-to-patch variation in $V_h(Q_{fast})$, individual Q_{fast} -V curves were aligned to the mean half-activation voltage in 0 or 70 μM Ca^{2+} before averaging (Horrigan and Aldrich, 1999) (see MATERIALS AND METHODS). The resulting plots (Fig. 7, C and D) are well fit by Boltzmann functions (solid lines) with identical valence (0.58 e) but different half-activation voltages, implying a small increase in the equilibrium constant for voltage sensor activation upon Ca^{2+} binding, as predicted by Scheme II when $E > 1$. The good fit by Boltzmann functions is also consistent with the assumption that voltage sensor activation can be described by a single R-A transition and that voltage sensors act independently when channels are closed.

Ca^{2+} Slows Voltage Sensor Deactivation

The kinetics of fast charge movement are altered slightly by Ca^{2+} , consistent with a small increase in the equilibrium constant for voltage sensor activation. The mean I_{gfast} time constants (τ_{gfast}) from Fig. 7, A and B, and similar experiments are plotted versus voltage in Fig. 7 E. At negative voltages, τ_{gfast} was determined by fitting the fast component of I_{gOFF} evoked after brief pulses (0.06–0.25 ms) that activate voltage sensors while most channels remain closed. The τ_{gfast} -V rela-

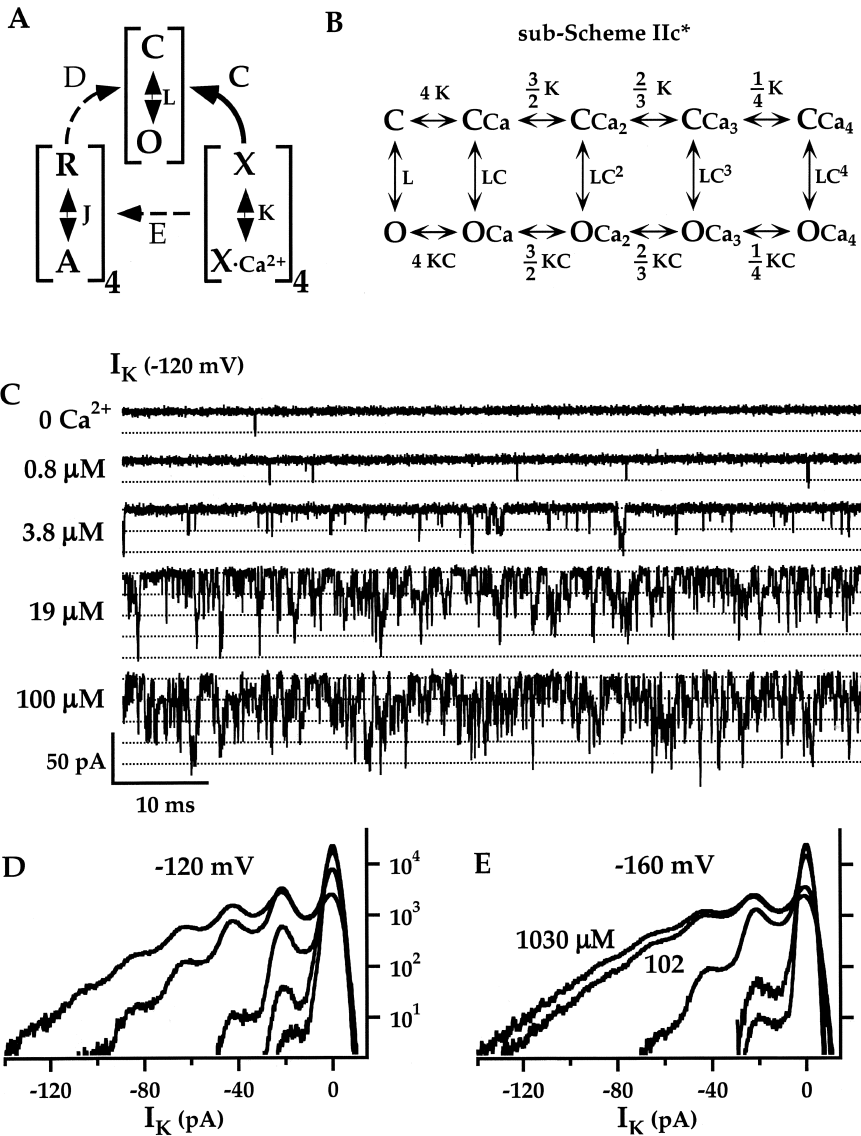


FIGURE 8. The Ca^{2+} dependence of P_o . (A) Scheme II predicts Ca^{2+} binding may affect the C-O transition directly (solid arrow) or indirectly (dashed arrow) by altering voltage sensor activation. (B) At low voltages Scheme II specifies an MWC-type gating scheme (Sub-Scheme IIc*) that is independent of voltage sensor activation. (C) Inward potassium currents recorded at -120 mV and filtered at 20 kHz from a macro patch in the indicated $[\text{Ca}^{2+}]$ demonstrate that P_o increases in a Ca^{2+} -dependent manner when voltage sensors are not activated. The corresponding all-point amplitude histograms are plotted in (D) on a semi-log scale and were constructed from 10-s recordings. (E) Similar histograms from another experiment at -160 mV over a wider $[\text{Ca}^{2+}]$ range ($0, 0.8, 8.2, 102, 1,030\text{ }\mu\text{M}$) reveal saturation of P_o near $100\text{ }\mu\text{M Ca}^{2+}$.

tionships were fit (Fig. 7 E, solid lines) with bell-shaped functions $\tau_{g\text{fast}} = (\alpha + \beta)^{-1}$ as predicted for a two-state model of voltage sensor activation where $\alpha = \alpha_0 \exp(-z_\alpha/kT)$ and $\beta = \beta_0 \exp(-z_\beta/kT)$ represent the forward and backward rate constants for voltage sensor activation when channels are closed. The partial charges associated with these rate constants (z_α, z_β) were determined from the best fit to the 0 Ca^{2+} data when $z_L = |z_\alpha| + |z_\beta|$ was constrained to $0.55\text{ }e$ (Horrigan and Aldrich, 1999). Attempts to constrain $z_L = 0.58\text{ }e$ as for the Q_{fast} - V fits produced $\tau_{g\text{fast}}$ - V fits that were too steep (unpublished data). Ca^{2+} shifts the peak of the $\tau_{g\text{fast}}$ - V fit by -20 mV , consistent with the shift in Q_{fast} - V . Ca^{2+} mainly reduces the backward rate for voltage sensor activation, and therefore increases $\tau_{g\text{fast}}$ at negative voltages, but has little effect on $\tau_{g\text{fast}}$ at positive voltages where the forward rate predominates (e.g., Fig. 7, A and B, at 160 mV).

Quantifying the Interaction between Ca^{2+} -binding and Voltage Sensor Activation

Fig. 7, A-E, show that Ca^{2+} has a small direct effect on voltage sensor movement. However, Q_{fast} - V relationships in 0 and $70\text{ }\mu\text{M Ca}^{2+}$ were rarely obtained from the same patch because I_g is small and extensive signal averaging was required. Thus, the change in mean $V_h(Q_{\text{fast}})$ ($\Delta V_h(Q_{\text{fast}}) = \langle V_h(Q_{\text{fast}})[0\text{ Ca}]\rangle - \langle V_h(Q_{\text{fast}})[70\text{ Ca}]\rangle = 20\text{ mV}$) may not represent accurately the Q_{fast} - V shift in individual experiments.

A more accurate estimate of the Q_{fast} - V shift (-33 mV) was obtained using admittance analysis. Admittance analysis provides an alternative method for selectively measuring fast gating charge movement (Fernandez et al., 1982). When the membrane is clamped with a sinusoidal voltage command, a non-linear gating capacitance (C_g) proportional to dQ_{fast}/dV

can be determined (Horrigan and Aldrich, 1999) (see MATERIALS AND METHODS). This technique provides a rapid assay of $Q_{\text{fast}}(V)$ such that the effects of 0 Ca^{2+} and 70 μM Ca^{2+} can be compared in the same patch. Fig. 7 F shows the C_g -V relationship is altered by Ca^{2+} . To estimate the Q_{fast} -V relationships for closed channels, the C_g -V traces were fit by the derivative of Boltzmann functions with respect to voltage over a voltage range where P_O is small (Horrigan and Aldrich, 1999). The 0 Ca^{2+} fit determined for $V < 100$ mV (solid line) was shifted along the voltage-axis by -32 mV to fit the 70 μM Ca^{2+} data from the same patch for $V < -10$ mV. Similar analysis in several different experiments indicate a mean Q_{fast} -V shift of -33 ± 4 mV (mean \pm SEM, $n = 6$).

The Energetic Relationship between Ca^{2+} -binding and Voltage Sensor Activation

A -33 mV shift in $Q_{\text{fast}}(V)$ upon Ca^{2+} binding can be accounted for by Scheme II if the allosteric factor E is assigned a value of 2.1 ($z_j = 0.58 e$). Thus, Ca^{2+} -binding increases the R-A equilibrium constant 2.1-fold, altering the energetics of voltage sensor activation by 0.45 kcal/mole. This represents a lower limit for the interaction energy because 70 μM Ca^{2+} may not be sufficient to completely saturate Ca^{2+} binding sites and the saturating shift in $Q_{\text{fast}}(V)$ may therefore be underestimated.

Effects of Ca^{2+} on Voltage Sensor Activation Cannot Account for the Shift in P_O -V

To determine whether the Ca^{2+} -dependent shift in the half-activation voltage of the P_O -V relationship ($\Delta V_h[P_O]$) can be accounted for by an effect of Ca^{2+} on voltage sensor activation, we examined the behavior of Scheme II when there is no direct interaction between Ca^{2+} binding and channel opening (i.e., $C = 1$). If we set $E = 2.1$ to account for the -33 mV shift in the Q_{fast} -V relationship produced by 70 μM Ca^{2+} then the model predicts $\Delta V_h(P_O) = -19$ mV, only 11% of the observed value ($\Delta V_h[P_O] = -166$ mV, Fig. 4 C). Even if E is infinite, Scheme II cannot reproduce a -166 mV shift when $C = 1$. If E is large then Ca^{2+} binding will effectively lock voltage sensors in the activated conformation (i.e., $JE \gg 1$) such that in saturating $[\text{Ca}^{2+}]$ the channel can only occupy a single closed and open state with a C-O equilibrium constant of LC^4D^4 , hence:

$$P_0 = \frac{LD^4C^4}{1 + LD^4C^4}$$

and

$$V_{hE\infty}(P_0) = \frac{kT}{z_L} \ln(L_0 C^4 D^4). \quad (2)$$

$V_{hE\infty}(P_0)$ represents, for any z_L , L_0, D , and C in saturating Ca^{2+} , the lower limit of $V_h(P_O)$ as E becomes large.

Given the parameters (z_L, L_0, D) used previously (0.4 e , $2 \times 10^{-6}, 17$) (Horrigan et al., 1999) or in the present study (0.3 e , $0.98 \times 10^{-6}, 25$), Eq. 2 predicts $V_{hE\infty}(P_O) = 81$ or 113 mV, respectively, when $C = 1$ as compared with the observed $V_h(P_O) = 20 \pm 8$ mV in 70 μM Ca^{2+} . Thus, interaction of Ca^{2+} binding with voltage sensor activation is insufficient to account for the observed $\Delta V_h(P_O)$, even if E is large. We conclude that Ca^{2+} binding must affect the C-O transition directly (i.e., $C > 1$).

Effects of Ca^{2+} on the C-O Transition

The weak Ca^{2+} -sensitivity of fast charge movement and data presented in Figs. 8 and 9 show that the primary mechanism of Ca^{2+} action involves direct interaction between Ca^{2+} -binding and the C-O transition.

The ability of Ca^{2+} to speed I_K activation, slow deactivation, increase open probability (Fig. 4), and produce analogous effects on the kinetics and amplitude of slow charge movement (Figs. 5 and 6) are consistent with Ca^{2+} causing a change in the rate-limiting C-O transition. However, Ca^{2+} may alter this transition through two different pathways: a direct interaction between Ca^{2+} binding and channel opening (Fig. 8 A, solid arrow) (C-factor), or an indirect interaction (Fig. 8 A, dashed arrows) involving a Ca^{2+} -dependent increase in voltage sensor activation (E-factor) that, in turn, promotes channel opening (D-factor). To isolate the direct interaction we measured open probability (P_O) at very negative voltages in the presence and absence of Ca^{2+} .

Ca^{2+} Increases P_O when Voltage Sensors Are Not Activated

At sufficiently negative voltages, voltage sensors should remain in the resting (R) state even when Ca^{2+} is bound. The Q_{fast} -V relationships in Fig. 7, C and D, show that the fraction of activated voltage sensors is small ($< 10^{-2}$) for $V < 0$ mV in 0 or 70 μM Ca^{2+} . With voltage sensors effectively locked in the R conformation, Scheme II reduces to sub-Scheme IIc (Fig. 3), which specifies a 10 state Monod-Wyman-Changeux (MWC)-type gating scheme (Fig. 8 B, sub-Scheme IIc*). Under this extreme condition, channels can open in a Ca^{2+} -dependent manner only through direct interaction between Ca^{2+} binding and the C-O transition. At negative voltages P_O is highly Ca^{2+} sensitive (Figs. 8 and 9), confirming that a strong interaction exists between Ca^{2+} binding and channel opening and providing a direct estimate of the allosteric factor C that embodies this interaction.

Fig. 8 C compares I_K recorded at -120 mV from a single patch in various $[\text{Ca}^{2+}]$. The corresponding amplitude histograms are superimposed in Fig. 8 D. Although the patch contains hundreds of *mSl01* channels, P_O is low in the absence of Ca^{2+} and activity is observed as the infrequent and brief opening of single channels.

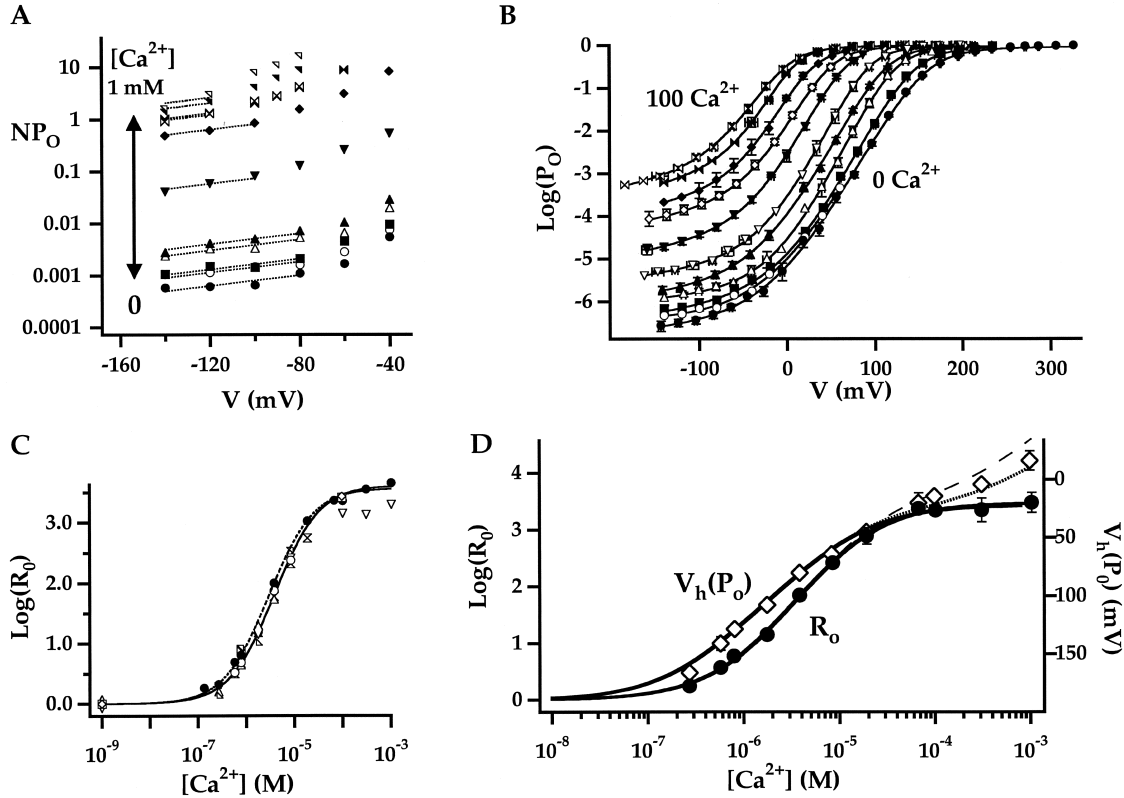


FIGURE 9. The Ca^{2+} dependence of P_0 . (A) NP_0 determined from the patch in Fig. 8 C is plotted on a semi-log scale vs. voltage for different $[\text{Ca}^{2+}]$ (in μM : 0 (●), 0.13 (○), 0.27 (■), 0.58 (△), 0.79 (▲), 3.8 (▼), 19 (◆), 68 (▣), 102 (▢), 313 (▨), 1030 (▢)). Dashed lines are exponential fits with $z = 0.3$ e. (B) P_0 -V relationships determined from normalized G-Vs at different $[\text{Ca}^{2+}]$ (in μM : 0 (●), 0.27 (■), 0.58 (△), 0.81 (▲), 1.8 (▽), 3.8 (▼), 8.2 (◇), 19 (◆), 68 (▣), 99 (▢)) are plotted on a semilog scale versus voltage (mean \pm SEM). Data for $P_0 < 10^{-2}$ were obtained from amplitude histograms as in A but were filtered at 5 kHz such that openings near the K^+ reversal potential could be distinguished from noise based on a half-amplitude criterion (see MATERIALS AND METHODS). The data were fit (solid lines) by Scheme I* (Fig 1 B) allowing all parameters (L_0 , z_L , J_0 , z_j , D) to vary freely at each $[\text{Ca}^{2+}]$. (C) A dose-response relationship for the effect of Ca^{2+} on P_0 at negative voltages is obtained by plotting the log-ratio of NP_0 in the presence and absence of Ca^{2+} ($\log[R_0]$) versus $[\text{Ca}^{2+}]$ for several experiments (symbols). $NP_0(V)$ was determined from exponential fits to the data with $z = 0.3$ e as in A. $\log(R_0)$ from A (●) spans the entire $[\text{Ca}^{2+}]$ range and is fit (dashed line) by Eq. 4 ($C = 7.8$, $K_D = 8.2 \mu\text{M}$). (D) The mean $\log(R_0)$ - $[\text{Ca}^{2+}]$ relationship is fit (solid line) by Eq. 4 ($C = 7.4$, $K_D = 9.3 \mu\text{M}$) and compared with the half activation voltage (V_h) of P_0 (open symbols). Solid lines in C and D represent predictions of Scheme II for $\log(R_0)$ and $V_h(P_0)$, respectively, using the Fit B parameters in Table II ($C = 8$, $K_D = 11 \mu\text{M}$; Table II, Fit B). The change in $V_h(P_0)$ from 100–1,000 μM Ca^{2+} can be reproduced (dotted line) if Scheme II is modified to include an additional low affinity binding site in each subunit that interacts with the C-O transition through an allosteric mechanism analogous to that embodied by the C-factor in Scheme II. The parameters for the low affinity site ($K_{D,\text{LOW}} = 2.33 \text{ mM}$, $C_{\text{LOW}} = 3.53$) were taken from Zhang et al. (2001). However, this model predicts a marked increase of R_0 in 100–1,000 μM Ca^{2+} (dashed line) that is inconsistent with the data.

Application of Ca^{2+} causes a large increase in open probability, resulting in multichannel openings. NP_0 increases 2,130-fold, from 6.1×10^{-4} in 0 Ca^{2+} to 1.3 in 100 μM Ca^{2+} . Histograms in Fig. 8 E demonstrate for a different patch at -160 mV that the increase in NP_0 saturates above 100 μM Ca^{2+} .

To characterize the interaction between Ca^{2+} -binding and channel opening in detail, and to confirm that the P_0 increase in Fig. 8 C can be described by sub-Scheme IIc, channel activity was measured over a range of negative voltages and $[\text{Ca}^{2+}]$. Fig. 9 A plots NP_0 versus voltage for the patch in Fig. 8 C at many $[\text{Ca}^{2+}]$. The NP_0 -V relations become weakly voltage dependent at negative potentials, consistent with the assumption that voltage sensors are not activated under these con-

ditions (Horrigan et al., 1999). This limiting behavior is also seen in Fig. 9 B, which plots $\log(P_0)$ over a wider voltage range at different $[\text{Ca}^{2+}]$ from many experiments (mean \pm SEM).

Fig. 9, A and B, show that P_0 increases $>1,000$ -fold in response to Ca^{2+} at negative potentials. Thus Ca^{2+} binding strongly affects channel opening through a pathway that does not involve voltage sensor activation. Sub-Scheme IIc predicts:

$$P_0 = \frac{L(1 + KC)^4}{L(1 + KC)^4 + (1 + K)^4}.$$

Because P_0 at extreme negative voltages is small ($<10^{-2}$), even in saturating $[\text{Ca}^{2+}]$, this expression can be approximated:

$$P_O = L \left(\frac{1 + KC}{1 + K} \right)^4. \quad (3)$$

Since the C-O equilibrium constant (L) is the only voltage-dependent parameter in sub-Scheme IIc, the voltage dependence of P_O should be identical to that of L and independent of $[Ca^{2+}]$. Consistent with this prediction, the NP_O -V relations in Fig. 9 A at all $[Ca^{2+}]$ can be fit reasonably by exponential functions (dashed lines) with identical voltage dependences (e -fold per 84 mV) reflecting the partial charge of L ($z_L = 0.3 e$).

Determining the Parameters Associated with Ca^{2+} -dependent Activation (K_D , C)

The parameters that define sub-Scheme IIc (L , K_D , C) are well determined by the properties of P_O at extreme negative voltages. L can be measured directly in 0 Ca^{2+} where Eq. 3 reduces to $P_O = L$. Then K_D and C can be determined from the Ca^{2+} dependence of P_O (Eq. 3). However, for some experiments (e.g., Fig. 9 A), P_O could not be determined because macroscopic currents were large and the number of channels in the patch (N) could not be estimated accurately. Errors in the estimation of N in other experiments may contribute to the variability in P_O at negative voltages in Fig. 9 B. Therefore, to evaluate K_D and C independent of N , we determined the ratio (R_O) of NP_O in the presence and absence of Ca^{2+} where (based on Eq. 3):

$$\begin{aligned} R_O([Ca^{2+}]) &= \frac{NP_O[V, [Ca^{2+}]]}{NP_O[V, 0]} \\ &= \left(\frac{1 + KC}{1 + K} \right)^4 = \left(\frac{1 + C[Ca^{2+}]/K_D}{1 + [Ca^{2+}]/K_D} \right)^4 \end{aligned} \quad (4)$$

R_O is independent of L as well as N and therefore depends only on Ca^{2+} binding (K_D) and its interaction with channel opening (C).

Fig. 9 C plots R_O on a log scale versus $[Ca^{2+}]$ for several experiments. R_O is highly reproducible and well fit by Eq. 4 (solid line). According to Eq. 4, R_O increases from a minimum of 1 in 0 Ca^{2+} to a maximum of C^4 in saturating Ca^{2+} ($[Ca^{2+}]_{sat}$). Thus, C can be determined from the saturating value of R_O ($C = [R_O([Ca^{2+}]_{sat})]^{-4}$). The dashed line in Fig. 9 C is the fit ($C = 7.8 \pm 0.1$, $K_D = 8.2 \pm 0.5 \mu M$) to the data from Fig. 9 A (solid symbols), representing the only single experiment to span the entire $[Ca^{2+}]$ range. A solid line represents the parameters used in the final model ($C = 8$, $K_D = 11 \mu M$). The best fit to mean $\log(R_O)$ yielded $C = 7.4 \pm 0.1$ and $K_D = 9.3 \pm 0.4 \mu M$ (Fig. 9 D, solid line).

The Energetic Relationship between Ca^{2+} Binding and Channel Opening

The ability of Ca^{2+} to increase P_O at extreme negative voltages shows that Ca^{2+} binding affects channel opening directly and provides an estimate of the interaction energy between these two processes. A C -fold increase in C-O equilibrium constant where $C = 8$ indicates that the free energy difference between closed and open increases 1.25 kcal mol⁻¹ for each Ca^{2+} bound ($\Delta\Delta G_{CO} = 0.6 \ln(C)$) or 5.0 kcal mol⁻¹ for the Ca^{2+} -saturated condition.

The Ca^{2+} Dependence of $V_h(P_O)$

Another measure of BK channel gating commonly used to characterize Ca^{2+} sensitivity is the half-activation voltage of the P_O -V relationship ($V_h(P_O)$) (Moczydlowski and Latorre, 1983). Fig. 9 D plots mean values of $V_h(P_O)$ and $\log(R_O)$ against $[Ca^{2+}]$. For certain gating schemes, a simple relationship between $V_h(P_O)$ and $\log(R_O)$ is expected. For instance, a voltage-dependent MWC scheme (sub-Scheme IIc) predicts $\Delta V_h(P_O[Ca^{2+}]) = -(kT/z_L) \ln(R_O)$ where $\Delta V_h(P_O[Ca^{2+}]) = V_h(P_O[Ca^{2+}]) - V_h(P_O[0])$. That is, changes in $V_h(P_O)$ and $\log(R_O)$ should be directly proportional. However, this prediction is not generally valid for Scheme II. And, although the two dose-response curves in Fig. 9 D are similar in shape, differences are evident. First, $V_h(P_O)$ is more Ca^{2+} -sensitive than $\log(R_O)$. That is, when the two curves are scaled as in Fig. 9 D to give identical Y-axis excursions between 0 and 100 $\mu M Ca^{2+}$, $V_h(P_O)$ -[Ca^{2+}] is left-shifted relative to $\log(R_O)$ -[Ca^{2+}]. Such a difference is predicted by Scheme II (Fig. 9 D, solid line) because $V_h(P_O)$, unlike R_O , is measured under conditions where voltage sensors are activated, thereby producing an E -fold increase in Ca^{2+} affinity. Another difference between the dose-response curves in Fig. 9 D is that $\log(R_O)$ saturates for $[Ca^{2+}] \geq 100 \mu M$, as predicted by Eq. 4, whereas $V_h(P_O)$ has a biphasic appearance, beginning to saturate around 100 $\mu M Ca^{2+}$ but continuing to change by more than 30 mV between 100 and 1,000 $\mu M Ca^{2+}$. The failure of $V_h(P_O)$ to saturate has been noted previously (Moczydlowski and Latorre, 1983; Cox et al., 1997a; Cui et al., 1997; Schreiber and Salkoff, 1997) and can be accounted for by the action of Ca^{2+} at distinct high affinity (micromolar) and low affinity (millimolar) binding sites (dotted line Fig. 9 D) (Shi and Cui, 2001; Zhang et al., 2001).

The apparent saturation of $\log(R_O)$ in 100–1,000 $\mu M Ca^{2+}$ is consistent with R_O reflecting the action of Ca^{2+} at high affinity binding sites. The differential effect of 100–1,000 $\mu M Ca^{2+}$ on $V_h(P_O)$ and $\log(R_O)$ has implications for the mechanism of Ca^{2+} action at low affinity binding sites that will be discussed below.

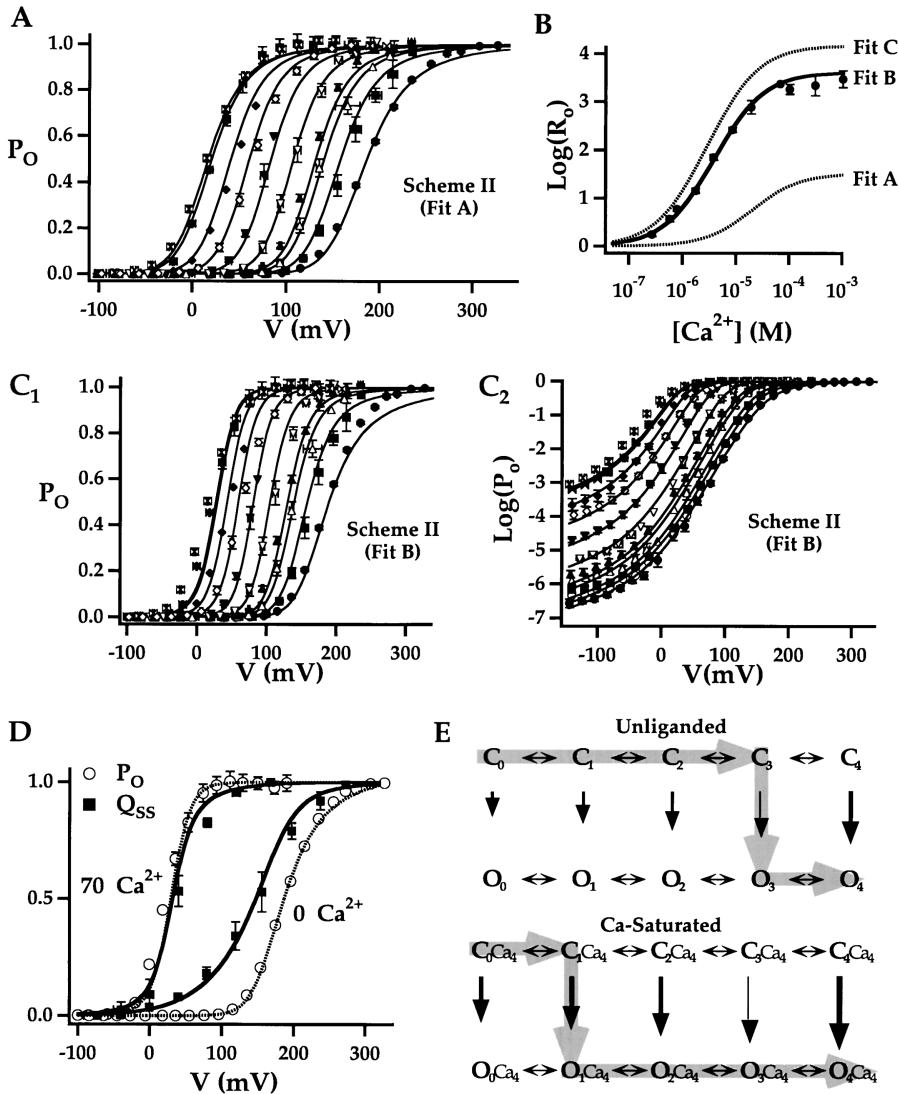


FIGURE 10. Fitting steady-state data with Scheme II. (A) Mean P_O -V relationships in different $[Ca^{2+}]$ (in μM : 0 (●), 0.27 (■), 0.58 (Δ), 0.81 (\blacktriangle), 1.8 (∇), 3.8 (\blacktriangledown), 8.2 (\diamond), 19 (\blacklozenge), 68 (\blacksquare), 99 (\blacksquare)) were fit by Scheme II by holding L_0 , z_L constant and allowing the other parameters to vary (Fit A, Table II). (B) Mean $\log(R_O)$ - $[Ca^{2+}]$ relationship (symbols) is compared with predictions of Scheme II based on different fits to the P_O data (Table II, Fits A, B, and C). (C) Mean P_O (C_1) and $\log(P_O)$ (C_2) are plotted versus voltage for different $[Ca^{2+}]$ (symbols) and are fit by Scheme II (Table II, Fit B). The linear and log transformed data were fit simultaneously using a weighting function to compensate for the greater amplitude range of $\log(P_O)$. (D) Scheme II reproduces (lines) the observed change in relationship between mean steady-state Q - V and P_O - V relationships (Table II, Fit B parameters). (E) Gating schemes for unliganded and Ca^{2+} -saturated channels illustrate the changes in equilibria induced by Ca^{2+} binding. By increasing the C-O equilibrium constants Ca^{2+} has the effect of changing the primary activation pathway, accounting in part for the altered relationship between Q - V and G - V .

Scheme II Reproduces the Ca^{2+} and Voltage Dependence of P_O

Thus far we have examined the gating of *mSl01* channels under extreme conditions to isolate interactions involved in Ca^{2+} -dependent activation and to test a general allosteric gating mechanism (Scheme II). Our results show that the interaction between Ca^{2+} binding and channel opening is strong and independent of voltage sensor activation. The interaction between Ca^{2+} binding and voltage sensor activation is weak and independent of channel opening.

Together with previous analysis of the voltage-dependent gating of unliganded channels (Horrigan and Aldrich, 1999; Horrigan et al., 1999) these results support Scheme II. However, an important test of the model is its ability to describe the combined effects of Ca^{2+} and voltage over a broad range of conditions. In general, the Ca^{2+} and voltage dependence of P_O will depend on all the parameters in Scheme II (Eq. 1). Thus, by fitting $P_O(V,[Ca^{2+}])$ it is theoretically possible to test the model

and define its parameters. Excellent fits to the P_O - V relationships for $[Ca^{2+}] \leq 100 \mu M$ were obtained (Fig. 10 A) when L_0 and z_L were set to 2×10^{-6} and $0.4 e$, respectively, based on previous estimates (Horrigan et al., 1999) and all other parameters were allowed to vary (Table II, Fit A). However several parameters in addition to L_0 and z_L are poorly constrained by this procedure and the ability of Eq. 1 to fit P_O is an inadequate test of Scheme II. Although the values of z_j (0.55 e), $V_h(J)$ (154 mV), and D (18.4) obtained from the fit are similar to those estimated previously from 0 Ca^{2+} data ($z_j = 0.55 e$, $V_h(J) = 145$ mV, and $D = 17$) (Horrigan et al., 1999), the values of C (2.4) and K_D (32 μM) are inconsistent with the $\log(R_O)$ - $[Ca^{2+}]$ relationship (Fig. 10 B, Fit A). And the value of E (31) predicts a -158 mV shift in the Q_{fast} - V relationship upon Ca^{2+} binding, much larger than the observed -33 mV shift in 70 μM Ca^{2+} .

One reason why the P_O fit fails to constrain L_0 , z_L , C , K_D is that it places little weight on the data at extreme negative voltages where P_O is small. These parameters

are better constrained by fitting $\log(P_O)$. Obviously the fit also excludes information available from gating currents. The final parameters assigned to Scheme II (Table II, Fit B) are a compromise determined by constraining many of the parameters within a restricted range and then fitting both P_O and $\log(P_O)$ simultaneously in an attempt to weigh equally the data at extreme negative voltage and near $V_h(P_O)$. Fig. 10 C plots P_O (Fig. 10 C₁) and $\log(P_O)$ (Fig. 10 C₂) together with the predictions of Scheme II (lines). The parameters were restricted as follows:

$V_h(J)$, the voltage where $J = 1$ ($V_h(J) = (kT/z_J) \ln(J_0)$), was restricted to a range from 145 to 155 mV. The upper limit corresponds to the half activation voltage of Q_{fast} -V determined from gating currents in 0 Ca^{2+} . The lower limit is based on previous analysis that suggests $V_h(J)$ may be reduced slightly under the ionic conditions used to measure P_O (Horrigan and Aldrich, 1999).

z_J , the voltage sensor charge was set to 0.58 e representing the mean value determined from Boltzmann fits to Q_{fast} -V relationships in 0 and 70 μM Ca^{2+} .

C and K_D were set to 8 and 11 μM , respectively, based on a fit to the R_O -[Ca^{2+}] data where C was fixed and K_D allowed to vary (Fig. 9 C). C was chosen as the maximum value judged consistent with the amplitude range of R_O because higher C consistently produced better fits to $P_O(V, [\text{Ca}^{2+}])$ by least-squares criteria. In addition, since C and E both contribute to the Ca^{2+} -dependent shift in $V_h(P_O)$, higher values of C allowed E to be reduced to a value (2.4) consistent with gating current measurements (see below). Allowing K_D to vary during the P_O -V fits consistently produced higher values (15–16 μM) than indicated by the R_O -[Ca^{2+}] data (11 μM). This may reflect the contribution of low affinity Ca^{2+} -binding sites estimated by Zhang et al. (2001) to shift $V_h(P_O)$ by –7 mV in 100 μM Ca^{2+} . When P_O -V data in 100, 70, 21, and 10 μM Ca^{2+} were shifted by –7, –5, –2, –1 mV to correct for the effect of low affinity sites, a lower K_D of 12 μM was obtained from P_O -V fits, consistent with the R_O data.

E was constrained to a range of 2.1–2.7 indicated by a 33–43 mV shift in the charge distribution for closed (Q_C) and open (Q_O) channels, respectively, in 70 μM Ca^{2+} . Q_C was determined from gating currents when channels are closed (i.e., Q_{fast} , Fig. 7). Q_O was estimated from the limiting voltage dependence of $\log(P_O)$ as described later (see Fig. 12).

z_L , the partial charge associated with the C-O transition was adjusted to 0.3 e based on the limiting slope of $\log(P_O)$ and the voltage dependence of $\tau(I_K)$. Larger values of z_L were clearly inconsistent with the weak voltage dependence of $\log(P_O)$ at extreme negative voltages, whereas smaller values, as discussed later, appear inconsistent with the voltage dependence of $\tau(I_K)$ at extreme negative and positive voltages.

D, L_0 were allowed to vary freely. L_0 is highly constrained by P_O at negative voltages in 0 Ca^{2+} where

TABLE II
Steady-State Parameters

	L_0	z_L	z_J	$V_h(J)$	K_D	C	D	E
		e	e	mV	μM			
Fit A	2×10^{-6}	0.4	0.55	154	32	2.4	18.4	31
Fit B	9.8×10^{-7}	0.3	0.58	150	11	8	25	2.4
Fit C	9.8×10^{-7}	0.3	0.58	150	11	11	25	1

Eq. 3 reduces to $P_O = L = L_0 \exp(-z_L V/kT)$. D , as discussed later, is constrained by the shape of the $\log(P_O)$ - V relationship.

Using the above constraints Scheme II does a reasonable job of reproducing P_O over a broad range of conditions while also reproducing results obtained under extreme conditions. $\log(P_O)$ is well fit at all [Ca²⁺] (Fig. 10 C₂) although fits to P_O tend to be too steep in intermediate [Ca²⁺] (e.g., 10 μM). The allosteric factors $C = 8$ and $E = 2.4$ demonstrate that a combination of strong direct and weak indirect interactions between Ca²⁺ binding and channel opening is sufficient to account for the Ca²⁺-dependent shift in $V_h(P_O)$ (Fig. 9 D).

We also attempted to fit the data with $E = 1$ (Table II, Fit C) to determine whether weak interaction between Ca²⁺ binding sites and voltage sensors is necessary for obtaining an adequate fit. In this case, increasing C from 8 to 11 was sufficient to reproduce the Ca²⁺-dependent shift in $V_h(P_O)$ (unpublished data). However, such an increase in C is inconsistent with the Ca²⁺ dependence of R_O , predicting a larger increase in R_O than is actually observed (Fig. 10 B, Fit C). Thus, a small but significant interaction between Ca²⁺ binding and voltage sensor activation is required to account for the Ca²⁺ dependence of P_O .

The parameters used to fit steady-state P_O (Table II, Fit B) also account for the change in shape and shift of the steady-state Q-V relation along the voltage axis in response to 70 μM Ca²⁺ as shown in Fig. 10 D. Ca²⁺ alters the relationship between open probability and charge movement by increasing the C-O equilibria, thus increasing the likelihood that channels will open at voltages where voltage sensors are not activated. Thus, the predominant activation pathway is altered by Ca²⁺ as illustrated in Fig. 10 E.

In the following section (Figs. 11–15) we test Scheme II further and refine the parameters by fitting the model to additional features of the ionic and gating current data.

The Reciprocity of Allosteric Interactions

A fundamental prediction of an allosteric mechanism (Scheme II) is the reciprocal nature of sensor–gate interactions. That is, if Ca²⁺ and voltage affect channel opening then channel opening should also affect Ca²⁺ binding and voltage sensor movement. Specifically, opening should increase the affinity of binding sites for Ca²⁺ n -fold, and increase the equilibrium constant for voltage

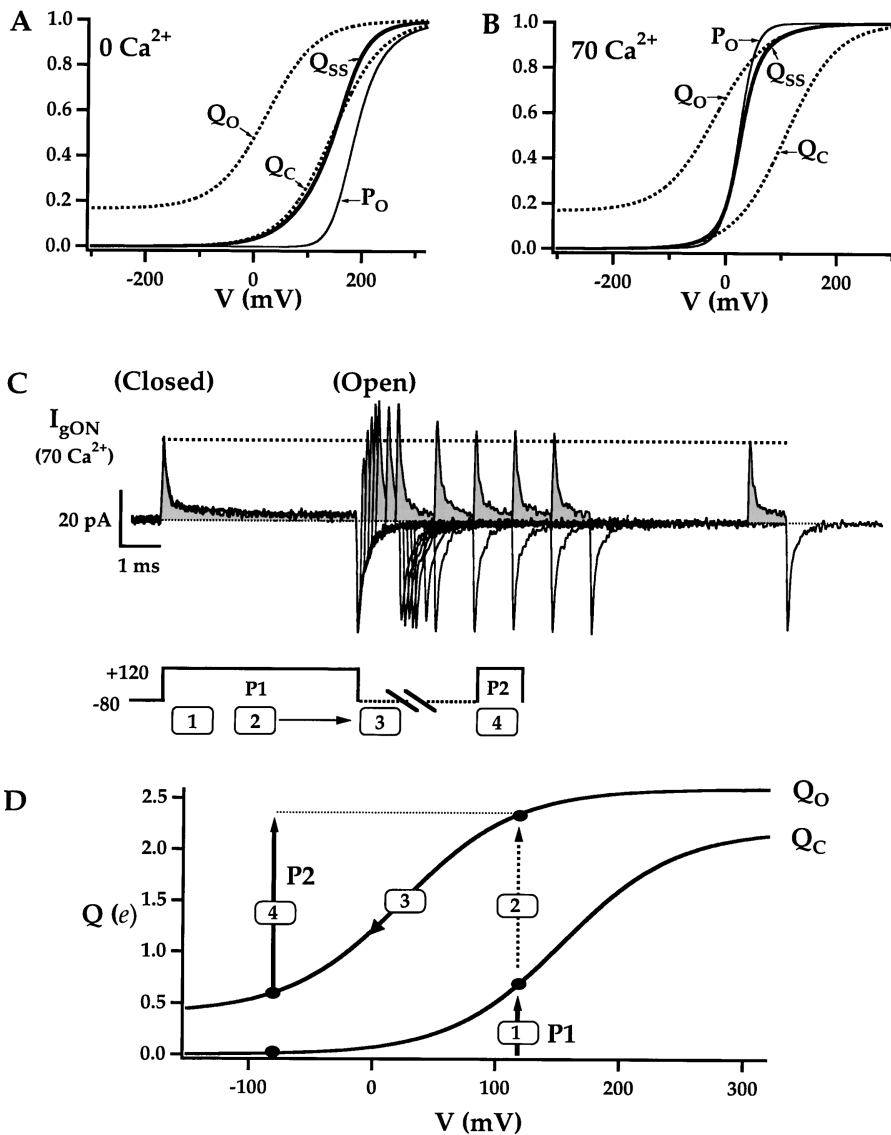


FIGURE 11. Charge distribution of open and closed channels. Normalized plots of Q_C , Q_O , P_O , and Q_{SS} versus voltage predicted by Scheme II (Table II, Fit B parameters) are compared in (A) 0 Ca^{2+} and (B) $70 \mu\text{M} \text{ Ca}^{2+}$. (C) A double pulse experiment in $70 \mu\text{M} \text{ Ca}^{2+}$ shows that peak I_g evoked by the second pulse (P2) is larger than that evoked by the first pulse (P1) when the interpulse interval is brief. This behavior is consistent with the predicted difference between Q_C and Q_O as illustrated by the numbered arrows in (D) corresponding to the pulse intervals in C. Arrows 1 and 4 represent the amount of charge that should move in response to a step from -80 to $+120$ mV if channels are closed or open, respectively.

sensor activation D-fold (Fig. 3, compare sub-Schemes IIe and IIif). The first prediction cannot be tested directly because we observe the binding of Ca^{2+} indirectly via its effects on channel function. As discussed later, the differential sensitivity of $\tau(I_K)$ to Ca^{2+} observed at extreme positive and negative voltages is consistent with an increase in Ca^{2+} binding affinity upon channel opening. Technical factors prevent detailed comparison of gating charge movement in open versus closed channels. However several lines of evidence (below) confirm that channel opening affects voltage sensor movement in a manner predicted by Scheme II.

Channel Opening Promotes Voltage Sensor Activation

The change in relationship between $Q_{SS}-V$ and P_O-V (Fig. 10 D) reflects in large part a marked steepening of $Q_{SS}-V$ in $70 \mu\text{M} \text{ Ca}^{2+}$. This increase in apparent voltage dependence seems surprising given that the shape of the P_O-V and $Q_{fast}-V$ relationships are relatively unaf-

fected by Ca^{2+} (Figs. 4 C₂ and 7 C). However, the steepening of $Q_{SS}-V$ is explained by the change in voltage sensor activation that is predicted to accompany channel opening.

According to Scheme II, the steady-state charge distribution for closed channels (Q_C ; approximated by Q_{fast} in Fig. 7) is determined by the R-A equilibrium constant (J in 0 Ca^{2+} ; JE in saturating Ca^{2+}) and by the charge associated with voltage sensor activation (z_J):

$$\text{in } 0 \text{ Ca}^{2+}: \quad Q_C = 4z_J \left[\frac{J}{1+J} \right]$$

$$\text{in saturating Ca}^{2+}: \quad Q_C = 4z_J \left[\frac{JE}{1+JE} \right]$$

When channels open, charge associated with the C-O transition (z_L) moves and the R-A equilibrium constant increases D-fold, producing an open channel charge distribution:

$$\text{in } 0 \text{ Ca}^{2+}: \quad Q_O = z_L + 4z_J \left[\frac{DJ}{1 + DJ} \right] \quad (5a)$$

$$\text{in saturating Ca}^{2+}: \quad Q_O = z_L + 4z_J \left[\frac{DJE}{1 + DJE} \right] \quad (5b)$$

Channel opening increases the R-A equilibrium constant, thus shifting the Q_O -V to more negative voltages than Q_C -V with little change in shape (Fig. 11, A and B).

The steady-state charge distribution (Q_{ss}) can be expressed in general as a sum of Q_C and Q_O , weighted by open probability:

$$Q_{ss} = (1 - P_O)Q_C + (P_O)Q_O \quad (6)$$

In 0 Ca^{2+} , P_O is small at voltages where Q_C and Q_O increase, so Eq. 6 can be approximated:

$$Q_{ss} \approx Q_C$$

Q_{ss} deviates from Q_C only at high voltages where P_O becomes significant and, even then, the Q_{ss} -V relationship is only slightly steeper than Q_C -V (Fig. 11 A). In the presence of $70 \mu\text{M Ca}^{2+}$, however, the relationship between Q_C , Q_O , and P_O changes (Fig. 11 B). The P_O -V relation shifts to more negative voltages while Q_C -V and Q_O -V are relatively unaffected. Consequently, P_O increases at voltages where Q_C is small ($Q_C \ll 1$) and Eq. 6 can be approximated:

$$Q_{ss} \approx P_O Q_O$$

In addition, Scheme II predicts Q_O will increase at more negative voltages than P_O and is relatively constant over the voltage-range where P_O increases most steeply. Thus Q_{ss} is roughly proportional to P_O . That Q_{ss} in 0 Ca^{2+} is proportional to Q_C and P_O respectively accounts for the marked change in shape of the Q_{ss} -V relationship upon application of Ca^{2+} .

Although the Q_{ss} -V relationship does not reveal the voltage dependence of Q_O in detail, the observation that Q_{ss} -V and P_O -V superimpose in $70 \mu\text{M Ca}^{2+}$ (Fig. 10 D) is consistent with Q_O increasing over a more negative voltage range than P_O , as predicted by Scheme II. Additional evidence presented below defines the Q_O -V relationship in more detail.

Channel Opening Produces “Charge Mobilization”

A double pulse gating current experiment in Fig. 11 C provides additional evidence that gating charge distribution differs for open and closed channels. In the presence of $70 \mu\text{M Ca}^{2+}$, the membrane voltage was stepped to 120 mV for 5 ms , returned to the holding potential (-80 mV) for various durations ($0.1\text{--}5 \text{ ms}$), and then stepped again to 120 mV . The amplitude of I_{gON} evoked by the first and second pulse (P1, P2) are equal when the interpulse interval is $\geq 3 \text{ ms}$ (Fig. 11 C, dashed line). However, with shorter intervals ($0.25\text{--}2 \text{ ms}$) peak I_{gON}

increases significantly during P2. A maximal increase in peak I_{gON} of 55% is observed together with a 43% increase in Q_{fast} using an interpulse interval of 0.5 ms .

The increase in Q_{fast} observed during the second pulse can be understood in terms of the relationship between Q_O and Q_C illustrated in Fig. 11 D. Initially, channels are closed at -80 mV , so Q_{fast} during P1 is determined by the voltage dependence of Q_C , and a pulse to 120 mV moves less than half of the total charge rapidly (Fig. 11 D, arrow 1). However, a 5-ms pulse to 120 mV in $70 \mu\text{M Ca}^{2+}$ is sufficient to activate *mSlo1* channels maximally (Fig. 4 C) and to saturate the Q_{ss} -V relationship (Fig. 6 E). Therefore, additional charge must move as channels open. This slow component of Q_{ON} can be described in terms of a transition between Q_C and Q_O (Fig. 11 D, arrow 2). After P1, repolarization to -80 mV moves voltage sensors rapidly back to their resting state while many channels remain open (Fig. 11 D, arrow 3) and channels subsequently close. With an interpulse interval of 3 ms or more, most channels are closed at the beginning of P2, so I_g evoked by P1 and P2 are identical. However, as the interpulse interval is reduced, some channels remain open at the beginning of P2 and an increase in Q_{fast} is observed because a step from -80 to 120 mV produces a greater increase in Q_O (Fig. 11 D, arrow 4) than it does in Q_C (arrow 1). That is, P2 evokes charge movement among open states (O-O), whereas P1 only evokes charge movement among closed states (C-C).

If all channels remain open and all voltage sensors are deactivated during the interpulse interval, then a 2.5-fold increase in Q_{fast} would be expected during P2 (Fig. 11 D, compare arrows 1 and 4). However, with a 0.5-ms interpulse interval only 37% of channels should remain open ($P_O = 0.375$) based on I_K deactivation kinetics ($\tau[I_K] = 0.51 \pm 0.04 \text{ ms}$ at -80 mV). In addition, 92% of the voltage sensors will reach the resting state ($P_R = 0.92$) based on the time constant of voltage sensor deactivation in open channels ($\tau = 0.2 \text{ ms}$ at -80 mV , see Fig. 13). Therefore, a 49% increase in Q_{fast} is predicted for P2 similar to the observed 43% increase ($Q_{fast}[P2] = [Q_O(+120) - Q_O(-80)] P_O P_R + [Q_C(+120) - Q_C(-80)] (1 - P_O) = [(2.5)(0.375)(0.92) + (1 - 0.375)] Q_{fast}[P1] = 1.49 Q_{fast}[P1]$).

The increase in charge mobilization revealed by the double pulse experiment is consistent with Q_O being shifted to more negative voltages than Q_C and further demonstrates that Q_O increases from -80 to 120 mV . This finding is completely consistent with the proposed allosteric relationship between voltage sensor activation (charge movement) and channel opening.

The Limiting Voltage Dependence of P_O Reveals the Q_O -V Relationship

To determine the voltage dependence of Q_O in more detail we analyzed the voltage dependence of P_O . The mean activation charge displacement $\langle q_a \rangle$ can be de-

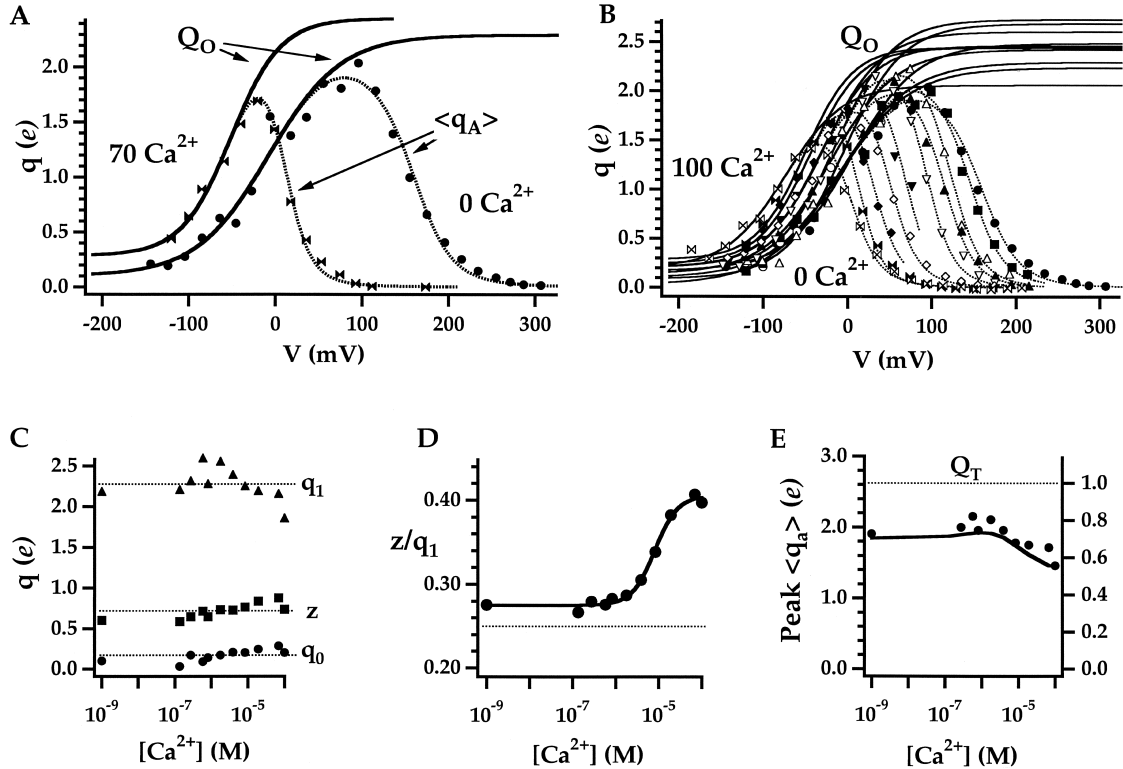


FIGURE 12. Estimating Q_O from the limiting voltage dependence of P_O . (A) $\langle q_a \rangle$ - V relationships representing the derivative with respect to voltage of mean $\log(P_O)$ (Eq. 7) are plotted for 0 and 70 μM Ca^{2+} . Dashed lines are smoothing functions determined from fits to mean $\log(P_O)$ in Fig. 9 B. Q_O - V relationships (solid lines) were estimated by fitting the smoothing functions with Eq. 12 at voltages where Q_C and P_O are small (0 Ca^{2+} : $V \leq 0$ mV; 70 μM Ca^{2+} : $V \leq -50$ mV). (B) Q_O is estimated as in A for all Ca^{2+} (0 to 100 μM). $\langle q_a \rangle$ was determined from mean $\log(P_O)$ in Fig. 9 B after excluding some data points that represent single measurements at the most positive or negative voltages. (C) Parameters for the Q_O - V fits are plotted versus $[\text{Ca}^{2+}]$. Dashed lines indicate mean values. (D) The ratio of the valence (z) and amplitude (q_1) of the voltage-dependent component of Q_O is plotted versus $[\text{Ca}^{2+}]$ and fit by a Hill equation ($n = 1.6$, $K_{1/2} = 8.1 \mu\text{M}$). (E) Peak $\langle q_a \rangle$ determined from smoothing functions in (B) (symbols) is reproduced by Scheme II (solid line; Table II, Fit B parameters). Peak $\langle q_a \rangle$ decreases with increasing $[\text{Ca}^{2+}]$ and underestimates total gating charge assigned to Scheme II (Q_T , dashed line).

fined in terms of the logarithmic slope of the P_O - V relationship (Sigg and Bezanilla, 1997):

$$\langle q_a \rangle = kT \frac{d(\ln[P_0])}{dV} \quad (7)$$

Sigg and Bezanilla (1997) derived a general expression for $\langle q_a \rangle$ in terms of the free energy and conductance of each state in an arbitrary gating scheme:

$$\langle q_a \rangle = \left[\frac{\sum_i q_i f_i \exp\left(-\frac{F_i}{kT}\right)}{\sum_i f_i \exp\left(-\frac{F_i}{kT}\right)} - \frac{\sum_i q_i \exp\left(-\frac{F_i}{kT}\right)}{\sum_i \exp\left(-\frac{F_i}{kT}\right)} \right] \quad (8)$$

where $F_i = G_i + q_i V$, and q_i , G_i , and f_i are the charge displacement, free energy at $V = 0$, and fractional conductance ($0 \leq f_i \leq 1$) respectively, of state i .

Rearrangement of Eq. 8 yields an expression for Q_O in terms of $\langle q_a \rangle$, P_O , and Q_C (Eq. 9, below) provided that all open states have the same conductance (i.e., $f_i = 1$ for open states and $f_i = 0$ for closed states). This ap-

pears to be a reasonable assumption for BK channels, since subconductance events are rare (Barrett et al., 1982; Rae et al., 1990) or brief (Ferguson et al., 1993). Thus,

$$Q_O = \frac{\langle q_a \rangle}{(1 - P_0)} + Q_C, \quad (9)$$

where

$$Q_C = \frac{\sum_i q_i f_i \exp\left(-\frac{F_i}{kT}\right)}{\sum_i f_i \exp\left(-\frac{F_i}{kT}\right)},$$

$$P_0 = \frac{\sum_i f_i \exp\left(-\frac{F_i}{kT}\right)}{\sum_i \exp\left(-\frac{F_i}{kT}\right)}$$

Combining Eqs. 7 and 9 yields an expression for Q_O in terms of P_O and Q_C :

$$Q_0 = \frac{kT}{(1-P_0)} \left[\frac{d(\ln(P_0))}{dV} \right] + Q_C \quad (10)$$

Thus, in theory, Q_0 can be determined in a model-independent manner at any voltage and $[Ca^{2+}]$ by measuring P_0 and Q_C (i.e., Q_{fast}). However, several experimental factors limit the conditions under which Eq. 10 can be evaluated accurately. First, at high voltages and/or $[Ca^{2+}]$ the P_0 of BK channels approaches unity (Rothberg and Magleby, 2000), such that the first term of Eq. 10 becomes large and sensitive to errors in P_0 . That our experiments measure normalized open probability (P_0/P_{OMAX}) rather than absolute P_0 introduces an additional systematic error when P_0 approaches P_{OMAX} . Second, the method of estimating Q_C is model dependent. The voltage dependence of Q_C can be determined from the Q_{fast} -V relationship (Fig. 7), if we assume, as in Scheme II, that Q_{fast} represents the movement of four independent and identical voltage sensors. In this case the maximal amplitude of Q_C is $4z_j$, where z_j , the voltage sensor charge, can be determined by fitting the Q_{fast} -V relationship to the Boltzmann distribution.

Q_0 can be determined in a model-independent manner that is insensitive to the use of normalized P_0 if we restrict our analysis to conditions where both P_0 and Q_C are small. If $P_0 \ll 1$, Eq. 10 reduces to:

$$Q_0 = kT \frac{d(\ln(P_0))}{dV} + Q_C.$$

If, in addition, $Q_C \ll Q_0$, then Q_0 can be approximated by the mean activation charge displacement:

$$Q_0 = kT \frac{d(\ln(P_0))}{dV} = \langle q_a \rangle. \quad (11)$$

According to Scheme II, Q_0 should increase to roughly half of its maximal value before Q_C or P_0 become significant (i.e., $>10^{-1}$) (see Fig. 11, A and B). Thus, over a range of negative voltages, the Q_0 -V relationship can be determined solely from the voltage dependence of P_0 . Since Eq. 11 is insensitive to the scaling of P_0 , normalized P_0 or NP_0 can be used without introducing additional errors. Since Eq. 11 is independent of Q_C , evaluation of Q_0 is not restricted to those $[Ca^{2+}]$ where gating currents have been measured.

Fig. 12 A plots $\langle q_a \rangle$ determined from mean P_0 in 0 and 70 μM Ca^{2+} (Fig. 9 B). The $\langle q_a \rangle$ -V relations are bell-shaped and are expected to approximate the Q_0 -V relation only at negative voltages where Q_C and P_0 are small and Eq. 11 is valid (i.e., $V < \sim 0$ in 0 Ca^{2+} , $V < -50$ in 70 μM Ca). The Q_0 -V relationships are estimated (Fig. 12 A, solid lines) by fitting the foot of the $\langle q_a \rangle$ -V curves with functions of the form:

$$Q_0 = q_0 + q_1 B[V], \quad (12)$$

where $B[V] = [1 + e^{(V-V_h)z/kT}]^{-1}$ is a Boltzmann function characterized by a half-activation voltage (V_h) and gating valence (z), whereas q_0 and q_1 represent the amplitudes of the voltage-independent and voltage-dependent components of Q_0 , respectively. The prediction of Scheme II (Eq. 5) can be expressed in terms of Eq. 12 when $q_0 = z_L$, $q_1 = 4z_j$, $z = z_j$ and $V_h = (kT/z_j)\ln(DJ_0)$ in 0 Ca^{2+} or $V_h = (kT/z_j)\ln(DEJ_0)$ in saturating Ca^{2+} .

$\langle q_a \rangle$ is very sensitive to experimental discontinuities in the P_0 -V relationship. Consequently, increased variation in $\langle q_a \rangle$ is observed near the potassium reversal potential (0 mV), where P_0 was not measured, and near the peak of the $\langle q_a \rangle$ -V relationship corresponding to the transition between microscopic and macroscopic P_0 measurements. These local regions of increased variability can strongly influence Q_0 -V fits, especially the estimated amplitude of Q_0 (q_1 in Eq. 12). Therefore, to limit the effects of local variation, the $\langle q_a \rangle$ -V relationships were fit first with approximating functions (Fig. 12, A and B, dashed lines) to provide smoothly varying curves through the data. The Q_0 -V relationships were then determined from the foot of these curves rather than from individual data points. The approximating functions represent the derivative with respect to voltage of fits to the mean $\log(P_0)$ -V data (Fig. 9 B, solid lines) using a 10-state gating scheme (Scheme I*, Fig. 1 B) where all the parameters (L_0 , z_L , J_0 , z_j , D) were allowed to vary freely at each $[Ca^{2+}]$. In this case, Scheme I was used simply to reproduce the shapes of the $\log(P_0)$ -V and $\langle q_a \rangle$ -V relations; the parameters have no mechanistic meaning. Although fits produced in this way appear to be excellent, it is possible that the use of a particular approximating function biases the Q_0 -V fits. Similar Q_0 -V curves were obtained when the approximation function was determined by smoothing spline interpolation (Reinsch, 1967) (unpublished data). However, this alternative method required subjective adjustment of smoothing parameters at each $[Ca^{2+}]$, thus fits to Scheme I* based on least squares criteria were more consistent.

Q₀ Confirms That Channel Opening and Ca²⁺ Binding Increase the Voltage Sensor Equilibrium

As predicted by Scheme II, the Q_0 -V relationship is similar in shape to the Q_C -V relationship but shifted to more negative voltages, consistent with an increase in the R-A equilibrium constant upon channel opening. In 0 Ca^{2+} , Q_0 -V is characterized by a valence $z = 0.60$ e (Fig. 12 A) indistinguishable from that estimated for the Q_C -V relationship ($z_j = 0.59 \pm 0.03$ e, 0 Ca^{2+} ; $z_j = 0.57 \pm 0.03$ e, 70 Ca^{2+}). The amplitude of the voltage-dependent component of Q_0 ($q_1 = 2.19$ e, 0 Ca; $q_1 = 2.16$ e, 70 μM Ca) is also similar to that predicted by Scheme II ($4z_j = 2.32$ e). Finally, $V_h(Q_0)$ shifts by -43 mV in 70 μM Ca^{2+} , similar to the -33 mV shift in Q_C determined from admittance

analysis (Fig. 7 F). Thus, the limiting voltage dependence of P_O confirms that Ca^{2+} binding has a small direct effect on voltage sensor movement.

To examine further the Ca^{2+} dependence of Q_O , $\langle q_a \rangle$ was plotted in different $[\text{Ca}^{2+}]$ from 0 to 100 μM (Fig. 12 B) and $Q_O\text{-V}$ was determined (solid lines) as in Fig. 12 A. The $Q_O\text{-V}$ relations shift along the voltage axis in a Ca^{2+} -dependent manner while maintaining similar shapes and amplitudes. The parameters q_0 , q_1 , and z derived from the $Q_O\text{-V}$ fits are plotted against $[\text{Ca}^{2+}]$ in Fig. 12 C. Mean values of each parameter are indicated by dashed lines ($q_0 = 0.17 \pm 0.02$, $q_1 = 2.28 \pm 0.06$, $z = 0.72 \pm 0.03$).

Ca^{2+} Alters the Apparent Voltage Dependence of Channel Opening and Voltage Sensor Activation

Although the results in Fig. 12, A and B, are generally consistent with Scheme II, several details are not. Ca^{2+} appears to increase both the steepness of the $Q_O\text{-V}$ relationship (z) and the amplitude of the voltage-independent component (q_0) (Fig. 12 C). According to Scheme II these parameters, reflecting the voltage dependence of channel opening (z_L) and voltage sensor activation (z_J), respectively, should be Ca^{2+} independent (compare Eqs. 5a and b). Below, we consider refinements to Scheme II that could conceivably account for these results. However, given the possibilities for measurement error in Q_O and the failure of other types of data to confirm a Ca-dependent change in z_L or z_J , the necessity of altering Scheme II is questionable.

Z or q_0 might increase with Ca^{2+} if Ca^{2+} binding sites are displaced through the membrane electric field when *mSl01* channels change conformation. That is, Ca^{2+} ions might contribute to the gating charge associated with voltage sensor activation (z_J) or channel opening (z_L). However, several lines of evidence argue against this possibility. In the case of voltage sensor activation, $Q_{\text{fast}}\text{-V}$ relationships in 0 and 70 μM Ca^{2+} (Fig. 7 C) are characterized by similar valence (0.59 e , 0.57 e), indicating that z_J in closed channels is not altered by Ca^{2+} -binding. Similarly, the voltage-dependent component of Q_O (q_1), representing the total voltage sensor charge when channels are open, is relatively unaffected by Ca^{2+} (Fig. 12 C). In the case of the C-O transition, I_K kinetics appear inconsistent with a large Ca^{2+} -dependent change in z_L , suggesting that q_0 in low Ca^{2+} may be underestimated (see below).

Although the $Q_O\text{-V}$ relationships in Fig. 12 B are similar to one another, they are derived from P_O measurements that differ by three orders of magnitude (Fig. 9 B). It is conceivable that the apparent Ca^{2+} -dependence of z and q_0 reflects systematic measurement errors correlated with a large Ca^{2+} -dependent increase in P_O . Although a particular source of error is not evident, the variance of $\log(P_O)$ is greatest in low Ca^{2+} and it is

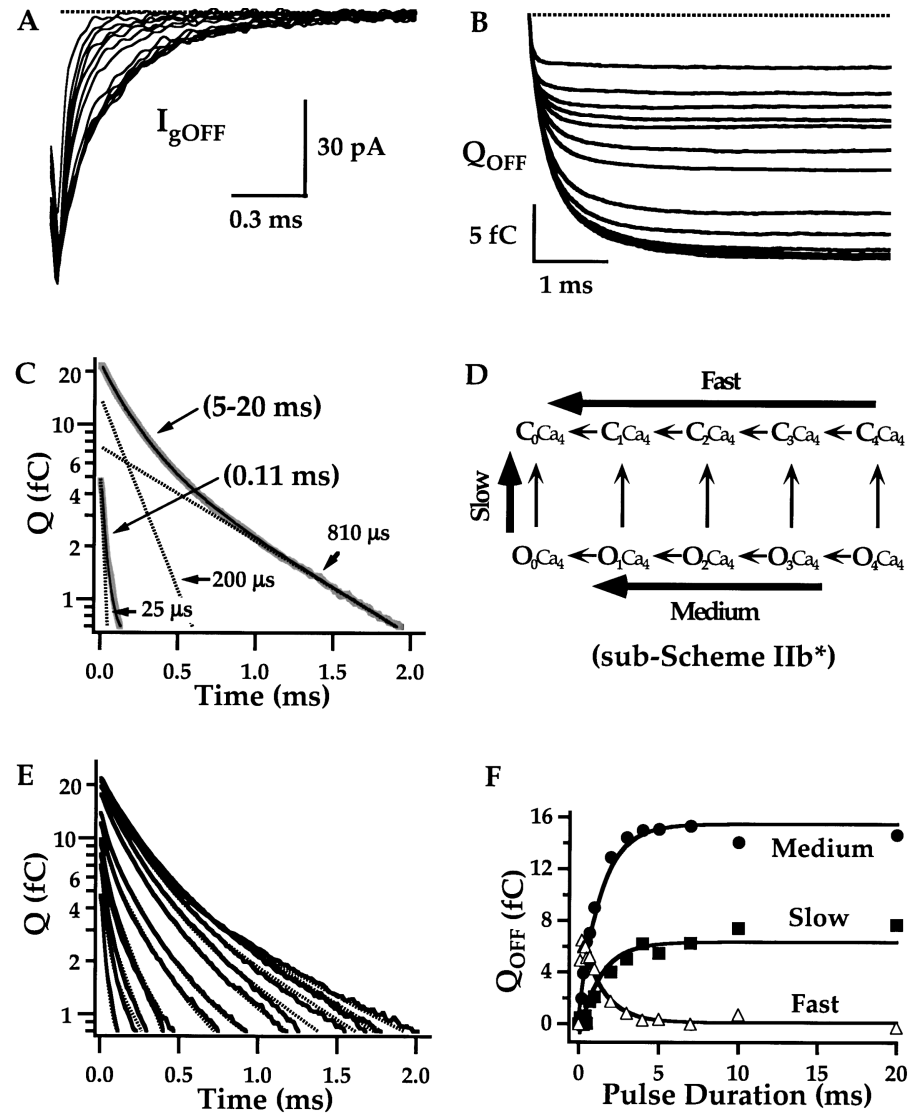
likely that sources of error that contribute to P_O in low Ca^{2+} are negligible in high Ca^{2+} . One potential source of error in q_0 , evident from Fig. 12, A and B, is that the data do not in general extend to sufficiently negative voltages to achieve saturation of $\langle q_a \rangle$. Thus, q_0 is extrapolated from a Boltzmann fit to $\langle q_a \rangle\text{-V}$ and is not measured directly.

A possible mechanism for the Ca^{2+} dependence of z is that Ca^{2+} binding increases the cooperativity of voltage sensor activation. Cooperativity could increase the steepness of $Q_O\text{-V}$ (z) without altering the total open channel charge (q_1). In the extreme case that voltage sensor activation is fully cooperative (i.e., concerted), we expect $z/q_1 = 1$; in contrast, an independent mechanism such as Scheme II predicts $z/q_1 = 0.25$. Fig. 12 D plots the ratio z/q_1 against $[\text{Ca}^{2+}]$. From 0 to 1 μM Ca^{2+} , z/q_1 remains relatively constant with a mean value 0.28 ± 0.003 , consistent with an independent mechanism (Fig. 12 D, dashed line). But z/q_1 increases with $[\text{Ca}^{2+}]$ to a maximum of 0.41. The data are fit by a Hill equation (solid line) with $n = 1.6$ and $K_{1/2} = 8.1 \mu\text{M}$, similar to the K_D determined from the $R_O\text{-}[Ca^{2+}]$ relationship. These results are consistent with the idea that Ca^{2+} binding increases the cooperativity of voltage sensor activation. Cooperativity might also explain why the $P_O\text{-V}$ relationships in high Ca^{2+} tend to be steeper than predicted by Scheme II (Fig. 10 C).

The Maximum Voltage Dependence of P_O Underestimates Total Gating Charge in a Ca^{2+} -dependent Manner

For channels containing a single open state, $\langle q_a \rangle$ is expected to attain a maximum at limiting negative voltages. This “limiting slope” indicates the total gating charge (Q_T) associated with channel activation representing the sum of charges associated with voltage sensor activation and channel opening (Almers, 1978; Sigg and Bezanilla, 1997). However, in *mSl01* channels the limiting and maximal values of $\langle q_a \rangle$ are different and neither provides a direct measure of Q_T . The limiting slope merely indicates the charge associated with the C-O transition (z_L). And Q_T , representing the maximum amplitude of Q_O , is always greater than peak $\langle q_a \rangle$ (Fig. 12, A and B). Since Q_T must be estimated in a model-dependent manner by fitting $Q_O\text{-V}$ to the foot of the $\langle q_a \rangle\text{-V}$ relationship it is of interest to determine to what extent peak $\langle q_a \rangle$ underestimates Q_T . Fig. 12 E plots peak $\langle q_a \rangle$ (solid symbols) determined from Fig. 12 B against $[\text{Ca}^{2+}]$ and demonstrates that the maximal voltage dependence of P_O varies with $[\text{Ca}^{2+}]$, attaining a maximum ($\sim 2.1 e$) at intermediate $[\text{Ca}^{2+}]$ and a minimum ($\sim 1.5 e$) at high $[\text{Ca}^{2+}]$. The allosteric model (Scheme II) reproduces this behavior (Fig. 12 E, solid line) and shows that peak $\langle q_a \rangle$ underestimates the value of Q_T in the model (dashed line, $Q_T = 4z_J + z_L = 2.62 e$) by 26–44%, depending on $[\text{Ca}^{2+}]$.

FIGURE 13. I_{gOFF} components. (A) OFF gating currents recorded at -80 mV in $70 \mu\text{M} \text{Ca}^{2+}$ following pulses of different duration (0.11–20 ms) to 120 mV decay more slowly as pulse duration increases. I_{gOFF} traces were integrated to obtain Q_{OFF} time courses in B. Q_{OFF} saturates for pulses of 5 ms or greater duration. (C) OFF kinetics following brief (0.11 ms) or prolonged (5–20 ms) pulses are compared by plotting the quantity $Q_{OFF}(t) - Q_{OFFSS}$ on a log scale versus time where Q_{OFFSS} is the mean value of $Q_{OFF}(t)$ for $t = 4\text{--}5$ ms. The 5–20 ms trace is the average of 5, 7, 10, and 20 ms records and is fit by a double exponential function (solid line, $q_{\text{MED}} = 14.1 \text{ fC}$, $\tau_{\text{MED}} = 200 \mu\text{s}$, $q_{\text{SLOW}} = 7.4 \text{ fC}$, $\tau_{\text{SLOW}} = 810 \mu\text{s}$) with dashed lines representing the two components. The 0.11-ms trace is fit by a triple exponential function (solid line, $q_{\text{FAST}} = 4.9 \text{ fC}$, $\tau_{\text{FAST}} = 25 \mu\text{s}$, $q_{\text{MED}} = 0.6 \text{ fC}$, $\tau_{\text{MED}} = 200 \mu\text{s}$, $q_{\text{SLOW}} = 0.4 \text{ fC}$, $\tau_{\text{SLOW}} = 810 \mu\text{s}$) with a dashed line indicating the fast component. (D) The Ca^{2+} -saturated gating scheme (sub-Scheme IIb*) indicates the origin of the three OFF components which are determined by voltage sensor deactivation when channels are closed (Fast) or open (Medium), or by channel closing (Slow). (E) OFF kinetics for all pulse durations are plotted as in C using the data in B. Dashed lines are triple exponential fits ($\tau_{\text{FAST}} = 25 \mu\text{s}$, $\tau_{\text{MED}} = 200 \mu\text{s}$, $\tau_{\text{SLOW}} = 810 \mu\text{s}$). (F) The amplitude of the three OFF components are plotted versus pulse duration and fit by exponential functions with 1.4-ms time constants representing the time course of channel opening.



Effects of Channel Opening on the Kinetics of OFF Charge Movement

The voltage and Ca^{2+} dependence of Q_C and Q_O indicate that channel opening strongly affects voltage sensor activation, whereas Ca^{2+} binding does not (i.e., D \gg E in Scheme II). That $70 \mu\text{M} \text{Ca}^{2+}$ greatly slows the decay of I_{gOFF} following a 1-ms pulse to 160 mV (Fig. 5 A) may appear to contradict the conclusion that direct interaction between Ca^{2+} binding sites and voltage sensors is weak. However, the Ca^{2+} -sensitivity of OFF charge movement can be understood in terms of an indirect interaction, mediated by the allosteric factors C and D in Scheme II, whereby Ca^{2+} promotes channel opening and channel opening affects voltage sensor movement.

In the presence of $70 \mu\text{M} \text{Ca}^{2+}$, OFF currents evoked after pulses to 160 mV decrease in amplitude and decay more slowly as pulse duration is increased (Figs. 5 B and 13 A). This phenomenon is also evident in the absence

of Ca^{2+} at more positive pulse voltages, is associated with the time course of channel opening, and is predicted by an allosteric voltage-gating mechanism (Horrigan and Aldrich, 1999). Channel opening biases the R-A equilibrium toward the activated state, with the result that voltage sensor deactivation, and therefore OFF charge movement, is slowed and peak I_{gOFF} is reduced.

The effect of pulse duration on I_{gOFF} in Fig. 5 B is more prominent in $70 \mu\text{M} \text{Ca}^{2+}$ than in 0Ca^{2+} because Ca^{2+} promotes channel opening. OFF currents evoked after brief pulses, when channels remain closed, decay rapidly in the presence or absence of Ca^{2+} (Fig. 5 B) because Ca^{2+} has little direct effect on voltage sensor deactivation kinetics (Fig. 7 E, compare τ_{gfast} at -80 mV in 0 and $70 \mu\text{M} \text{Ca}^{2+}$). The marked slowing of I_{gOFF} in $70 \mu\text{M} \text{Ca}^{2+}$ after a 1-ms pulse (Fig. 5 A) reflects that channel opening is both more complete and more rapid in the presence of Ca^{2+} . Therefore, the effect of Ca^{2+} on I_{gOFF} in Fig. 5 A reflects a difference in voltage sensor deacti-

vation for open and closed channels, rather than a direct effect of Ca^{2+} on voltage sensor movement.

Multiple Components of OFF Gating Charge Movement

The effects of channel opening on OFF charge movement in 70 μM Ca^{2+} are examined in more detail in Fig. 13. OFF currents evoked at -80 mV following pulses to 120 mV of different duration (0.11–20 ms) are superimposed on an expanded timescale in Fig. 13 A and exhibit a slowing in the decay of $I_{g\text{OFF}}$ that saturates for pulses of ≥ 5 ms duration. The integrals of these traces (Q_{OFF} , Fig. 13 B) reveal an additional slow component of charge relaxation after prolonged depolarizations that is not obvious in the $I_{g\text{OFF}}$ records and requires ~ 4 ms to reach a steady-state.

The kinetics of Q_{OFF} relaxation were analyzed by plotting the quantity $Q_{\text{OFF}}(t) - Q_{\text{OFFSS}}$ on a semi-log scale (Fig. 13, C and E), where Q_{OFFSS} is the steady-state value of $Q_{\text{OFF}}(t)$. Fig. 13 C compares OFF kinetics after the most brief (0.11 ms) and prolonged (5–20 ms) depolarizations. The 5–20-ms trace is fit by a double exponential function (solid line) with time constants of 200 and 810 μs (dashed lines) termed “Medium” and “Slow” components. The 0.11-ms record is fit by a triple-exponential function with a primary “Fast” 25- μs component (dashed line) in addition to the 200- and 810- μs components. Qualitatively similar results were reported previously in the absence of Ca^{2+} (Horrigan and Aldrich, 1999).

These kinetics can be understood in terms of sub-Scheme IIb* (Fig. 13 D). A prolonged depolarization to 120 mV in 70 μM Ca^{2+} is sufficient to activate *mSlo1* channels maximally. Therefore, the biexponential decay of Q_{OFF} after a 5–20-ms pulse represents the relaxation of open channels back to their resting state and is determined by voltage sensor deactivation while channels are open (O-O transitions labeled Medium in Fig. 13 D) and by channel closing (Slow). A brief depolarization is sufficient to activate voltage sensors but does not allow many channels to open. Thus, the decay of Q_{OFF} after a 0.11-ms pulse is dominated by a Fast component representing the deactivation of voltage sensors while channels are closed (C-C transitions labeled Fast in Fig. 13 D).

Sub-Scheme IIb* predicts that Q_{OFF} measured after pulses of intermediate duration will be best fit by a combination of all three time constants, since some channels will be open and some will be closed. Fig. 13 E shows that $Q_{\text{OFF}}(t) - Q_{\text{OFFSS}}$ derived from the OFF currents in Fig. 13 A for all pulse durations can be fit by triple-exponential functions with 25-, 200-, and 810- μs time constants. The amplitudes of the different exponential components are plotted versus pulse duration in Fig. 13 F. The fast component increases rapidly as voltage sensors are activated and then decreases as

channels leave the closed state. At the same time, the Medium and Slow components increase in parallel reflecting the increased occupancy of open states. The time courses of the amplitudes of all three components are fit by exponential functions with a time constant of 1.4 ms, representing the kinetics of channel opening.

The Kinetics of I_K Relaxation

In response to a voltage step, I_K activates or deactivates with an exponential time course after a brief delay (Fig. 4 B) (Horrigan et al., 1999). The $\tau(I_K)$ -V relationship characterizing this relaxation exhibits a complex voltage dependence. Increasing Ca^{2+} from 0 to 70 μM shifts the relation with little effect on its shape (Fig. 4 D). A similar pattern is observed at intermediate $[\text{Ca}^{2+}]$ (Fig. 14 A).

I_K kinetics were characterized primarily in 0 Ca^{2+} or high Ca^{2+} (70–100 μM) and the data at intermediate $[\text{Ca}^{2+}]$ often do not include the most positive voltages. Nonetheless, trends in the behavior of $\tau(I_K)$ are evident that help to constrain the parameters in Scheme II and provide important information about the Ca^{2+} and voltage dependence of gating. In particular, the response of $\tau(I_K)$ to Ca^{2+} at negative voltages suggests that a complex relationship exists between the Ca^{2+} - and voltage dependence of the rate limiting C-O transition.

The Voltage Dependence of $\tau(I_K)$

If voltage sensor activation and Ca^{2+} binding are fast and assumed to equilibrate on the timescale of channel opening, then $\tau(I_K)$ can be written (Cox et al., 1997a; Horrigan et al., 1999):

$$\tau(I_K) = [\sum (\delta_{ij} pC_{ij} + \gamma_{ij} pO_{ij})]^{-1}, \quad (13)$$

where i and j represent the number of activated voltage sensors and occupied Ca^{2+} -binding sites, respectively, δ_{ij} and γ_{ij} are forward and backward rate constants for the $C_{ij} - O_{ij}$ transitions and pC_{ij} , pO_{ij} are conditional occupancies of the open and closed states ($pC_{ij} = p(C_{ij}|C)$, $pO_{ij} = p(O_{ij}|O)$). Comparison of I_g and I_K kinetics in 0 and 70 μM Ca^{2+} supports the notion that voltage sensor activation is always faster than channel opening. The exponential relaxation of I_K and the similar voltage dependence of $\tau(I_K)$ in the presence and absence of Ca^{2+} are consistent with the assumption that Ca^{2+} binding is fast and that $\tau(I_K)$ is not limited by Ca^{2+} -binding transitions (Cox et al., 1997a).

The similar shape of $\tau(I_K)$ -V relations in different $[\text{Ca}^{2+}]$ is not surprising since, in the presence or absence of Ca^{2+} , $\tau(I_K)$ is governed by voltage sensor activation and by voltage-dependent changes in the rate constants for the C-O transition. These two processes define four regions in the $\tau(I_K)$ -V relationship (Eqs. 14–17 below).

At negative voltages where forward rate constants (δ_{ij}) are small compared with backward rates constants (γ_{ij}) Eq. 13 reduces to:

$$\tau(I_K) = \left(\sum \gamma_{ij} p O_{ij} \right)^{-1}. \quad (14)$$

Conversely, at positive voltages the backward rates are small, and Eq. 13 reduces to:

$$\tau(I_K) = \left(\sum \delta_{ij} p C_{ij} \right)^{-1}. \quad (15)$$

The equilibrium constants and rate constants for the C-O transitions vary with the number of activated voltage sensors. Consequently, Eqs. 14 and 15 define regions to either side of the peak in the $\tau(I_K)$ -V relationship where the voltage dependence of $\tau(I_K)$ is steepest, reflecting that different C-O transitions dominate I_K relaxation at different voltages (Horrigan et al., 1999). At more extreme potentials, by contrast, voltage sensor activation is saturated, and $\tau(I_K)$ reflects only the weak voltage dependence of the C-O rate constants (Eqs. 16 and 17 below).

At extreme negative voltages where voltage sensors are not activated ($i = 0$, Fig. 3 sub-Scheme IIC), Eq. 14 simplifies to:

$$\tau_N(I_K) = \left(\sum \gamma_{0j} p O_{0j} \right)^{-1}. \quad (16)$$

Thus, τ_N depends only on the closing rate constants and the distribution of Ca^{2+} -bound open states. Eq. 16 is valid when voltage sensors in the open channel are not activated and Q_O is therefore at a minimum. Based on Fig. 12 B, this condition is satisfied for all $[\text{Ca}^{2+}]$ at voltages less than approximately -150 mV. Consistent with this prediction, $\tau(I_K)$ in all $[\text{Ca}^{2+}]$ exhibits a similar exponential voltage dependence for $V < -150$ mV (Fig. 14 A), presumably reflecting the voltage dependence of the closing rates (γ_{0j}). In Fig. 14 B the mean $\tau(I_K)$ -V relationships in 0, 1, and $70 \mu\text{M}$ Ca^{2+} are fit (dashed lines) by exponential functions ($\tau_N = \exp(z_N V/kT)$) from -300 to -150 mV. The exponential voltage dependence of τ_N was shown previously to extend to at least -500 mV in 0 Ca^{2+} (Horrigan et al., 1999). The partial charges, z_N , determined from fits to individual $\tau(I_K)$ -V relationships are plotted versus $[\text{Ca}^{2+}]$ in Fig. 14 C (open circles) and exhibit little Ca^{2+} -dependence, with mean values (solid circles) of $-0.124 \pm 0.003 e$ in 0 Ca^{2+} ($n = 21$) and $-0.145 \pm 0.007 e$ in high ($70-100 \mu\text{M}$) Ca^{2+} ($n = 5$).

At extreme positive voltages, where all voltage sensors are activated ($i = 4$, Fig. 3, sub-Scheme IID), Eq. 15 simplifies to:

$$\tau_P(I_K) = \left(\sum \delta_{4j} p C_{4j} \right)^{-1}. \quad (17)$$

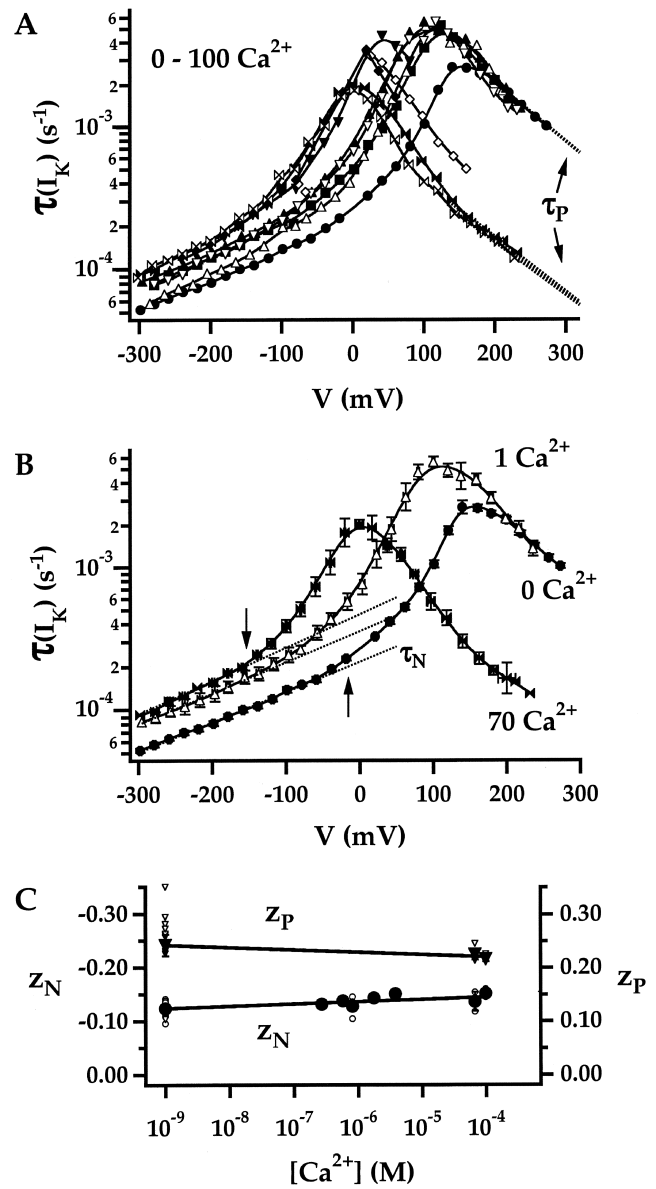


FIGURE 14. I_K kinetics. (A) Mean $\tau(I_K)$ -V relationships for different $[\text{Ca}^{2+}]$ (in μM): 0 (●), 0.27 (■), 0.58 (△), 0.81 (▲), 1.8 (▽), 3.8 (▼), 8.2 (◇), 19 (◆), 68 (▣), 99 (▢). Dashed lines are fits to exponential functions at extreme positive voltages ($V \geq 200$ mV in 0 Ca^{2+} or for $V \geq 140$ mV in high Ca^{2+} (68 and 99 μM)). (B) Comparison of $\tau(I_K)$ -V (mean \pm SEM) in 0, 0.81, and 68 μM . Dashed lines are fits to exponential functions between -300 and -150 mV, indicating that the voltage dependence of $\tau(I_K)$ at extreme negative voltages is not appreciably Ca^{2+} sensitive. However, the voltages where $\tau(I_K)$ begins to deviate from these fits in 0 and 68 $\mu\text{M} \text{ Ca}^{2+}$ differ by approximately -150 mV (arrows). (C) The partial charges determined from exponential fits to $\tau(I_K)$ at extreme positive (z_P) and negative (z_N) voltages as in A and B, respectively, are plotted against $[\text{Ca}^{2+}]$ and fit by lines ($z_P = 0.203 - 0.0044 \log[\text{Ca}^{2+}]$, $z_N = -0.161 - 0.0042 \log[\text{Ca}^{2+}]$). Individual data points (open symbols) and mean \pm SEM (solid symbols) are shown. The fits in A and B were constrained to the mean values of z_P and z_N respectively for each $[\text{Ca}^{2+}]$.

Thus, τ_p depends only on the opening rate constants and the distribution of Ca^{2+} -bound closed states. Eq. 17 is valid when voltage sensors in closed channels are activated such that Q_C is maximal. Because Q_C saturates at ~ 250 mV (Fig. 7 C), τ_p cannot be measured over a large voltage range. Therefore, the voltage dependence of τ_p was estimated by fitting the $\tau(I_K)$ -V relationships in 0, 70, and 100 μM Ca^{2+} with exponential functions (dashed lines Fig. 14 A) at voltages where Q_C is not completely saturated (> 200 mV, 0 Ca^{2+} , > 140 mV, 70–100 μM Ca^{2+}). These fits are consistent with $\tau(I_K)$ at the most positive voltages and are characterized by similar partial charges in different $[\text{Ca}^{2+}]$ (z_p , Fig. 14 C), reflecting the charge associated with opening rate constants. However, z_p may be overestimated slightly because Q_C is not completely saturated.

Ca^{2+} Mainly Affects Opening Rates at Limiting Negative Voltages

Fig. 14 B shows that $\tau_N(I_K)$ at -150 mV increases approximately twofold as $[\text{Ca}^{2+}]$ increases from 0 to 70 μM Ca^{2+} , implying that the closing rate (γ_{0j}) decreases only twofold when Ca^{2+} is bound (i.e., $\gamma_{00}/\gamma_{04} = 2$). By contrast, P_O at extreme negative voltages (-140 to -120 mV) increases $\sim 1,000$ -fold (Fig. 9 A). Therefore, the main effect of Ca^{2+} on the C-O transition at negative voltages must be to increase the forward (opening) rates.

$\tau(I_K)$ Reflects the Differential Affinities of Ca^{2+} for Open and Closed Channels

Although the change in $\tau(I_K)$ at negative voltages is small, it is remarkably Ca^{2+} sensitive. Fig. 14 B shows that 1 μM Ca^{2+} produces an almost maximal increase in $\tau_N(I_K)$, similar to that in 70 μM Ca^{2+} . By contrast, 1 μM Ca^{2+} has almost no effect on $\tau(I_K)$ measured at extreme positive voltages (Fig. 14 B). The Ca^{2+} dependence of $\tau(I_K)$ depends on the C-O rate constants as well as the distribution of Ca^{2+} -bound states (Eq. 13) and therefore does not provide a direct measure of Ca^{2+} binding. However, the differential Ca^{2+} sensitivities of $\tau_N(I_K)$ and $\tau_p(I_K)$ are qualitatively consistent with an allosteric effect of channel opening on Ca^{2+} binding affinity. $\tau_N(I_K)$ depends on the distribution of Ca^{2+} -bound open states (Eq. 16) and should therefore reflect the higher Ca^{2+} affinity of open channels, whereas $\tau_p(I_K)$ will reflect the lower affinity of closed channels (Eq. 17).

The Voltage Dependence of $\tau_N(I_K)$ and $\tau_p(I_K)$ Suggest z_L Is Ca^{2+} Independent and K_D Is Voltage Independent

The charge q_0 estimated from the limiting voltage dependence of P_O increases with $[\text{Ca}^{2+}]$ (Fig. 12 C), suggesting that bound Ca^{2+} ions may contribute to gating charge associated with the C-O equilibrium (z_L) and,

conversely, that Ca^{2+} binding may be voltage dependent. However, the voltage dependence of $\tau_N(I_K)$ and $\tau_p(I_K)$ in different $[\text{Ca}^{2+}]$ do not support these possibilities and suggest instead that q_0 in low Ca^{2+} may underestimate z_L .

Fig. 14 C plots the partial charges (z_N, z_p) determined from exponential fits to $\tau_N(I_K)$ and $\tau_p(I_K)$ at different $[\text{Ca}^{2+}]$. According to Eqs. 16 and 17, z_N and z_p reflect the voltage dependence of the backward and forward rate constants, respectively, for the C-O transition. In 0 Ca^{2+} and saturating Ca^{2+} , z_N and z_p should be determined by single rate-constants (0 Ca^{2+} : $z_N = z[\gamma_{00}]$ and $z_p = z[\delta_{40}]$, saturating Ca^{2+} : $z_N = z[\gamma_{04}]$ and $z_p = z[\delta_{40}]$).

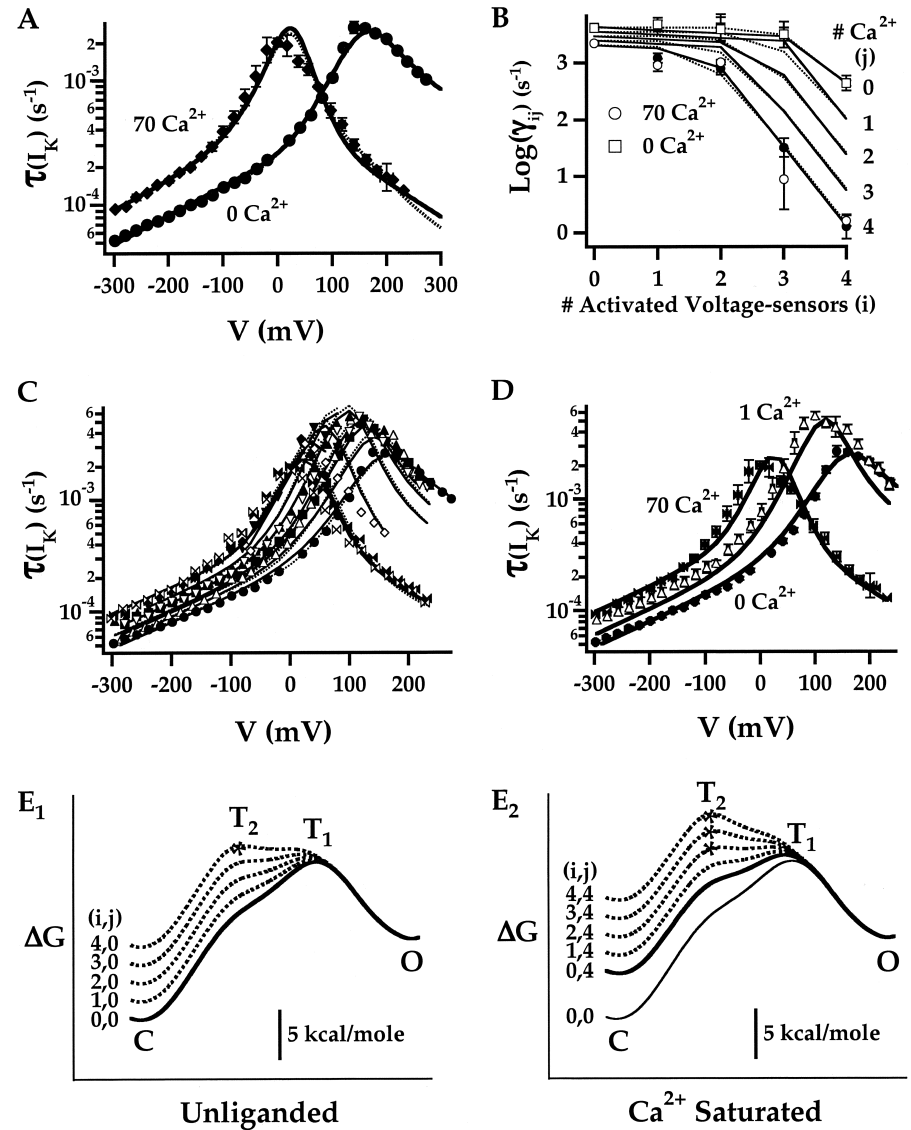
Fig. 14 C shows that neither z_N nor z_p are strongly Ca^{2+} sensitive. z_N increases in magnitude 1.16-fold from -0.124 ± 0.003 e in 0 Ca^{2+} ($n = 21$) to an average of -0.145 ± 0.007 e in high (70–100 μM) Ca^{2+} ($n = 5$). z_p decreases 1.1-fold from 0.24 ± 0.02 e (0 Ca^{2+} , $n=12$) to 0.22 ± 0.005 e in high Ca^{2+} ($n = 6$). The sum $z_T = |z_N| + |z_p|$ is identical in 0 Ca^{2+} and high Ca^{2+} ($z_T = 0.37$ e), suggesting that z_L is not Ca^{2+} dependent. z_T is expected to equal z_L only in the simple case that the C-O transition can be represented as single energy barrier; it is formally possible for z_T to be greater or less than z_L . Furthermore, z_T may be overestimated if z_p was not measured at sufficiently positive voltages. Nonetheless, the weak Ca^{2+} -sensitivity of z_N , z_p and z_T argue against the idea that the partial charge for channel opening (z_L) depends on Ca^{2+} .

If z_L is not Ca^{2+} dependent, then q_0 , determined from the limiting slope of P_O , is probably underestimated in low Ca^{2+} . q_0 in high Ca^{2+} (~ 0.3 e) is comparable to z_T (0.37 e) and may therefore represent a reasonable estimate of z_L . But q_0 in low Ca^{2+} (~ 0.1 e) appears underestimated since it is much smaller than z_T and smaller even than z_N . As noted above, factors that might contribute to errors in determining q_0 include failure to measure P_O at sufficiently negative voltages and large Ca^{2+} -dependent changes in the magnitude of P_O . In contrast, measurements of z_N and z_p are less subject to these types of errors. z_N , in particular, should be accurate since $\tau_N(I_K)$ was routinely measured over a large voltage range (-300 to -150 mV) where voltage sensors are not activated and $\tau(I_K)$ -V is exponential. Moreover, systematic Ca^{2+} -dependent errors in the measurement of z_N should be small because the amplitude of $\tau_N(I_K)$ changes only twofold in response to Ca^{2+} .

The Ca^{2+} and Voltage Dependence of C-O Transition Kinetics

The effects of Ca^{2+} on steady-state activation and I_K kinetics superficially resemble each other in that the P_O -V and $\tau(I_K)$ -V relationships are shifted similarly along the voltage axis with little change in shape (Fig. 4, C and D). Although the shift in P_O -V can be reproduced by assuming Ca^{2+} and voltage act almost independently

FIGURE 15. The Ca^{2+} and voltage dependence of C-O rate constants. (A) Mean $\tau(I_K)$ -V relationships in 0 and 68 μM Ca^{2+} are fit by Scheme I* (unliganded, Fig. 1 B) and sub-Scheme IIb* (Ca^{2+} saturated, Fig. 4 E), respectively, with the assumption the voltage sensors are equilibrated (Eq. 13). Each model contains five C-O transitions whose equilibrium constants are defined by the steady-state parameters (Table II, Fit B), increasing D-fold (25-fold) for each voltage sensor activated. (B) The backward rate constants for the C-O transitions (γ_{ij}) determined from the fits are plotted (symbols) versus the number of activated voltage sensors (i). The forward rate constants (δ_{ij}) are specified by γ_{ij} and the equilibrium constants. Dashed lines in A and open symbols B represent fits where γ_{ij} was allowed to vary freely. Similar fits (solid lines [A] and closed symbols [B]) were obtained when γ_{ij} was constrained to decrease by at most D^{-1} -fold when a voltage sensor activates such that δ_{ij} increases monotonically. (C) Mean $\tau(I_K)$ -V at all $[\text{Ca}^{2+}]$ (0–100 μM) are fit by Scheme II using the steady-state parameters in Table II (Fit B) and a two-barrier transition state model to describe the C-O rate constants (dashed lines, Eq. 20; solid lines, Eq. 21). The corresponding values of γ_{ij} are plotted in B (lines). (D) $\tau(I_K)$ -V relationships (mean \pm SEM) in 0, 0.81, and 68 μM Ca^{2+} are compared with fits (Eq. 21). (E) Transition state diagrams illustrate how a model with two transition states (T_1 , T_2) can account for a complex relationship between Ca^{2+} , voltage, and closing rates. Free energy (ΔG) relative to the open state is plotted against the C-O reaction coordinate for the unliganded (E_1) and Ca^{2+} -saturated (E_2) case. Solid lines represent the transition when voltage sensors are not activated ($i = 0$). Dashed lines indicate the additive perturbations produced by activation of 1–4 voltage sensors. The relative energies of C versus O and T_1 versus T_2 and the perturbations to each of these states produced by Ca^{2+} binding and voltage sensor activation were determined from the fits in (C) using Eq. 21. The ΔG between the open and transition states is not determined by the data and was adjusted arbitrarily. (E_1) In the unliganded state when voltage sensors are not activated (solid line) the transition rate is dominated by a single barrier (T_1). Voltage sensor activation produces a small perturbation to T_1 ($\Psi_V^1 = 0.041$) such that γ_{ij} is not sensitive to voltage sensor activation for $i = 1–3$. However, T_2 is strongly perturbed ($\Psi_V^2 = 1$) such that it becomes rate-determining when $i = 4$ (starred barrier). (E_2) Ca^{2+} binding also perturbs T_2 more than T_1 ($\Psi_{Ca}^2 = 0.7$; $\Psi_{Ca}^1 = 0.089$) such that when the channel is Ca^{2+} saturated (thick solid line) T_2 becomes rate determining when $i = 2–4$ (starred traces).



to alter the C-O equilibrium (Scheme II), the shift in $\tau(I_K)$ -V implies that a more complex relationship exists between the Ca^{2+} and V dependence of the C-O transition kinetics. We can show that this is the case by focusing on the foot of the $\tau(I_K)$ -V relation.

As membrane potential increases at negative voltages, $\tau(I_K)$ deviates from its limiting exponential voltage dependence ($\tau_N(V)$), implying that $\tau(I_K)$ can no longer be described by Eq. 16. However, this deviation

occurs at voltages where P_O is small and closing rates are presumably much greater than opening rates. Therefore, Eq. 14 should be valid. Comparing Eqs. 14 and 16, it is evident that two conditions must be satisfied for a deviation from exponential voltage dependence to occur. First, voltage sensors must activate so that open states other than O_{0j} are occupied. That is, the open channel charge distribution Q_O must increase from its minimum level. Second, voltage sensor activa-

tion must reduce the closing rates. The voltage (V_{dN}) where deviation from $\tau_N(V)$ occurs reflects both the voltage dependence of Q_O and the effect of voltage sensor activation on the O to C transition rates.

V_{dN} decreases by almost 150 mV as $[Ca^{2+}]$ increases from 0 to 70 μM (arrows, Fig. 14 B). This shift is not accounted for entirely by a Ca^{2+} -dependent change in voltage sensor activation, because Q_O shifts by only ~ 40 mV over the same Ca^{2+} -range (Fig. 12 B). Therefore, the change in V_{dN} must reflect a Ca^{2+} -dependent change in the sensitivity of closing rates to voltage sensor activation. To test this hypothesis, we fit the $\tau(I_K)$ - V relationships in 0 Ca^{2+} and 70 μM Ca^{2+} to Scheme II (Fig. 15 A).

Ca²⁺ Alters the Sensitivity of Closing Rates to Voltage Sensor Activation

Scheme II reduces to a 10-state gating scheme containing five C-O transitions in either 0 Ca^{2+} (Scheme I*, Fig. 1 B) or saturating Ca^{2+} (sub-Scheme IIb*, Fig. 4 E). The equilibrium constants for the C-O transitions are determined by the steady-state parameters, leaving five additional kinetic parameters to specify the opening and closing rate constants. The mean $\tau(I_K)$ - V relationships in 0 Ca^{2+} and 70 μM Ca^{2+} are plotted in Fig. 15 A together with fits to the unliganded and Ca^{2+} -saturated schemes respectively. The log closing rate constants are plotted in Fig. 15 B (symbols) against the number of voltage sensors activated (i). Similar fits were obtained when the closing rates were allowed to vary freely (Fig. 15 A, dashed lines, and B, open symbols) or constrained such that opening and closing rates change monotonically with voltage sensor activation (Fig. 15 A, solid lines, and B, filled symbols).

The closing rates (Fig. 15 B) reveal a different response to voltage sensor activation in 0 Ca^{2+} and 70 μM Ca^{2+} . In 0 Ca^{2+} , closing rates remain relatively constant until the fourth voltage sensor is activated. In 70 μM Ca^{2+} , however, closing rates begin to decrease when one voltage sensor is activated and decrease more sharply when three or four are activated. This change in the pattern of closing rates is necessary to explain the large shift in the foot of the $\tau(I_K)$ - V relationship with Ca^{2+} . In high Ca^{2+} , V_{dN} coincides roughly with the foot of the Q_O - V relationship, whereas, in 0 Ca^{2+} , V_{dN} occurs at more positive voltages where Q_O has already increased substantially and several voltage sensors have been activated.

$\tau(I_K)$ in Intermediate $[Ca^{2+}]$

$\tau(I_K)$ - V relationships in intermediate $[Ca^{2+}]$ are similar in shape to those in 0 Ca^{2+} and 70 μM Ca^{2+} and can also be fit by 10-state gating schemes (unpublished data). However, such fits are of limited value since many more than 10 states are accessible at intermediate

$[Ca^{2+}]$. Even with the simplifying assumption that Ca^{2+} -binding and voltage sensor transitions are equilibrated, the 70-state gating scheme specified by Scheme II contains 35 C-O transitions that can influence $\tau(I_K)$. The equilibrium constants for these transitions are specified by Scheme II and constrained by the steady-state data. Yet the forward and backward rate constants are, in principle, free to vary within this constraint, adding 35 kinetic parameters.

Fitting $\tau(I_K)$ in 0 Ca^{2+} and high Ca^{2+} and at extreme voltages helps to constrain subsets of the kinetic parameters in Scheme II. Nonetheless, attempts to fit the entire $\tau(I_K)$ dataset to Eq. 13 were problematic. The $\tau(I_K)$ data were not sufficient to constrain the large number of free kinetic parameters. Fits often failed to converge or did not converge to unique solutions. In some cases, the model traces “oscillated” about the $\tau(I_K)$ - V plots, exhibiting periodic changes in voltage dependence caused when neighboring C-O transitions in Scheme II were assigned rate constants of different orders of magnitude (unpublished data). Such fits fail to capture the gradual changes in voltage dependence that are evident in the data. This suggests that neighboring rate constants in the model are not completely free to vary but are to some extent correlated.

A Transition State Model for the C-O Conformational Change

To reduce the number of free parameters in Scheme II and to better reproduce the voltage dependence of $\tau(I_K)$ by imposing a correlation among rate constants, we attempted to devise a model to account for the Ca^{2+} and voltage dependence of the rate constants. It is likely that C-O transition kinetics might be described in terms of a simple mechanism since the steady-state data are reproduced reasonably well by Scheme II. That is, the effect of Ca^{2+} and voltage on the C-O equilibrium is accounted for with the assumption that perturbations in ΔG_{CO} caused by Ca^{2+} binding ($\Delta\Delta G_{CO}^{Ca} = -kT\ln[C]$) or by voltage sensor activation ($\Delta\Delta G_{CO}^V = -kT\ln[D]$) are additive and independent (Cui and Aldrich, 2000). Thus, a linear relationship exists between ΔG_{CO} and the number of bound Ca^{2+} (j) or activated voltage sensors (i). Given this simple relationship, it seems plausible that C-O rate constants might also be altered systematically by Ca^{2+} binding and voltage sensor activation.

Although perturbations in equilibria and kinetics need not be related, simple correlations are often observed for protein conformational changes, including the opening of acetylcholine receptor channels (Grosman et al., 2000), the allosteric transition of hemoglobin (Eaton et al., 1991; Hofrichter et al., 1991), and protein folding reactions (Fersht, 1995). A simple example in the case of *mSlc1* is that $\tau(I_K)$ and P_O both exhibit exponential voltage dependencies at extreme negative voltages (Figs. 9 A and 14 B). Thus, a linear re-

lationship exists between the log closing rate constant ($\ln[\gamma]$) and log C-O equilibrium constant ($\ln[\kappa]$) in response to voltage perturbation when voltage sensors are not activated. Such relationships can be explained in terms of transition state theory.

According to transition state theory, the C-O conformational change may be described as a reaction whose kinetics are dominated by an energy barrier, represented as a transiently occupied state (T). The C-O equilibrium constant is determined by the free energy difference (ΔG_{CO}) between C and O states ($L = \exp(-\Delta G_{CO}/kT)$), whereas the closing rate is determined by the difference (ΔG_{OT}) between O and T ($\gamma = A \exp(-\Delta G_{OT}/kT)$). Thus, proportional changes in $\ln(\gamma)$ and $\ln(\kappa)$ imply proportional changes in ΔG_{CO} and ΔG_{OT} (i.e., $\Delta\Delta G_{OT} = \Psi \Delta\Delta G_{CO}$). In the case of a voltage-dependent transition, such a rate-equilibrium linear-free energy relationship could arise if the gating charge moved during the O-T transition is a constant fraction of that moved during the O-C transition. In a more general sense, proportional changes in ΔG_{CO} and ΔG_{OT} are thought to occur when the transition state has structural features intermediate between the C and O conformations and is therefore sensitive to perturbations that affect C and O (Leffler, 1953; Hammond, 1955).

A Single Barrier Model Cannot Account for the Voltage Dependence of $\tau(I_K)$

To describe the rate constants in Scheme II we first considered the possibility that the C-O conformational change can be represented by a single energy barrier with a transition state (T) and that perturbations in the barrier energy produced by Ca^{2+} -binding ($\Delta\Delta G_{OT}^{\text{Ca}}$) or voltage sensor activation ($\Delta\Delta G_{OT}^V$) are additive and proportional to perturbations in ΔG_{CO} where $\Delta\Delta G_{CO}^{\text{Ca}} = -kT\ln(C)$ and $\Delta\Delta G_{CO}^V = -kT\ln(D)$. In this case three parameters, in addition to the equilibrium parameters in Scheme II, are required to specify the rate constants:

$$\gamma_{ij} = A e^{-\Delta G_{OT}/kT} = \gamma_{00} D^{-i\Psi_V} C^{-j\Psi_{Ca}}, \quad (18)$$

where γ_{00} is the closing rate for the unliganded channel ($j = 0$) with no voltage sensors activated ($i = 0$). Ψ_V and Ψ_{Ca} represent the fractional perturbations of ΔG_{OT} produced by voltage sensor activation or Ca^{2+} -binding, respectively ($\Delta\Delta G_{OT}^X = \Psi \Delta\Delta G_{CO}^X$).

Although Eq. 18 only specifies 25 rate constants, this is sufficient to characterize the 35 C-O transitions in Scheme II, provided we make the simplifying assumption that transitions with identical equilibrium constants have identical rate constants. Scheme II predicts that multiple C-O transitions exist for some combinations of i and j, owing to direct interactions between voltage sensors and Ca^{2+} binding sites represented by

the E-factor in Scheme II. However, these interactions do not alter the C-O equilibrium constants which are identical for any one combination of i and j.

The single barrier model predicts a linear relationship between log closing rate and the number of activated voltage sensors (i) or bound Ca^{2+} (j):

$$\ln(\gamma_{ij}) = \ln(\gamma_{00}) - i\Psi_V \ln[D] - j\Psi_{Ca} \ln[C].$$

This prediction is inconsistent with the observed relationships between $\log(\gamma_{ij})$ and i in 0 Ca^{2+} or 70 μM Ca^{2+} (Fig. 15 B). Thus, a single barrier model is inadequate to describe the observed voltage dependence of $\tau(I_K)$.

A Two Barrier Model Reproduces the Apparent Ca^{2+} and Voltage Dependence of C-O Transition Kinetics

The relationship between $\log(\gamma_{ij})$ and voltage sensor activation in 0 Ca^{2+} (Fig. 15 B) suggests that perturbations in ΔG_{CO} by activation of each voltage sensor produce small $\Delta\Delta G_{OT}$ when the first three voltage sensors activate, but a larger $\Delta\Delta G_{OT}$ for the fourth voltage sensor. This biphasic pattern might arise if the C-O transition is characterized by two barriers that become rate limiting over different ranges of ΔG_{CO} . It seems reasonable that a complex protein conformational change such as channel opening might be characterized by a complex energy landscape rather than a single uniform barrier (Fersht, 1995; Sigg et al., 1999). Thus, we considered a model in which the C-O transition is represented by two transition states (T_1, T_2); Ca^{2+} and voltage are assumed to perturb the energy of the transition states to different extents as determined by the perturbation factors $\Psi_V^1, \Psi_{Ca}^1, \Psi_V^2, \Psi_{Ca}^2$.

Modeling the C-O transition rates in terms of a complex energy barrier using Eyring rate theory is a simplification and requires additional assumptions about the energy landscape. A two-barrier model suggests that an energy well defining an intermediate state (S_I) might exist between C and O. However, a variety of macroscopic and single channel kinetics data imply that the C-O transition is concerted (i.e., highly cooperative), such that any intermediate states must have a low equilibrium occupancy and brief dwell time (see DISCUSSION). Thus, we make the simplifying assumption that the free energy of any intermediate is high relative to both C and O such that the sum of the rate constants for leaving S_I are fast relative to those for entering. If this general condition is satisfied then it is not necessary to include intermediate states explicitly in our kinetic scheme. The overall closing rate constant from O to C (γ) is determined by the product of the rate constant from O to S_I and the conditional probability that a channel in S_I will exit to C rather than O. Consequently, the closing rate can be ex-

pressed in terms of the free energy differences between the open state and the two transition states (ΔG_{OT1} , ΔG_{OT2}):

$$\gamma = Ae^{-\Delta G_{OT2}} \left[\frac{Ae^{-\Delta G_{ST1}}}{Ae^{-\Delta G_{ST1}} + Ae^{-\Delta G_{ST2}}} \right] = \frac{Ae^{-\Delta G_{OT1}} e^{-\Delta G_{OT2}}}{e^{-\Delta G_{OT1}} + e^{-\Delta G_{OT2}}} \quad (19)$$

$$\text{or } \gamma_{ij} = \frac{\gamma_{ij}^1 \gamma_{ij}^2}{\gamma_{ij}^1 + \gamma_{ij}^2} \text{ where} \quad (20)$$

$$\gamma_{ij}^M = Ae^{-\Delta G_{OTM}} = \gamma_{00}^M D^{-i\Psi_V^M} C^{-j\Psi_{Ca}^M},$$

where M = 1,2 and γ_{ij}^1 and γ_{ij}^2 represent the closing rates determined by T₁ and T₂, respectively.

When the free energies of T₁ and T₂ are comparable, Eq. 19 depends on both barriers. But as the difference between barriers increases, the rate constant becomes limited by the highest barrier. Alternatively, the closing rate may be determined by the highest barrier under all conditions if there is no energy well (intermediate state) between the two barriers when they are of similar height:

$$\gamma_{ij} = \min(\gamma_{ij}^1, \gamma_{ij}^2). \quad (21)$$

In Fig. 15 C the $\tau(I_K)$ -V relationships for all Ca²⁺ were fit simultaneously using the alternative 2-barrier models described by Eqs. 20 (dashed lines) and 21 (solid lines). The steady-state parameters were held constant (Table II, Fit B) while the kinetic parameters were allowed to vary (Table III).

The two-barrier models provide reasonable fits to the 0 Ca²⁺ and 70 μM Ca²⁺ data, and reproduce the large shift in V_{DN} (Fig. 15 D). The models also approximate the $\tau(I_K)$ -V relationship in 1 μM Ca²⁺ (Fig. 15 D) and capture the envelope of time constants observed over a range of intermediate Ca²⁺ (Fig. 15 C). The model lacking an intermediate state (Eq. 21, Fig. 15, C and D, solid lines) provided slightly better fits than Eq. 20 (dashed lines) based on chi-squared criteria. Improved fits at intermediate Ca²⁺ were obtained if K_D was reduced (unpublished data). However, a reduction in K_D is not consistent with the R_O-[Ca²⁺] relationship. The poorest fits were obtained in 10 μM Ca²⁺, which is not surprising since the steady-state model underestimates the steepness of the P_O-V relationship in 10 Ca²⁺ (Fig. 10 C₁).

The closing rate constants predicted by the two barrier models are plotted in Fig. 15 B (Eq. 20, dashed lines; Eq. 21, solid lines) for different numbers of bound Ca²⁺ (j). The models not only reproduce the biphasic pattern of closing rates in 0 Ca²⁺ but also the modification of this pattern that occurs in saturating Ca²⁺.

TABLE III
Scheme II: Two-barrier Model Kinetic Parameters

	γ_{ij}^1	γ_{ij}^2	Ψ_V^1	Ψ_{Ca}^1	Ψ_V^2	Ψ_{Ca}^2
	s^{-1}	s^{-1}				
Eq. 20	4,193	1.90×10^8	0.0	0.083	1.0	0.70
Eq. 21	4,322	1.74×10^8	0.041	0.089	1.0	0.70

The steady-state parameter were from Table II, Fit B: L₀ = 9.8 × 10⁻⁷, z_L = 0.3 e, z_j = 0.58 e, V_h(J) = 150 mV, K_D = 11 mM, C = 8, D = 25, E = 2.4.

The mechanism by which the two barrier model reproduces the different patterns of backward rates observed in 0 Ca²⁺ and 70 μM Ca²⁺ is illustrated by the transition state diagrams in Fig. 15 E. In 0 Ca²⁺ at extreme negative voltages the closing rate (γ_{00}) is determined by the highest barrier (T₁). Voltage sensor activation produces little change in ΔG_{OT1} (Ψ_V^1 is small) such that γ_{ij} is not greatly altered by activation of one or two voltage sensors (Fig. 15 E₁). However, the energy of the second barrier (ΔG_{OT2}) is altered by voltage sensor activation (Ψ_V^2 is large) such that T₂ becomes rate-limiting, and γ becomes sensitive to voltage sensor activation, when more than three voltage sensors are activated (starred trace Fig. 15 E₁) thereby producing a biphasic pattern in the relationship between ln(γ_{ij}) and i. Ca²⁺ binding also increases ΔG_{OT2} (Ψ_{Ca}^2 is large) such that, in 70 μM Ca²⁺, T₂ becomes rate limiting when fewer than three voltage sensors are activated (starred traces Fig. 15 E₂). By the same logic, Ca²⁺ exerts little effect on the closing rate when voltage sensors are not activated (Ψ_{Ca}^1 is small), but has a much bigger effect at high voltages when T₂ becomes rate limiting. In this way, additive effects of Ca²⁺ binding and voltage sensor activation on the C-O equilibrium free energy change can produce nonlinear changes in ln(γ_{ij}).

DISCUSSION

The combined effects of Ca²⁺ and voltage on BK channel gating are important to understand because they underlie physiological processes in many cell types, but also because they provide information about channel gating that is difficult to obtain from channels that are purely ligand or voltage gated. For example, the voltage dependence of BK channels allows us to compare the gating of liganded and unliganded channels to an extent that is not possible for most ligand-gated channels. BK channels can be activated maximally by voltage in the absence of Ca²⁺, allowing the detailed study of transitions among unliganded states (Cui et al., 1997; Stefani et al., 1997; Horrigan and Aldrich, 1999; Horrigan et al., 1999; Nimigean and Magleby, 2000; Talukder and Aldrich, 2000). Such openings support allosteric models where ligand-bound and unliganded channels undergo similar conformational changes, but

ligand binding alters the energetics of certain transitions. Here we compare the gating of Ca^{2+} -bound and unliganded BK channels to identify Ca^{2+} -sensitive transitions and determine the mechanism of Ca^{2+} action.

Relationship to Previous Studies

Previous studies support the basic conclusion that both voltage sensor activation and Ca^{2+} binding act to promote BK channel opening through allosteric mechanisms (Cox et al., 1997a; Cui et al., 1997; Horrigan and Aldrich, 1999; Horrigan et al., 1999; Rothberg and Magleby, 1999, 2000; Cox and Aldrich, 2000; Cui and Aldrich, 2000; Talukder and Aldrich, 2000; Zhang et al., 2001). However, as discussed below, none of these studies have fully tested the assumptions and predictions of a particular mechanism such as Scheme II.

In general, BK channels distribute among a large number of states in a Ca^{2+} - and voltage-dependent manner. Scheme II predicts a gating architecture (i.e., connectivity among states) and equilibrium constants that are determined by the model parameters and by assumptions about the functional properties of sensors and gates and their interactions with each other. Thus, in theory, the gating mechanism can be tested by determining the arrangement of states and the relationships among the equilibria.

Single channel I_K kinetic analysis confirms that BK channels can occupy many different open and closed states consistent with the allosteric assumption that no combination of sensor and gate conformations are disallowed (Rothberg and Magleby, 1999; Talukder and Aldrich, 2000). Moreover, these kinetics can be reproduced by gating schemes with separate voltage- and Ca^{2+} -dependent transitions (Rothberg and Magleby, 2000) consistent with a mechanism where Ca^{2+} - and voltage sensors are capable of nonconcerted action. However, the number of accessible states is large, transitions associated with voltage and Ca^{2+} sensor activation are fast, and single channel recordings at extreme voltages are difficult. Hence, some states are rarely occupied or are difficult to resolve so that many rate constants, and the corresponding equilibrium constants, are poorly determined. Restricting the analysis to the unliganded or Ca^{2+} -saturated conditions reduces the number of accessible states and improves, but does not solve, the problem of determining the relationship among equilibrium constants (Rothberg and Magleby, 1999; Talukder and Aldrich, 2000).

The Ca^{2+} and voltage dependence of BK channel open probability also provide information about the underlying gating mechanism. Models similar to Scheme II have been used to fit the shape and Ca^{2+} dependence of macroscopic G-V relationships successfully over a wide range of conditions (Cox and Aldrich,

2000; Cui and Aldrich, 2000; Zhang et al., 2001). However, some parameters in Scheme II are poorly constrained by such data and others covary, and thus are not determined uniquely (Zhang et al., 2001). As we have shown in Fig. 10 A, excellent fits can be obtained when some parameters are adjusted to unrealistic values. Thus, our ability to test many aspects of the mechanism by the G-V data alone is questionable.

Additional tests of the BK channel gating mechanism are provided by combining I_K data with manipulations of channel function. The effect on G-V relationships of the accessory $\beta 1$ subunit (Cox and Aldrich, 2000) or mutations in the S4 voltage sensor (Cui and Aldrich, 2000) are consistent with mechanisms similar to Scheme II. In addition the effects of voltage sensor, mutations suggest that the interaction between Ca^{2+} binding sites and voltage sensors are weak. However, the extent to which this conclusion is model dependent or can be quantified is unclear.

Testing the Allosteric Gating Mechanism

To test the mechanism of BK channel gating we have measured gating currents, extended I_K measurements to extreme negative voltages, and employed conditions in which subsets of the processes and interactions depicted in Scheme II can be studied in isolation. Gating currents allow us to characterize voltage sensor function directly and to examine the interaction of voltage sensors with Ca^{2+} binding and channel opening. The limiting voltage dependence of P_O provides additional information about the interaction between voltage sensor activation and channel opening that is not obtained readily from gating currents. Measurements of P_O and macroscopic I_K relaxation kinetics at extreme negative voltages provide direct information about the C-O transition properties and allow us to test the interaction between Ca^{2+} binding and channel opening in a way that is independent of voltage sensor activation. Although we do not monitor the Ca^{2+} -bound state of the channel directly, the Ca^{2+} dependence of P_O at extreme negative voltages provides a more direct indication of Ca^{2+} binding properties than previous measurements based on Ca^{2+} dependence of the half activation voltage. By focusing on conditions of high (70–100 μM) and low (1 nM) $[\text{Ca}^{2+}]$ we are able to examine gating when the state of the Ca^{2+} binding site is well defined (i.e., saturated or unliganded).

Another important strategy used in this investigation was to examine the reciprocal nature of interactions between sensors and gates. Such reciprocal interactions are a hallmark of allosteric mechanisms and provide alternative methods to measure each interaction factor in Scheme II.

Our results allow us to make a number of conclusions about the properties and relationships between voltage sensor activation, calcium binding, subunit interac-

tions, and channel opening that are outlined in the following sections.

Isolation of Channel Opening, Voltage Sensor Activation, and Ca²⁺ Binding

A basic prediction of an allosteric gating mechanism is that all combinations of sensor and gate conformation are allowed. We have tested this hypothesis by examining *mSlo1* gating under a variety of extreme conditions. Channel opening is weakly voltage dependent at extreme negative voltages in the absence of Ca²⁺. This shows that the C-O conformational change occurs whether or not voltage sensors or Ca²⁺-binding sites are activated. Similarly, gating currents are observed when channels are closed or open in the presence or absence of Ca²⁺. Thus, voltage sensors can activate whether channels are closed or open, unliganded or Ca²⁺ bound. That Ca²⁺ sensors activate whether or not voltage sensors are activated is indicated by the ability of Ca²⁺ to increase P_O at extreme positive and negative voltages. Similarly, the ability of Ca²⁺ to shift the open and closed channel charge distributions (Q_O, Q_C) and to alter τ(I_K) at both extreme positive and negative voltages indicates that Ca²⁺ binds whether channels are open or closed.

The Functional Properties of Sensor Activation and Channel Opening

Scheme II assumes that voltage sensor activation, Ca²⁺ binding, and channel opening can each be described by simple two-state processes and that voltage and Ca²⁺ sensors in different subunits act independently. These assumptions appear reasonable within the resolution of our measurements, although indirect evidence suggests that channel opening may not be completely concerted and that voltage sensors in different subunits may interact weakly.

The R-A Transition

Consistent with a two-state model of voltage sensor activation, gating currents recorded in the absence of Ca²⁺ activate without a detectable delay and decay with a rapid exponential time course while channels are closed (Horrigan and Aldrich, 1999). In the presence of 70 μM Ca²⁺, a slow component of I_{gON} decay is evident, and slow components of both ON and OFF charge movement are observed. However, these observations are readily accounted for by interactions between channel opening and voltage sensor movement and do not imply a complex voltage sensor activation mechanism. Q_{fast}-V relationships determined by fitting the fast component of I_{gON} in either 0 or 70 Ca²⁺ reflect the voltage sensor equilibrium for closed channels (Q_C) and are fit well by single Boltzmann functions, again consistent with a two-state process and a voltage

sensor charge z_f = 0.58 e. The limiting slope of the P_O-V relationship that reveals the voltage sensor equilibrium for open channels (Q_O) is also fit reasonably by a single Boltzmann function. Although exponential kinetics and a Boltzmann equilibrium distribution are consistent with the assumption of independent voltage sensor movement, the increased slope of the Q_O-V relationship caused by Ca²⁺ is not predicted by Scheme II. This effect may indicate a small cooperative interaction among voltage sensors or may represent a systematic measurement error related to large Ca²⁺-dependent increases in P_O.

The C-O Transition

Scheme II represents the C-O conformational change as a concerted two-state process that is rate limiting for channel activation and has a weak intrinsic voltage dependence. Consistent with a two-state C-O transition, macroscopic I_K relaxation kinetics are single exponential after a brief delay, over a wide range of voltage and [Ca²⁺] (Cox et al., 1997a; Cui et al., 1997; Horrigan et al., 1999). The delay can be attributed to voltage sensor activation (Horrigan and Aldrich, 1999; Horrigan et al., 1999) and does not imply a complex C-O transition. The exponential voltage dependence of τ(I_K) over a large range of negative voltages is also consistent with a two-state process. The weak voltage dependence of τ(I_K) and P_O at negative voltages demonstrates that charge movement associated with the C-O transition is small (z_L = 0.3 e).

Single channel studies also support a two-state C-O conformational change. The number of detectable open and closed dwell-time components are comparable under a variety of conditions (McManus and Magleby, 1988; Rothberg and Magleby, 1999; Nimigean and Magleby, 2000; Talukder and Aldrich, 2000). This observation is consistent with an allosteric mechanism like Scheme II with a concerted C-O transition that implies gating schemes with an equal number of open and closed states directly connected in a two-tiered arrangement. Kinetic components can underestimate the accessible states and do not generally provide a precise comparison of closed versus open states. However, in 0 Ca²⁺ (Nimigean and Magleby, 2000; Talukder and Aldrich, 2000) and saturating (100–1,000 μM) Ca²⁺ (Rothberg and Magleby, 1999), where the accessible states are minimized, the number of open and closed components are less than or equal to the number of states predicted by Scheme II (five open, five closed), consistent with a concerted C-O transition. In addition, two-dimensional dwell time distributions are consistent with the connectivity of open and closed states specified by a two-tiered gating architecture (Rothberg and Magleby, 1999). And the detailed kinetics can be reproduced by models similar to Scheme II (Rothberg and Magleby, 1999, 2000).

Although the macroscopic and single channel kinetics are generally consistent with a two state C-O transition, the C-O transition maybe more complex. Brief “flicker” closings are commonly observed in single BK channel recordings. These events are not predicted by Scheme II and may represent intermediates during the C-O conformational change or closed states, such as blocking events, that lie outside of the activation pathway. Detailed single channel analysis cannot distinguish these possibilities (Rothberg and Magleby, 1998). In addition, as discussed below, the voltage and Ca^{2+} dependence of macroscopic $\tau(I_K)$ suggest that C-O transition kinetics respond in a complex fashion to voltage sensor activation and Ca^{2+} binding. To account for these results we have suggested that the C-O conformational change may be characterized by a complex energy landscape.

Ca^{2+} Binding

It is reasonable to describe Ca^{2+} binding to each high affinity binding site as a two-state process. However, we do not measure Ca^{2+} binding directly, and the indirect analysis of Ca^{2+} -binding properties based on the Ca^{2+} dependence of channel opening is complicated by the presence in *Slo1* channels of additional low affinity binding sites and by effects of Ca^{2+} on voltage sensor activation. Here we have measured open probability at extreme negative voltages to isolate the effect of Ca^{2+} binding on channel opening from its effect on voltage sensor activation. Under these conditions, the ratio (R_O) of NP_O in the presence and absence of Ca^{2+} should depend only on the Ca^{2+} dissociation constant (K_D) and the allosteric interaction between Ca^{2+} -binding and channel opening (C). The Ca^{2+} dependence of R_O is well fit by an MWC model (sub-Scheme IIc), consistent with independent and identical two-state binding reactions. The $K_{D\text{S}}$ determined in this fashion ($9.3 \pm 0.4 \mu\text{M}$) or used in Scheme II ($11 \mu\text{M}$) fall within the range of previous estimates for *mSlo1* ($7.4\text{--}11.2 \mu\text{M}$) (Cox et al., 1997a; Cox and Aldrich, 2000; Shi and Cui, 2001; Zhang et al., 2001).

It is important to realize that Scheme II specifies four different state-dependent Ca^{2+} dissociation constants for the high-affinity binding site. K_D represents the dissociation constant for closed channels when voltage sensors are in the resting state ($K_D[\text{CR}] = 11 \mu\text{M}$). Channel opening produces a C-fold (eightfold) increase in affinity ($K_D[\text{OR}] = 1.4 \mu\text{M}$). Voltage sensor activation produces an additional E-fold (2.4-fold) increase in affinity for both closed and open channels ($K_D[\text{CA}] = 4.6 \mu\text{M}$, $K_D[\text{OA}] = 0.57 \mu\text{M}$).

The extent to which Ca^{2+} binding may be voltage dependent has yet to be defined. The gating of unliganded channels rules out that voltage gating is determined solely by Ca^{2+} binding (Cui et al., 1997). However, voltage-dependent binding could potentially

contribute to voltage gating and provide clues as to the location of the Ca^{2+} binding site relative to the membrane electric field. P_O or $\tau(I_K)$ exhibit similar voltage dependencies in different $[\text{Ca}^{2+}]$, suggesting that Ca^{2+} binding is not strongly voltage dependent relative to voltage sensor activation (Cox et al., 1997a; Rothberg and Magleby, 2000). Assuming Ca^{2+} binding is not rate limiting for channel gating (Cox et al., 1997a; Cui et al., 1997), effects of voltage on Ca^{2+} binding should be evident only at intermediate $[\text{Ca}^{2+}]$ where the occupancy of binding sites can be altered by changes in binding affinity. Since P_O increases with Ca^{2+} occupancy, one consequence of voltage-dependent binding should be to increase the voltage dependence of P_O at intermediate $[\text{Ca}^{2+}]$ relative to saturated or unliganded conditions. Although a bell-shaped dependence on $[\text{Ca}^{2+}]$ is observed in the steepness of P_O -V relationships (Cui et al., 1997), this effect can be reproduced by a model similar to Scheme II without voltage-dependent Ca^{2+} binding (Cox and Aldrich, 2000). Our results indicate an apparent increase with $[\text{Ca}^{2+}]$ in the voltage dependence of P_O at extreme negative voltages (q_0 , Fig. 12 C). But this effect is not characterized by a bell-shaped Ca^{2+} dependence and may reflect measurement error at low open probability. $\tau(I_K)$, which can be measured with greater precision than P_O at extreme voltages, exhibits exponential voltage dependencies at both positive and negative voltages that are essentially Ca^{2+} independent (Fig. 14 C). From these kinetic results we conclude that the voltage dependence of Ca^{2+} binding must be weak relative to that of the C-O transition ($z_L = 0.3 e$). Therefore, we make the simplifying assumption in Scheme II that Ca^{2+} binding is voltage independent.

Interactions Among Sensors and Gates

We pursued several distinct goals in characterizing the interactions among voltage sensor activation, Ca^{2+} -binding, and channel opening. First was to quantify the interaction energies, i.e., the allosteric factors C, D, E in Scheme II. When possible, we determined these quantities by measuring the equilibrium (energetic) change in a target process produced by extreme (saturating) changes in the state of a coupled effector process. Second, we tested the allosteric prediction that such interactions are reciprocal in nature. Finally, to test the Scheme II prediction that the activation of an individual sensor has an additive effect on the C-O equilibrium constant, we fit the Ca^{2+} and voltage dependencies of P_O .

Interaction of Ca^{2+} Binding and Channel Opening

Interactions between Ca^{2+} binding and channel opening can in theory be studied in isolation from voltage sensor activation at extreme positive or negative voltages. However, at extreme positive voltages where all voltage sensors are activated, measurement of I_K is diffi-

cult and P_O saturates, even in the absence of Ca^{2+} , providing little information about the C-O equilibrium constant. The effect of Ca^{2+} on channel opening is best studied at extreme negative voltages where no voltage sensors are activated and P_O is small. Under these conditions, P_O increases in a Ca^{2+} -dependent manner by more than three orders of magnitude, indicating a strong interaction between Ca^{2+} binding and channel opening. To quantify this interaction, we determined the ratio (R_O) of $N P_O$ in the presence and absence of Ca^{2+} . According to Scheme II, $R_O = C^4$ in saturating Ca^{2+} , providing a direct measure of the interaction factor $C = 7.4 \pm 0.1$ (1.20 kcal mol⁻¹) based on mean R_O . This is lower than values of C reported previously for *mSlc1* ($C = 8.4\text{--}11.6$) (Cox et al., 1997a; Cox and Aldrich, 2000; Shi and Cui, 2001; Zhang et al., 2001). However, the previous estimates, based on P_O at more positive voltages, reflect interactions between Ca^{2+} binding and voltage sensor activation and therefore represent a composite of the allosteric factors C and E in Scheme II.

Once C was determined from the saturating value of R_O , the $R_O\text{-Ca}^{2+}$ relationship was fit well by an MWC model (sub-Scheme IIC) by simply adjusting K_D . The ability of sub-Scheme IIC to fit the Ca^{2+} dependence of R_O supports the assumption that Ca^{2+} sensors in different subunits have independent and identical additive effects on the free energy of the C-O transition.

The reciprocal effect of channel opening on Ca^{2+} -binding predicted by the allosteric model was not tested directly by measuring bound Ca^{2+} . However $\tau(I_K)$ measured at extreme positive voltage (τ_P) or negative voltages (τ_N) should reflect the distribution of Ca^{2+} -bound closed and open states respectively. That τ_N is sensitive to sub-micromolar Ca^{2+} while τ_P is not is therefore qualitatively consistent with the prediction that an increase in Ca^{2+} -affinity accompanies channel opening.

Interaction of Voltage Sensor Activation and Channel Opening

Interactions between voltage sensor and gate can be studied in isolation from Ca^{2+} binding in the unliganded or Ca^{2+} -saturated states. The $P_O\text{-V}$ relationships under these conditions reflect the effect of voltage sensor activation on channel opening. Specifically, the change in P_O that occurs from extreme negative voltages ($V_N < -100$ mV), where no voltage sensors are activated, to extreme positive voltages ($V_P > 250$ mV), where all voltage sensors are activated, reflects the interaction energy and the intrinsic voltage dependence of the C-O transition. Scheme II predicts:

$$\frac{\lambda_{A4}[V_P]}{\lambda_{A0}[V_N]} = D^4 e^{z_L(V_P - V_N)/kT}, \quad (22)$$

where (λ_{Ai}) is the C-O equilibrium constant when i voltage sensors are activated and z_L is its partial charge.

$\lambda_{A0}[V_N]$ is well determined in both 0 Ca^{2+} and high (70–100 μM) Ca^{2+} by measurements of P_O over a range of negative voltages, whereas z_L can be estimated from the weak voltage dependence of $P_o[V_N]$. Unfortunately $\lambda = P_O/(1 - P_O)$ cannot be measured accurately at extreme positive voltages because $P_O(V_P)$ saturates, near unity, even in 0 Ca^{2+} . Therefore, D cannot be determined from Eq. 22. However, we can place a lower limit on D by considering that $\lambda \leq \lambda_{A4}$ for any $V \leq V_P$. Thus:

$$\frac{\lambda[V_H(P_0)]}{\lambda_{A0}[V_N]} = \frac{1}{\lambda_{A0}[V_N]} \leq D^4 e^{z_L(V_H(P_0) - V_N)/kT}. \quad (23)$$

In 0 Ca^{2+} , the mean half-activation voltage $V_h(P_0)$ is 186 mV and $\lambda_{A0}[V_N] = P_O(-124 \text{ mV}) = 3.2 \times 10^{-7}$. Therefore, Eq. 23 yields $D \geq 17$ ($\Delta\Delta G = 1.7$ kcal mol⁻¹) if $z_L = 0.3$ e.

A best value of $D = 25$ ($\Delta\Delta G = 1.93$ kcal mol⁻¹) was ultimately determined by fitting P_O over the entire voltage range. The ability of Scheme II to fit the $P_O\text{-V}$ relationships supports the assumption that activation of each individual voltage sensor has an additive effect on channel opening.

Several lines of evidence confirm the allosteric prediction that channel opening has a reciprocal effect on voltage sensor activation. First, the decay of OFF gating current is slowed when channels are opened (Fig. 13). In addition I_{gON} increases in amplitude in response to a double pulse protocol (Fig. 11). Finally, the open channel charge distribution (Q_O) estimated from the limiting voltage dependence of P_O (Fig. 12 A) is shifted to more negative voltages than the closed channel distribution (Q_C) determined from I_{gON} (Fig. 7 C). The similar shapes of Q_O and Q_C are consistent with the prediction that channel opening has equivalent effects on all four voltage sensors.

The shift in half-activation voltage between Q_C and Q_O ($\Delta V_h(Q_{CO})$) provides an additional measure of the interaction factor $D = \exp(z_j \Delta V_h(Q_{CO})/kT)$. In 0 Ca^{2+} , the half-activation voltages for Q_C (155 mV) and Q_O (-4.3 mV) differ by 159 mV, yielding $D = 38.5$ ($\Delta\Delta G = 2.19$ kcal mol⁻¹) if $z_j = 0.58$ e. Although this estimate of D is 54% greater than that obtained by fitting the $P_O\text{-V}$ relationships ($D = 25$), the difference in energetic terms ($\Delta\Delta G = \ln[D]$) is only 13% and could be accounted for by a 19 mV overestimation of $\Delta V_h(Q_{CO})$. Several factors might contribute to an error of this magnitude, including patch-to-patch variation, the different ionic conditions used to measure Q_O and Q_C , and that Q_O is extrapolated from a fit to the foot of the $\langle q_a \rangle\text{-V}$ relationship.

Interaction of Ca^{2+} Binding and Voltage Sensor Activation

We isolated the effect of Ca^{2+} binding on voltage sensor activation from its effect on channel opening by taking advantage of the fact that C-O transition kinetics

are much slower than voltage sensor activation in *Slo1* channels. Fast components of gating charge movement occurring in the first 100–200 μ s after a voltage step reveal the kinetic and steady-state properties of voltage sensor activation while the open/closed state of the channel remains effectively constant (Horrigan and Aldrich, 1999). For closed channels, we find 70 μ M Ca^{2+} slows the fast component of $I_{g\text{OFF}}$ but has little or no effect on $I_{g\text{ON}}$. Consistent with a slowing of voltage sensor deactivation, the $Q_c\text{-V}$ relationship shifts by -33 mV in 70 μ M Ca^{2+} , as determined by gating-capacitance measurements. Similarly, the $Q_o\text{-V}$ relationship shifts by -43 mV. According to Scheme II, the shifts in Q_c and Q_o are produced by an E-fold increase in the equilibrium constant for voltage sensor activation where $E = \exp(z_f \Delta V_h [Q]/kT)$ ranges from 2.1 to 2.7 ($\Delta\Delta G = 0.45$ to 0.59 kcal mol $^{-1}$) based on Q_c and Q_o , respectively. The shift in Q_c may underestimate E because Ca^{2+} binding sites in the closed channel, with a K_D of 11 μ M, are expected to be 86% occupied in 70 μ M Ca^{2+} , whereas open channels with a higher Ca^{2+} affinity should be fully saturated. A final value of $E = 2.4$ was assigned to Scheme II based on fits to the $P_o\text{-V}$ relationships over a range of $[\text{Ca}^{2+}]$.

In Scheme II we assume that the effects of Ca^{2+} on voltage sensor activation and channel opening are mediated by the same Ca^{2+} binding sites. An alternative hypothesis is that Ca^{2+} can bind nonspecifically to the channel or membrane and shift the voltage dependence of voltage sensor activation through a charge screening mechanism. We cannot rule out this possibility based on gating current measurements because the dose-dependent effects of Ca^{2+} were not examined. However, I_K measurements over a range of Ca^{2+} support the assumption that effects of Ca^{2+} on voltage sensor activation are mediated by high affinity binding sites. First, the $Q_o\text{-V}$ relationship shifts even in low micromolar Ca^{2+} (Fig. 12 B), whereas surface charge effects are unlikely at such low concentrations. In addition, we have described a difference between the apparent Ca^{2+} sensitivities of $V_h(P_o)$ and P_o measured at extreme negative voltages (i.e., R_o), which can be accounted for by interactions between Ca^{2+} binding and voltage sensor activation. The discrepancy between $V_h(P_o)$ and R_o is evident even in submicromolar Ca^{2+} and is well described by Scheme II (Fig. 9 D) from 0 to 100 μ M Ca^{2+} , consistent with the assumption that effects of Ca^{2+} on voltage sensor activation and channel opening are mediated by the same binding sites.

Limitations of Limiting Slope Measurements

The maximal voltage dependence of P_o (i.e., peak $\langle q_a \rangle$) does not provide a direct indication of total gating charge for channels like *Slo1* that can occupy multiple open states (Sigg and Bezanilla, 1997; Horrigan et al.,

1999). We have shown that peak $\langle q_a \rangle$ underestimates the total gating charge of *mSlo1* by 26–44% in a Ca^{2+} -dependent manner (Fig. 12 E). The tendency of peak $\langle q_a \rangle$ to decrease with increasing $[\text{Ca}^{2+}]$ is reproduced by Scheme II without requiring that Ca^{2+} binding is voltage dependent or that Ca^{2+} ions contribute to gating charge. These observations have consequences for the interpretation of previous studies. For example, Diaz et al. (1998) studied the effect of charge altering point mutations in the S4 voltage sensor of *hSlo1*. The voltage dependence of P_o at low voltages was used to assess changes in total gating charge. Their conclusions concerning the contribution of different S4 residues to gating charge are difficult to evaluate given the tendency of this method to underestimate gating charge and because different mutants were studied in different $[\text{Ca}^{2+}]$.

Mechanism of Channel Activation by Low Affinity Ca^{2+} Binding Sites

Recent studies indicate that Ca^{2+} and Mg^{2+} at high concentrations (>100 μ M) can act at low affinity (millimolar) binding sites to promote channel opening (Shi and Cui, 2001; Zhang et al., 2001). These studies conclude that Ca^{2+} binding at low affinity sites increases the C-O equilibrium constant through an allosteric mechanism analogous to that embodied by the allosteric factor C in Scheme II. An alternative hypothesis, that low affinity sites interact exclusively with voltage sensors, was rejected (Zhang et al., 2001). However, the possibility that low affinity sites interact with both C-O and R-A transition as in Scheme II was not ruled out. Indeed, our results and analysis suggest that low affinity sites must interact with voltage sensors.

When Ca^{2+} is increased from 100 to 1,000 μ M we observe an approximately -30 mV shift in $V_h(P_o)$. This effect is consistent with previous reports (Cox et al., 1997a; Shi and Cui, 2001; Zhang et al., 2001) and can be reproduced (Fig. 9 D, dotted line) by modifying Scheme II after Zhang et al. (2001) to include additional low affinity binding sites ($K_{D\text{Low}} = 2.33$ mM) that are allosterically coupled to the C-O transition ($C_{\text{Low}} = 3.53$). If Ca^{2+} binding at these sites acts merely to increase the C-O equilibrium constant, then changes in $V_h(P_o)$ should be accompanied by proportional changes in P_o at extreme negative voltages. Consequently the modified model predicts a 27% increase in $\log(R_o)$ from 100 to 1,000 μ M Ca^{2+} (Fig. 9 D, dashed line) corresponding to a large ninefold increase in P_o . By contrast, we observe a 2.4% increase in mean $\log(R_o)$, similar to the 3.6% increase predicted by Scheme II, and a maximum 9% increase was observed in an individual experiment (Fig. 8 E). Thus, the R_o data are inconsistent with the hypothesis that Ca^{2+} binding to low affinity sites acts merely to increase the C-O equilibrium constant.

A discrepancy between the Ca^{2+} dependence of $V_h(P_O)$ and R_O is observed in 0–100 μM Ca^{2+} and can be accounted for by interactions between high affinity Ca^{2+} binding sites and voltage sensors. As shown in Fig. 9 D, Scheme II predicts $V_h(P_O)$ will begin to increase over a range of Ca^{2+} where R_O remains relatively constant. A similar mechanism involving interaction of low affinity sites with voltage sensors might account for the differential response of $V_h(P_O)$ and R_O to Ca^{2+} in the 100–1,000 μM range. If this is the case, measurements at $[\text{Ca}^{2+}] > 1 \text{ mM}$ may be necessary to reveal an effect of low affinity sites on R_O .

If Ca^{2+} binding at low affinity sites increases the voltage sensor equilibrium, then the charge distribution for open channels (Q_O) should shift to more negative voltages in high Ca^{2+} . Although we did not test this prediction, kinetic data reported by Zhang et al. (2001) are consistent with a shift in Q_O . According to our analysis, $\tau(I_K)$ achieves a weak exponential voltage dependence at extreme negative voltages and can deviate from this limiting voltage dependence only when Q_O begins to increase. Consistent with this prediction, $\tau(I_K)\text{-V}$ in 0–100 μM Ca^{2+} exhibit a similar limiting voltage dependence between –300 and –150 mV (Fig. 14, B and C) where Q_O has apparently achieved a minimum (Fig. 12 B). Similar behavior is observed in the $\tau(I_K)\text{-V}$ data reported by Zhang et al. (2001) for 0–100 μM Ca^{2+} with a limiting voltage dependence of e-fold per 195 mV ($z_N = -0.13 e$) from –200 to –150 mV in 1 μM Ca^{2+} (measured from Fig. 10 A [Zhang et al., 2001]). By contrast, $\tau(I_K)\text{-V}$ in 10–100 mM Ca^{2+} is approximately fourfold steeper ($z_N = -0.51 e$, 10 mM Ca^{2+}) over the same voltage range. This result suggests that the foot of the $Q_O\text{-V}$ relationship has shifted to voltages more negative than –200 mV in 10 mM Ca^{2+} . Thus, low affinity Ca^{2+} binding sites may interact with voltage sensor activation.

Kinetic Models and the Nature of the C-O Transition

Although we depict the C-O transition in Scheme II as a two-state reaction, it is likely to represent a complex quaternary conformational change involving the concerted movement of four subunits. The existence of concerted but asynchronous transitions are well recognized in the case of protein-folding reactions where multiple interactions may be broken and formed during a rapid transition between two stable conformations (Fersht, 1995). In such a case, the transition-free energy cannot be described as a smooth symmetrical barrier as might characterize a simple small molecule reaction. Rather, complex energy landscapes are observed where the barrier is often described as “broad” and may also be “rugged,” containing numerous local maxima and minima (Fersht, 1995; Oliveberg et al.,

1998). A complex barrier is not incompatible with apparent two-state behavior provided that the intermediate species are unstable and do not accumulate. Moreover, a complex transition with a single dominant barrier can exhibit simple kinetic behaviors, such as linear free energy relationships, in response to small equilibrium perturbations. However, large perturbations frequently alter the position or identity of the rate limiting barrier, producing complex changes in the relationship between equilibria and kinetics (Oliveberg et al., 1998; Oliveberg, 2001). In some cases, nonlinear free energy relationships are observed that have been interpreted in terms of a gradual shift in the position of the transition state along the reaction coordinate, the so called Hammond postulate behavior (Matouschek and Fersht, 1993; Hammond, 1955; Matouschek et al., 1995; Matthews and Fersht, 1995). In other cases, sudden or large changes in the slope of linear free energy relationships are observed that are thought to represent a switch in the rate-determining barrier similar to that proposed here for the C-O transition of *mSlo1* (Milla et al., 1995; Jonsson et al., 1996; Silow and Oliveberg, 1997; Oliveberg et al., 1998).

The voltage and Ca^{2+} dependence of $\tau(I_K)$ for *mSlo1* suggest that C-O transition kinetics respond in a complex fashion to voltage sensor activation and Ca^{2+} binding. In particular, biphasic relationships are observed between closing rate constants and voltage sensor activation in 0 Ca^{2+} and 70 μM Ca^{2+} . To account for this feature of the data we propose a two-barrier transition state model for the C-O conformational change. The model reproduces the biphasic pattern of closing rates as well as the changes that occur in that pattern between 0 Ca^{2+} and 70 μM Ca^{2+} (Fig. 15 B). The $\tau(I_K)\text{-V}$ relationships at intermediate Ca^{2+} are only approximated by this scheme and it is possible that a more complex model is required. However, this example illustrates the basic point that complex patterns of rate constants can be reproduced while maintaining the Scheme II assumptions that the C-O transition is concerted and that activation of individual voltage sensors and Ca^{2+} binding sites have additive effects on the C-O transition energy.

It is conceivable that the effects of Ca^{2+} binding and voltage sensor activation on the C-O transition energy are to some extent nonadditive (i.e., cooperative), and this might account for the tendency of Scheme II to overestimate the steepness of $P_O\text{-V}$ relationships in intermediate $[\text{Ca}^{2+}]$. Since the rate constants in Fig. 15 B were determined from fits to Scheme II, the pattern of closing rates could also be affected by the assumption of energy additivity. Regardless of this possibility, the behavior of $\tau(I_K)$ at negative voltages supports the general conclusion that Ca^{2+} binding alters the sensitivity of C-O rate constants to voltage sensor activation. $\tau(I_K)$

should only deviate from a limiting exponential voltage dependence at extreme negative voltages when voltage sensors begin to activate and the O-to-C rate constant decreases. The voltage at which this deviation occurs is strongly affected by Ca^{2+} , whereas voltage sensor activation (Q_O) is not. This implies that fewer voltage sensors need be activated in high Ca^{2+} to produce a decrease in the closing rate constant.

Our two-barrier model predicts a linear relationship between log closing rate and the free energy perturbation produced by activation of a few Ca^{2+} or voltage sensors, but deviation from a linear relationship as more sensors are activated. This hypothesis appears reasonable given the intrinsic voltage dependence of the C-O transition and the magnitude of the perturbations produced by voltage sensor activation and Ca^{2+} binding. At negative voltages in 0 Ca^{2+} , where voltage and Ca^{2+} sensors are not activated, $\tau(I_K)$ exhibits an exponential dependence on voltage over an ~ 400 mV voltage range (-500 to -100 mV) (Horrigan et al., 1999). We expect $1/\tau(I_K)$, at extreme negative voltages, to represent the closing rate constant, and the C-O equilibrium-free energy should change in proportion to voltage. Thus, the exponential voltage dependence of $\tau(I_K)$ shows that the C-O transition exhibits a rate-equilibrium linear free energy relationship over an ~ 120 -fold change in the C-O equilibrium constant (assuming $z_L = 0.3 e$). Linear free energy relationships were also reported for acetylcholine receptor channels in response to a three order of magnitude change in the C-O equilibrium constant (Grosman et al., 2000). We observe similar behavior in *mSlo1* in response to 2–3 order of magnitude perturbations in the C-O equilibrium constant by activation of two voltage sensors ($D^2 = 625$) or even Ca^{2+} -binding to all four high affinity sites ($C^4 = 4.1 \times 10^3$). However, we observe deviations from linearity when additional sensors are activated, since a large nine order of magnitude maximum perturbation is possible ($C^4D^4 = 1.6 \times 10^9$, 12.7 kcal mole $^{-1}$).

There is evidence in BK and other channels for activation-associated transiently occupied sub-conductance states that may support the notion of a complex C-O transition. Although stable subconductance events in BK channels are rare, brief (~ 50 μs) sojourns to a subconductance level (10–35% of fully open) are frequently observed during “flicker” closings or immediately before and after transitions to a fully closed state (Ferguson et al., 1993). Similarly, Shaker K $^+$ channels pass through two sequentially occupied substates with microsecond lifetimes during the transition between fully closed and open (Zheng et al., 2001). These brief subconductance events could represent metastable intermediates in what is an essentially concerted but complex C-O transition.

We thank Tom Middendorf, Richard Lewis, Jon Sack, Toshi Hoshi, and Merrit Maduke for helpful comments on the manuscript.

This work was supported by a grant from the National Institutes of Health (NS42901) for F.T. Horrigan and by a National Institute of Mental Health Silvio Conte Center for Neuroscience Research grant (MH48108) for R.W. Aldrich. R.W. Aldrich is an investigator with the Howard Hughes Medical Institute.

Submitted: 10 April 2002

Revised: 26 June 2002

Accepted: 27 June 2002

REFERENCES

- Almers, W. 1978. Gating currents and charge movements in excitable membranes. *Rev. Physiol. Biochem. Pharmacol.* 82:96–190.
- Armstrong, C.M., and F. Bezanilla. 1974. Charge movement associated with the opening and closing of the activation gates of the Na channels. *J. Gen. Physiol.* 63:533–552.
- Barrett, J.N., K.L. Magleby, and B.S. Pallotta. 1982. Properties of single calcium-activated potassium channels in cultured rat muscle. *J. Physiol.* 331:211–230.
- Butler, A., S. Tsunoda, D.P. McCobb, A. Wei, and L. Salkoff. 1993. *mSlo*, a complex mouse gene encoding “maxi” calcium-activated potassium channels. *Science*. 261:221–224.
- Cox, D.H., and R.W. Aldrich. 2000. Role of the beta1 subunit in large-conductance Ca^{2+} -activated K $^+$ channel gating energetics. Mechanisms of enhanced Ca^{2+} sensitivity. *J. Gen. Physiol.* 116: 411–432.
- Cox, D.H., J. Cui, and R.W. Aldrich. 1997a. Allosteric gating of a large conductance Ca-activated K $^+$ channel. *J. Gen. Physiol.* 110: 257–281.
- Cox, D.H., J. Cui, and R.W. Aldrich. 1997b. Separation of gating properties from permeation and block in *mSlo* large conductance Ca^{2+} -activated K $^+$ channels. *J. Gen. Physiol.* 109:633–646.
- Cui, J., and R.W. Aldrich. 2000. Allosteric linkage between voltage and Ca^{2+} -dependent activation of BK-type *mSlo1* K $^+$ channels. *Biochemistry*. 39:15612–15619.
- Cui, J., D.H. Cox, and R.W. Aldrich. 1997. Intrinsic voltage dependence and Ca^{2+} regulation of *mSlo* large conductance Ca^{2+} -activated K $^+$ channels. *J. Gen. Physiol.* 109:647–673.
- Diaz, F., M. Wallner, E. Stefani, L. Toro, and R. Latorre. 1996. Interaction of internal Ba $^{2+}$ with a cloned Ca^{2+} -dependent K $^+$ (*hslo*) channel from smooth muscle. *J. Gen. Physiol.* 107:399–407.
- Diaz, L., P. Meera, J. Amigo, E. Stefani, O. Alvarez, L. Toro, and R. Latorre. 1998. Role of the S4 segment in a voltage-dependent calcium-sensitive potassium (*hslo*) channel. *J. Biol. Chem.* 273: 32430–32436.
- DiChiara, T.J., and P.H. Reinhart. 1997. Redox modulation of *hslo* Ca^{2+} -activated K $^+$ channels. *J. Neurosci.* 17:4942–4955.
- Eaton, W.A., E.R. Henry, and J. Hofrichter. 1991. Application of linear free energy relations to protein conformational changes: the quaternary structural change of hemoglobin. *Proc. Natl. Acad. Sci. USA*. 88:4472–4475.
- Ferguson, W.B., O.B. McManus, and K.L. Magleby. 1993. Opening and closing transitions for BK channels often occur in two steps via sojourns through a brief lifetime subconductance state. *Bioophys. J.* 65:702–714.
- Fernandez, J.M., F. Bezanilla, and R.E. Taylor. 1982. Distribution and kinetics of membrane dielectric polarization. II. Frequency domain studies of gating currents. *J. Gen. Physiol.* 79:41–67.
- Fersht, A.R. 1995. Characterizing transition states in protein folding: an essential step in the puzzle. *Curr. Opin. Struct. Biol.* 5:79–84.
- Grosman, C., M. Zhou, and A. Auerbach. 2000. Mapping the conformational wave of acetylcholine receptor channel gating. *Nature*. 403:773–776.
- Hamill, O.P., A. Marty, E. Neher, B. Sakmann, and F.J. Sigworth. 1981. Improved patch-clamp techniques for high-resolution cur-

- rent recording from cells and cell-free membrane patches. *Pflug Arch.* 391:85–100.
- Hammond, G.S. 1955. A correlation of reaction rates. *J. Am. Chem. Soc.* 77:334–338.
- Herrington, J., and R.J. Bookman. 1995. Pulse Control. University of Miami Press, Miami, FL.
- Hofrichter, J., E.R. Henry, A. Szabo, L.P. Murray, A. Ansari, C.M. Jones, M. Coletta, G. Falcioni, M. Brunori, and W.A. Eaton. 1991. Dynamics of the quaternary conformational change in trout hemoglobin. *Biochemistry*. 30:6583–6598.
- Horrigan, F.T., and R.W. Aldrich. 1999. Allosteric voltage gating of potassium channels II. Mslo channel gating charge movement in the absence of Ca^{2+} . *J. Gen. Physiol.* 114:305–336.
- Horrigan, F.T., J. Cui, and R.W. Aldrich. 1999. Allosteric voltage gating of potassium channels I. Mslo ionic currents in the absence of Ca^{2+} . *J. Gen. Physiol.* 114:277–304.
- Islas, L.D., and F.J. Sigworth. 1999. Voltage sensitivity and gating charge in Shaker and Shab family potassium channels. *J. Gen. Physiol.* 114:723–742.
- Jonsson, T., C.D. Waldburger, and R.T. Sauer. 1996. Nonlinear free energy relationships in Arc repressor unfolding imply the existence of unstable, native-like folding intermediates. *Biochemistry*. 35:4795–4802.
- Leffler, J.E. 1953. Parameters for the description of transition states. *Science*. 117:340–341.
- Marks, T.N., and S.W. Jones. 1992. Calcium currents in the A7r5 smooth muscle-derived cell line. An allosteric model for calcium channel activation and dihydropyridine agonist action. *J. Gen. Physiol.* 99:367–390.
- Matouschek, A., and A.R. Fersht. 1993. Application of physical organic chemistry to engineered mutants of proteins: Hammond postulate behavior in the transition state of protein folding. *Proc. Natl. Acad. Sci. USA*. 90:7814–7818.
- Matouschek, A., D.E. Otzen, L.S. Itzhaki, S.E. Jackson, and A.R. Fersht. 1995. Movement of the position of the transition state in protein folding. *Biochemistry*. 34:13656–13662.
- Matthews, J.M., and A.R. Fersht. 1995. Exploring the energy surface of protein folding by structure-reactivity relationships and engineered proteins: observation of Hammond behavior for the gross structure of the transition state and anti-Hammond behavior for structural elements for unfolding/folding of barnase. *Biochemistry*. 34:6805–6814.
- McCormack, K., W.J. Joiner, and S.H. Heinemann. 1994. A characterization of the activating structural rearrangements in voltage-dependent Shaker K^+ channels [published erratum appears in *Neuron* 12:706]. *Neuron*. 12:301–315.
- McManus, O.B., and K.L. Magleby. 1988. Kinetic states and modes of single large-conductance calcium-activated potassium channels in cultured rat skeletal muscle. *J. Physiol.* 402:79–120.
- Milla, M.E., B.M. Brown, C.D. Waldburger, and R.T. Sauer. 1995. P22 Arc repressor: transition state properties inferred from mutational effects on the rates of protein unfolding and refolding. *Biochemistry*. 34:13914–13919.
- Moczydowski, E., and R. Latorre. 1983. Gating kinetics of Ca^{2+} -activated K^+ channels from rat muscle incorporated into planar lipid bilayers. Evidence for two voltage-dependent Ca^{2+} binding reactions. *J. Gen. Physiol.* 82:511–542.
- Neyton, J. 1996. A Ba^{2+} chelator suppresses long shut events in fully activated high-conductance Ca^{2+} -dependent K^+ channels. *Biophys. J.* 71:220–226.
- Nimigean, C.M., and K.L. Magleby. 2000. Functional coupling of the beta(1) subunit to the large conductance Ca^{2+} -activated $\text{K}(+)$ channel in the absence of Ca^{2+} . Increased Ca^{2+} sensitivity from a Ca^{2+} -independent mechanism. *J. Gen. Physiol.* 115:719–736.
- Oliveberg, M. 2001. Characterisation of the transition states for protein folding: towards a new level of mechanistic detail in protein engineering analysis. *Curr. Opin. Struct. Biol.* 11:94–100.
- Oliveberg, M., Y.J. Tan, M. Silow, and A.R. Fersht. 1998. The changing nature of the protein folding transition state: implications for the shape of the free-energy profile for folding. *J. Mol. Biol.* 277: 933–943.
- Rae, J.L., J. Dewey, J.S. Rae, and K. Cooper. 1990. A maxi calcium-activated potassium channel from chick lens epithelium. *Curr. Eye Res.* 9:847–861.
- Reinsch, C.H. 1967. Smoothing spline functions. *Numerische Mathematik*. 10:177–183.
- Rios, E., M. Karhanek, J. Ma, and A. Gonzalez. 1993. An allosteric model of the molecular interactions of excitation-contraction coupling in skeletal muscle. *J. Gen. Physiol.* 102:449–481.
- Rothberg, B.S., and K.L. Magleby. 1998. Kinetic structure of large-conductance Ca^{2+} -activated K^+ channels suggests that the gating includes transitions through intermediate or secondary states. A mechanism for flickers. *J. Gen. Physiol.* 111:751–780.
- Rothberg, B.S., and K.L. Magleby. 1999. Gating kinetics of single large-conductance Ca^{2+} -activated K^+ channels in high Ca^{2+} suggest a two-tiered allosteric gating mechanism. *J. Gen. Physiol.* 114: 93–124.
- Rothberg, B.S., and K.L. Magleby. 2000. Voltage and Ca^{2+} activation of single large-conductance Ca^{2+} -activated K^+ channels described by a two-tiered allosteric gating mechanism. *J. Gen. Physiol.* 116:75–99.
- Schreiber, M., and L. Salkoff. 1997. A novel calcium-sensing domain in the BK channel. *Biophys. J.* 73:1355–1363.
- Shi, J., and J. Cui. 2001. Intracellular Mg^{2+} enhances the function of BK-type Ca^{2+} -activated $\text{K}(+)$ channels. *J. Gen. Physiol.* 118:589–606.
- Sigg, D., and F. Bezanilla. 1997. Total charge movement per channel. The relation between gating charge displacement and the voltage sensitivity of activation. *J. Gen. Physiol.* 109:27–39.
- Sigg, D., H. Qian, and F. Bezanilla. 1999. Kramers' diffusion theory applied to gating kinetics of voltage-dependent ion channels. *Biophys. J.* 76:782–803.
- Sigworth, F.J. 1994. Voltage gating of ion channels. *Q. Rev. Biophys.* 27:1–40.
- Silow, M., and M. Oliveberg. 1997. High-energy channeling in protein folding. *Biochemistry*. 36:7633–7637.
- Stefani, E., M. Ottolia, F. Noceti, R. Olcese, M. Wallner, R. Latorre, and L. Toro. 1997. Voltage-controlled gating in a large conductance Ca^{2+} -sensitive K^+ channel (hslo). *Proc. Natl. Acad. Sci. USA*. 94:5427–5431.
- Talukder, G., and R.W. Aldrich. 2000. Complex voltage-dependent behavior of single unliganded calcium-sensitive potassium channels. *Biophys. J.* 78:761–772.
- Tang, X.D., H. Daggett, M. Hanner, M.L. Garcia, O.B. McManus, N. Brot, H. Weissbach, S.H. Heinemann, and T. Hoshi. 2001. Oxidative regulation of large conductance calcium-activated potassium channels. *J. Gen. Physiol.* 117:253–274.
- Zagotta, W.N., T. Hoshi, and R.W. Aldrich. 1994. Shaker potassium channel gating. III: Evaluation of kinetic models for activation. *J. Gen. Physiol.* 103:321–362.
- Zhang, X., C.R. Solaro, and C.J. Lingle. 2001. Allosteric regulation of BK channel gating by Ca^{2+} and Mg^{2+} through a nonselective, low affinity divalent cation site. *J. Gen. Physiol.* 118:607–636.
- Zheng, J., L. Vankataramanan, and F.J. Sigworth. 2001. Hidden Markov model analysis of intermediate gating steps associated with the pore gate of shaker potassium channels. *J. Gen. Physiol.* 118:547–564.